Master's thesis

NTNU
Norwegian University of Science and Technology
Faculty of Engineering
Department of Mechanical and Industrial Engineering

Maya Keilen

Investigation of Chemical Mechanical Polishing to Enhance Feature Resolution by Atomic Layer Deposition

Master's thesis in Mechanical Engineering
Supervisor: Jan Torgersen and Stephanie Burgmann
July 2020

NTNU
Norwegian University of
Science and Technology

Maya Keilen

Investigation of Chemical Mechanical Polishing to Enhance Feature Resolution by Atomic Layer Deposition

Master's thesis in Mechanical Engineering
Supervisor: Jan Torgersen and Stephanie Burgmann
July 2020

Norwegian University of Science and Technology
Faculty of Engineering
Department of Mechanical and Industrial Engineering

NTNU
Norwegian University of
Science and Technology

Preface

This master thesis was written during the spring semester of 2020, at the Department of Mechanical and Industrial Engineering (MTP), at the Norwegian University of Science and Technology (NTNU). The thesis is based on a project work, which was done during autumn 2019. Due to the COVID-19 pandemic, there was limited time for conducting the experimental work, and some of the results were obtained during the project work.

I want to thank my supervisor, Associate Professor Jan Torgersen, and Ph.D. Candidate Stephanie Burgmann for their help and guidance during this project. They always showed great interest and enthusiasm for what I was doing. I also want to thank Abdullah Bin Afif and Anup Dadlani for their help regarding the different equipment, and everyone at NanoLab, especially Jens Høvik and Mathilde Isabelle Barriet, for their help and moral support. Also, I would like to thank Markus Joakim Lid and Andreas Flaten, who were great members of our project group. I could always ask them for help if I needed something.

Honorable mentions go to my family, classmates, and friends. Especially, Vilde Årdal for making this year amazing. Finally, lots of love for Thomas V. Bjørge, for being the best team player ever. He made every day of this semester incredible with his positive attitude and amazing personality. I love you to the moon and back.

Abstract

Designing smaller and faster electronic devices requires control of the structure at the nanometer size. Increasing feature resolution by building underlying 3D structures of different materials and releasing those structures in a vapor etch process. To even out these structures chemical mechanical polishing (CMP) is used.

The CMP machine has many advantages such as very smooth surface results and low damage to the underlying structures, in addition to high efficiency at a low cost. Further, different parameters were changed to investigate the CMP on the nanometer scale. By changing one parameter at a time, it was possible to see how the slurry concentration, duration time, backside pressure, and working pressure influenced the roughness and material removal rate (MRR) of alumina (Al_2O_3), silica (SiO_2), and amorphous silicon (a-Si) (backside pressure and working pressure were not tested on a-Si). For a-Si adhesion and film quality, studies were conducted by changing deposition parameters and substrate material.

In conclusion, it is possible to see that a higher slurry concentration will increase the amount of material removed (AMR) from the surface. This occurs for all three materials. A-Si has a logarithmic relation, while alumina has a linear, and silica has a more polynomial relation. Higher working pressure yields almost a linear relation for both the silica and the alumina wafers. While there is no correlation between the AMR and the backside pressure, there is a trend of an increasing standard deviation of the surface roughness when the backside pressure is increased for silica and alumina wafers. To find out if there is a tighter correlation between the different parameters and the surface roughness, AMR, and standard deviation of the surface roughness, a bigger sample size should be investigated.

Sammendrag

For å designe mindre og raskere elektroniske enheter, kreves det å lage strukturer på nanometer størrelse. Å øke detaljoppløsningen ved å bygge underliggende 3D strukturer av forskjellige materialer og frigjøre disse strukturene ved hjelp av etseprosesser. For å jevne ut disse strukturene brukes kjemisk-mekanisk polering (CMP).

CMP maskinen har mange fordeler. For eksempel blir overflateresultatet veldig homogent, lagene får lite defekter, i tillegg til at maskinen har høy effektivitet til en lav pris. Videre ble ulike parameter endret for å undersøke hvordan CMP maskinen påvirket materialene på nanometerskala. Ved å endre en parameter av gangen, er det mulig å sjekke hvordan slikker-konsentrasjonen, poleringstiden, baktrykket og arbeidstrykket påvirker overflateruheten og hvor mye materiale som forsvinner (AMR), ved polering av aluminaoksid (Al_2O_3), silika (SiO_2) og amorft silisium (a-Si) (baktrykket og arbeidstrykket ble ikke testet på a-Si). Vedrørende a-Si heft og filmkvalitet ble flere studier utbragt ved å endre deponerings parametere og substratmaterialet.

Som konklusjon er det mulig å se at en høyere slikker-konsentrasjon vil øke mengde materialet som blir polert bort fra overflatene. Dette skjer for alle de tre materialene. A-Si har en logaritmisk relasjon, mens aluminaoksid har lineær relasjon og silika har en mer polynomisk relasjon. Et høyere arbeidstrykk gir nesten et lineært forhold mellom mengde materiale som blir polert bort og trykket for både silika og aluminiumoksid. Mens det er nesten ingen relasjon mellom materiale som blir polert bort og baksidetrykket, ser det ut som det er en trend med økende standardavvik for overflateruheten når baksidetrykker øker for både silika og aluminiumoksid. For å finne ut om det er en nærmere sammenheng mellom de ulike parameterne, overflateruhet, materiale som blir polert bort og standardavvik for overflateruheten, bør en større prøvestørrelse undersøkes.

Contents

List of Figures

List of Tables

Abbreviations

ALD	Atomic Layer Deposition
ALE	Atomic Layer Epitaxy
AMR	Amount of Material Removed
A-Si	Amorphous Silicon
BP	Backside Pressure
CARs	Chemically Amplified Resists
CVD	Chemical Vapor Deposition
CMP	Chemical Mechanical Polishing
DI-water	Deionized Water
DMD	Digital Micromirror Device
DOF	Depth of Focus
DUV	Deep Ultraviolet
EUV	Extreme Ultraviolet
GPC	Growth Per Cycle
GR	Growth Rate
ICs	Integrated Circuits
IPA	Isopropanol
LCVD	Laser Chemical Vapor Deposition
LER	Line Edge Roughness
MBE	Molecule Beam Epitaxy
MBEBL	Multi Beam Electron Beam Lithography
MEMS	Micro-electro-mechanical Systems
MMR	Mean Material Removed
MRR	Material Removal Rate
MSE	Mean Square Error
NA	Numerical Aperture
NIL	Nanoimprint Lithography
Non-CA	Nonchemically Amplified
OM	Optical Microscope

OPT	Oxford Plasma Technology
PEB	Post Exposure Bake
PECVD	Plasma Enhanced Chemical Vapor Deposition
PPM	Parts Per Million
PR	Photoresist
PVD	Physical Vapor Deposition
RF	Radio Frequency
RIE	Reactive Ion Etching
RR	Removal Rate
SEM	Scanning Electron Microscopy
TEM	Transmission Electron Microscopy
TMA	Trimethylaluminum
UV	Ultraviolet
WP	Working Pressure

1 Introduction

After being valid in the electronic industry for about 50 years, Moore's law is coming to an end. Now it is necessary to find a method that can make electronic devices faster, smaller, and more affordable. Knoops *et al.* [1] especially emphasized three metrics. The need for thickness control, uniformity and conformality, and the ability to deposit high-quality materials at low substrate temperatures. Bottom-up approaches, like atomic layer deposition (ALD) and plasma enhanced vapor deposition (PECVD), are some of the most precise methods, which can meet all these requirements [2]. With ALD and PECVD, it is possible to build the material atom-by-atom with thickness in the nanometer range, especially suited for microelectronic applications. Future devices in the electronics industry will rely on methods that can make films in nanometer size and free-standing 3D structures.

One of the main applications for the free-standing membrane is in micro-electro-mechanical systems (MEMS) based sensors and electronic devices with tremendous industrial implications. Winterkorn *et al*. [3] made a sandbox that can be used in MEMS devices, as can be seen in Figure 1.1. By a combination of ALD, PECVD, chemical mechanical polishing (CMP), lithography, and standard technologies in MEMS processing, it is possible to create almost anything. Unlike ALD and PECVD, CMP is a top-down method where layers are removed in the nanometer range. One can use CMP to achieve a homogeneous surface after the deposition of layers by either ALD, PECVD, lithography, or other MEMS processes [3]. Consequently, this method can be utilized to successfully make free-standing 3D structures and to control features down to nanometer precision.

Standard lithography is commonly used to make patterns on a chip. It is desired to know the etch rate of different materials to get the desired thickness. This will be used in combination with ALD, PECVD, and CMP to make a tunnel chip that can be used as a holder-chip in transmission electron microscopy (TEM). The CMP is not yet fully understood, and this paper will focus on how the CMP machine works and how it is possible to change some of the parameters to get the desired thickness. By changing the parameters, one at a time, one can investigate how they will affect the result. The parameters that have the highest effect and that will be tested in this paper are the slurry concentration, step duration, backside pressure, and working pressure. This paper aims to map the CMP machine and see how the different parameters change the homogeneity and removal rate of amorphous silicon (a-Si), alumina (Al_2O_3), and silica (SiO_2) on the wafer's surface. Since a-Si will be deposited on top of alumina in the holder-chip, it is desired to know how to influence the

adhesion between the two layers. Different thickness layer, temperatures, and a small layer of silica (SiO_2) are tested as solutions to achieve good adhesion between the two layers.

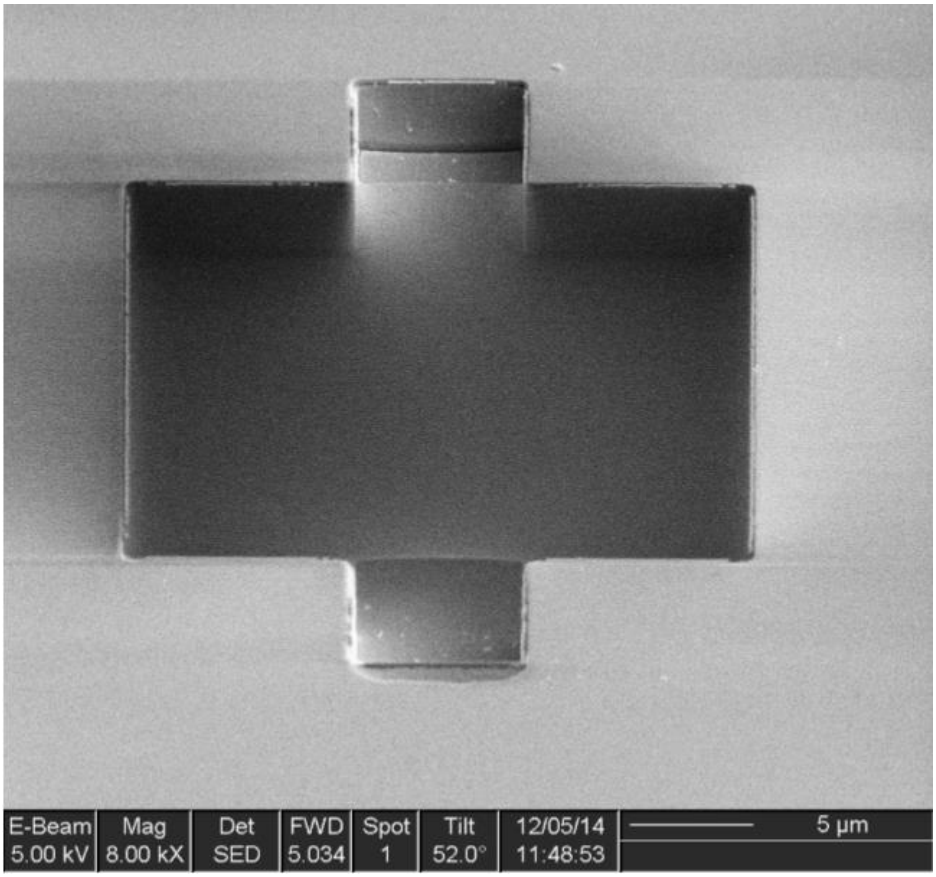

Figure 1.1: SEM characterization of a sandbox which can be used in MEMS devices [3]

2 Theory

The necessary theory required for understanding the procedures used for producing a microreactor for in-situ deposition characterization and optimizing the chemical mechanical polishing (CMP) is presented in this chapter. A lot of the theory is taken from the project work (TMM4560) written during autumn 2019.

2.1 Substrate Cleaning Procedure

Plasma cleaning is a commonly used method for cleaning wafers, and almost every material can be cleaned by the Plasma Cleaner (1450) at NanoLab shown in Figure 2.2. It is designed to accommodate both 2- and 4-inch wafers, but also tweezers, specimen clamping ring, and anything that can fit into the chamber can be cleaned by the plasma cleaner [4]. It is normal to use a plasma cleaner to remove unwanted artifacts from the top of the sample and minimize surface contamination [5][6], especially the samples that are prepared for scanning electron microscopy (SEM) or TEM [7]. The plasma cleaner cleans by bombarding the surface with ions and ionized gas, which is called plasma and is performed in low pressure. Ultraviolet (UV) radiation breaks down the long-chain complex carbon compounds, removing all the organic materials from the surface, and oxygen makes the surface hydrophilic. The plasma cleaner at NanoLab has a maximum generator frequency of 40 kHz and a maximum flow rate of 200 sccm [8]. It is possible to choose either argon, oxygen, or both in percent of the maximum value. The byproducts, such as carbon dioxide (CO_2) and water (H_2O), will be pumped out of the cleaner by the vacuum system [5]. A schematic view of a plasma cleaner system can be seen in Figure 2.1 [6].

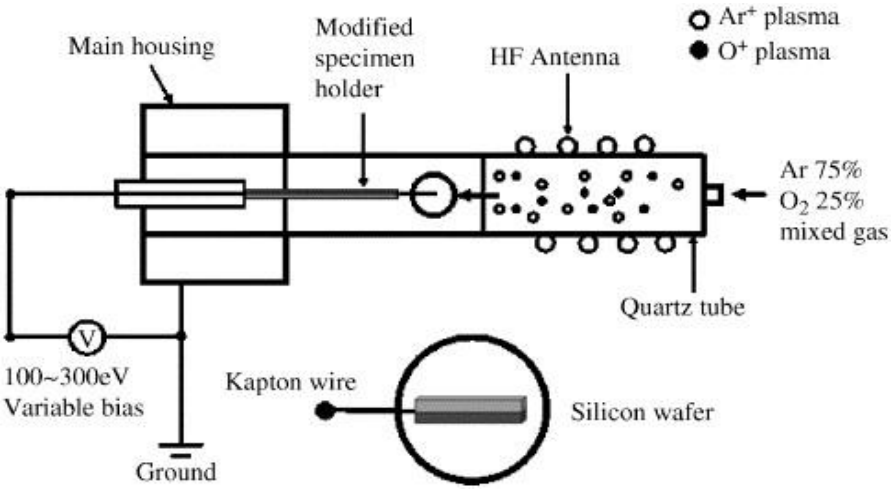

Figure 2.1: Schematic view of the plasma etching system [6]

Plasma cleaning is one of the most used methods as a pretreatment before any other treatment is done to the wafers, mostly because it does not affect the bulk material [9]. Argon and oxygen are commonly used together to clean both metallic and non-metallic materials [10]. Argon is used because it is cheap, it prevents oxidation, and it also has wide availability. Argon will not etch the surface and will remove any traces of organic matter. It also has small ionization energy and high ionization efficiency [11]. Oxygen is also cheap and has wide availability. Oxygen plasma removes organic matter and cleans the surface prior to bonding. Oxygen plasma is highly effective in removing hydrocarbons [4]. It is mostly used on non-metallic materials unless it is used in combination with argon. The difference between argon and oxygen is that oxygen etches the surface, while argon does not. Oxygen also has the capability of surface modification.

Figure 2.2: The plasma cleaner at NanoLab

2.2 Chemical Vapor Deposition (CVD)

The deposition of thin layers or films has been intensively studied for a long time, and many methods have been developed [2]. The two main methods are vapor phase deposition and liquid-based growth. Vapor phase deposition includes chemical vapor deposition (CVD), where a solid material is deposited from vapor by a chemical reaction, normally on a heated substrate [12]. There are many different CVD processes, but all are based on a reaction between the surface of the substrate and the vapor, where a thin film is formed. By varying the conditions like the composition of the reaction gas mixture and the temperature, it is possible to produce a coating with a uniform thickness on a substrate. The resulting layers have low porosity and can be deposited with high uniformity on complex shapes, such as carbon nanotubes [13]. As Carlsson *et al.* state [12], the reaction mechanism in every CVD process is complicated but always leads to a solid material and a gaseous byproduct. A new method called laser chemical vapor deposition (LCVD) uses a laser to deposit porous materials. It is a new approach, but it is still not clear how the growth mechanism in the LCVD works [14].

2.2.1 The CVD Process

S.M. George [15] explains that CVD reactions are based on binary reactions, as can be seen in the equations below.

$$\boldsymbol{A + B \rightarrow Product} \tag{2.1}$$

$$\boldsymbol{AX(g) \rightarrow A(s) + X(g)} \tag{2.2}$$

It can be seen in Figure 2.3 [12], that a gas mixture is going in from the inlet, passes over the surface of the material, molecules or atoms are being adsorbed, resulting in a solid layer on the surface. At the same time, gaseous byproducts are removed through the exhaust. Since there are a lot of different CVD machines and methods, every reaction is unique. But most depositions include chemical reactions, evaporations, adsorption, and desorption, and most processes are done in a vacuum [2], or ultra-high vacuum [16].

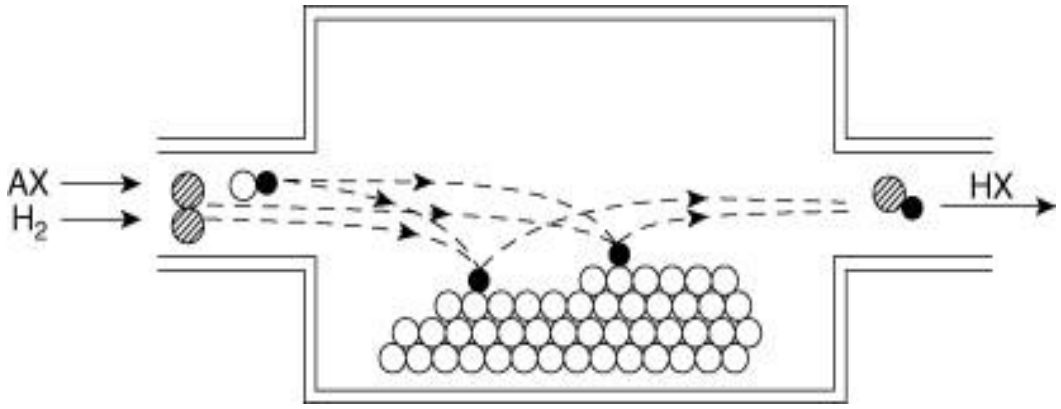

Figure 2.3: Illustration of how CVD works in the chamber [12]

By changing different conditions such as temperature, pressure, and reaction gas, it is possible to deposit many different materials. When using plasma to promote chemical reactions, it is called plasma enhanced chemical vapor deposition (PECVD), which will be discussed in the next section. CVD offers many possibilities to deposit different layers and has given birth to many other methods. For instance, a "very high frequency PECVD" technique which is a compatible PECVD technique [17][18].

2.3 Plasma Enhanced Chemical Vapor Deposition (PECVD)

PECVD is a CVD method where radio frequency (RF) energized electrode is used. Using PECVD, a variety of different thin films can be deposited on a substrate. During a PECVD process, plasma is sustained in the chamber where many simultaneous CVD reactions are occurring. Normally the PECVD operates at very low temperatures compared to many other CVD methods [19]. The layer is formed by microwaves at a frequency of around 2.45 GHz. The microwave energy is related to the natural resonant frequency of the plasma electrons, often in the presence of a static magnetic field [2]. The PECVD instrument at NanoLab operates at around 0.5-2 Torr pressure. The PECVD chamber has two electrodes, one for gas inlet and one for exhaust. The sample stage in the machine is heated up to a maximum of 700℃. The disadvantage of a single-chamber system PECVD, shown in Figure 2.4, is that each sample may take a long time to make since several purge and pump-down steps are needed [18], but the PECVD is famous for making excellent uniform layers on substrates [20].

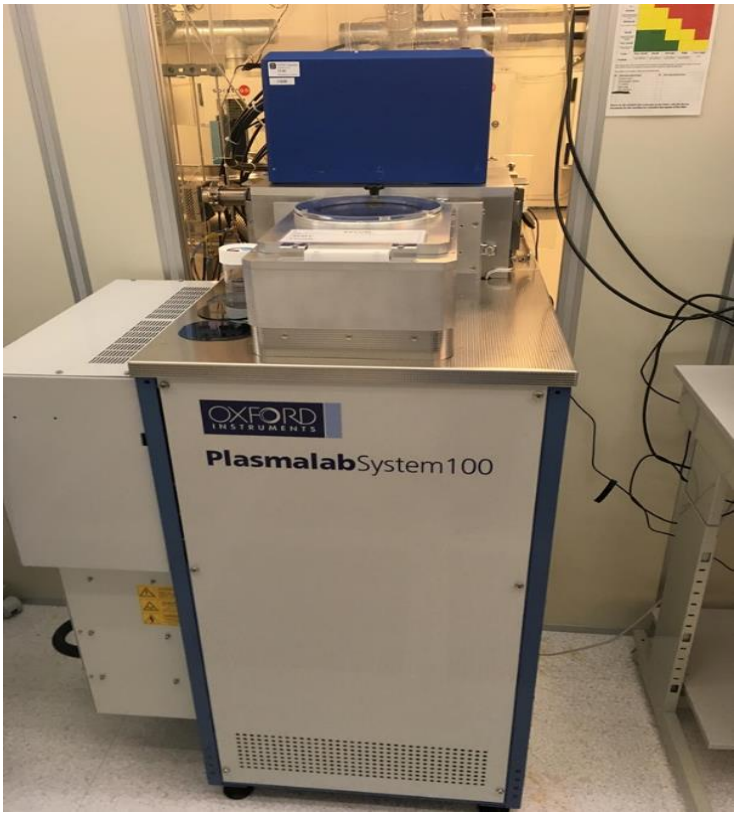

Figure 2.4: The single-chamber system, PECVD machine at NanoLab

2.3.1 Silica Deposition in PECVD

Most of the earlier research refers to the production of silica (SiO_2) when they talk about PECVD. This is due to the low cost, low optical loss properties, and high efficiency of the

silica deposition [21]. In the semiconductor industry, silica is widely used as a masking material to insulate active circuits, but as Subhash *et al.* [22] explain the properties of silica change drastically with the thickness of the layer. Silica is produced by pure SiH_4 and O_2 in a planar plasma reactor [23]. The thickness of the produced coating has a very high uniformity. The oxidation reaction that produces the silica layer can be seen in the equation below [2].

$$\boldsymbol{SiH_4\,(g) + O_2\,(g) = SiO_2\,(s) + 2H_2\,(g)} \quad \textbf{(2.3)}$$

2.3.2 Amorphous Silicon Deposition in PECVD

Amorphous silicon, often called a-Si, is the non-crystalline form of silicon used for many different applications, such as making silicon solar cells, image sensors, or electrophotography, and has received extensive research [24]. A-Si is also often used as a masking layer due to its resistance to hydrofluoric acid solutions [25] and is a cheap material expected to be used widely in components for new electronics [26]. Compared to silica, the a-Si changes its properties drastically when varying the thermal diffusion parameters, like time and deposition temperature in the PECVD. This is due to different passivating contacts when the temperature changes. Chen *et al.* [27] have studied which properties the a-Si film got after being manufactured at different temperatures. They observed that the density of defects, microcavities, crystallinity, and hydrogen concentration changes significantly, and a higher temperature yields more energy for crystallization. Silane (SiH_4) is used to produce a-Si, and the reaction that produces the a-Si layer can be seen in the equation below [27].

$$\boldsymbol{SiH_4\,(g) = Si\,(s) + 2H_2\,(g)} \quad \textbf{(2.4)}$$

The deposition process, which makes the a-Si, is very complicated. The plasma's physical and chemical interaction is dependent on the deposition surface, the power and frequency, the substrate temperature, the gas flow, and much more [18]. The standard deposition temperature for a-Si is 250℃, but researchers have tried temperatures down to 25℃, and up to above 300℃ [26]. J.P Conde *et al.* [26] state that by lowering the deposition temperature, significant hydrogen dilution is required to get adequate transport properties (95% hydrogen dilution when the deposition temperature is at 100℃). The deposition rate and the defect density drastically change when the deposition temperature changes. It is also shown that there will be fewer defects if the film thickness increases [24]. Y. Q. Fu *et al.* [28] state that by increasing the molecular hydrogen in the reaction, the hydrogen ion

will cause the formation of microvoids or form gas bubbles, increasing the mechanical stress value in the film. They suggest producing a-Si for micro-electro-mechanical systems (MEMS) devices with pure SiH_4 at a low plasma power with a high hydrogen dilution ratio due to low stress and smoothness of the films.

A-Si films can be deposited on various substrates, but it is preferred to be deposited on silicon or oxide substrate because it will have better adhesion and will not crack or peel off. It is normal to get hillocks when a-Si is deposited on crystalline substrates. As can be seen in Figure 2.5 [29], there are no hillocks and a smooth surface in (a) because the a-Si was deposited on oxide/Si substrate, while in (b), there are many hillocks because a-Si is deposited on a crystalline Si substrate.

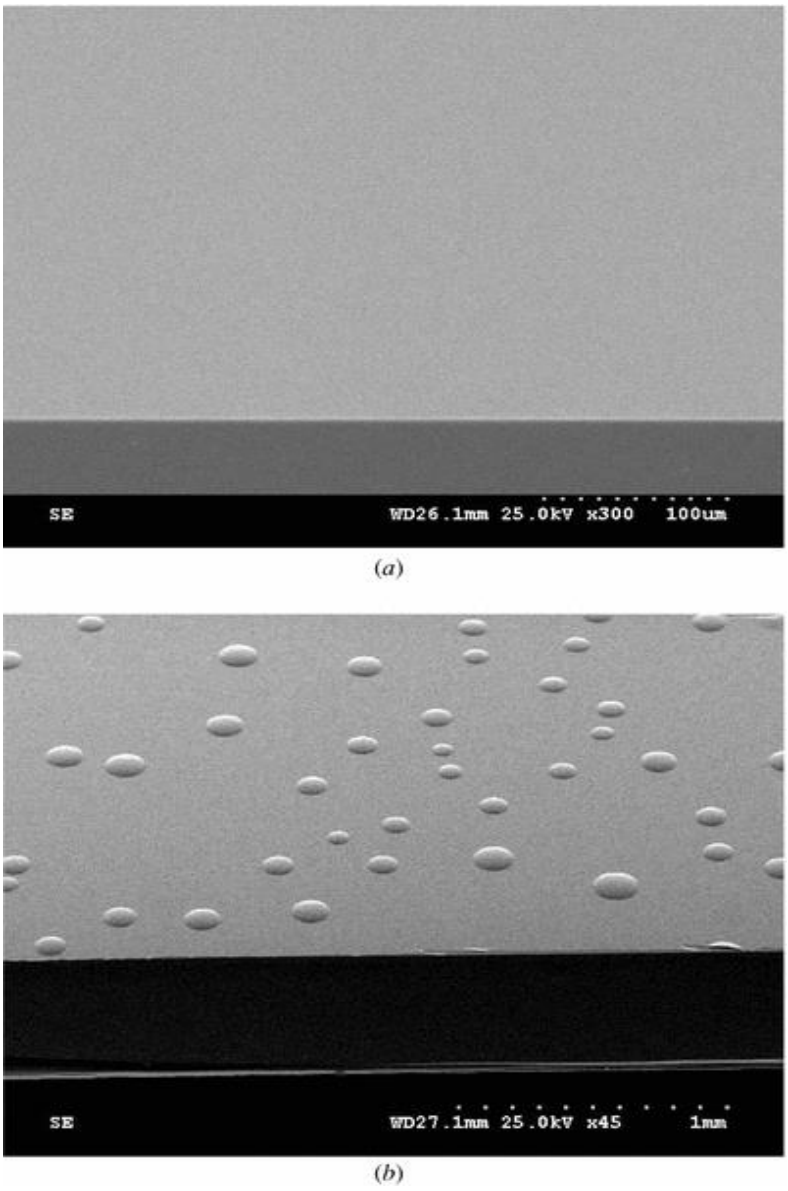

Figure 2.5: SEM picture of a-Si on (a) oxide substrate and (b) crystalline substrate [29]

2.4 Atomic Layer Deposition (ALD)

Already in the 1970s, atomic layer epitaxy (ALE) was a technique used to deposit one atomic layer at a time. ALE was a success, allowing both crystalline and polycrystalline materials to be deposited, but as Knoops *et al.* [1] state, it did not take a long time before other traditional methods like molecular beam epitaxy (MBE) outperformed ALE. Between the late 90s and the beginning of the 2000s, the silicon-based microelectronics industry expanded. With the ongoing trend toward making electronic devices smaller, a better method than ALE was needed. Atomic layer deposition (ALD), which uses a bottom-up approach, promised a better chance of obtaining a more homogeneous structure [2]. ALD has been an important mechanism to deposit different layers in almost all electronic applications. Now it is possible to deposit everything from perovskites [30], metal oxides, sulfides [31], nitrides, carbides, and pure elements [32]. The ALD machine at NanoLab is shown in Figure 2.6.

Figure 2.6: The ALD machine at NanoLab

Using ALD, film growth happens in a self-limiting fashion where each cycle leaves an atomic layer, thus leading to the main advantages of highly conformal layers on complex shapes with thicknesses of just a few nanometers. No other mechanism can achieve this accuracy. ALD uses a technology which has driven the down-scaling of silicon electronics over the last decades, managing to increase computer processing power and lower power consumption [33]. ALD has a wide variety of applications, such as fuel cells, batteries, solar panels, and membranes [32].

2.4.1 The ALD Process

ALD is very closely related to CVD [15]. While CVD uses binary reactions, the A and B reactions do not happen simultaneously in ALD. ALD has two or more precursor gases that are utilized in alternating pulses. Both CVD and ALD use vapor precursors to make a film and are based on thermo-chemical processes. However, ALD is mainly a surface chemistry process which changes the surface chemistry, and not a gas phase reaction like CVD [33]. ALD is based on cycles, which involve four steps, illustrated in Figure 2.7 [1]. In each cycle, a sub-monolayer of material is deposited, which yields a perfect conformality, and trench-fill capability [20].

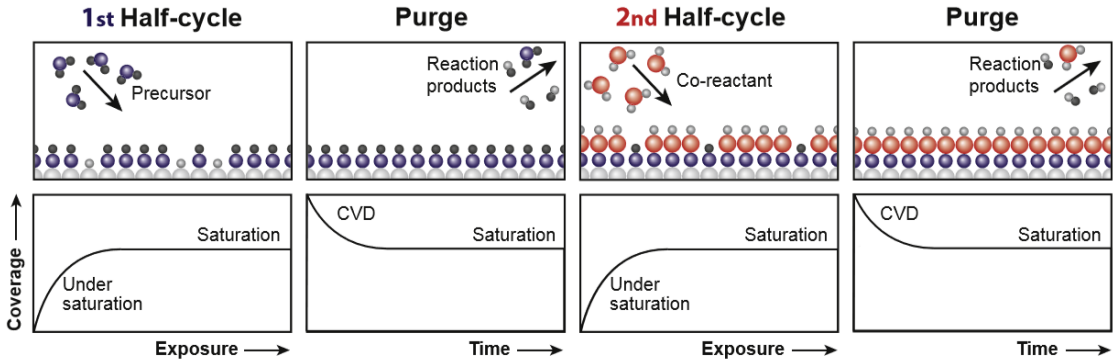

Figure 2.7: Illustration of how the ALD process works [1]

In the first step, a pulse of a precursor is introduced into the chamber. It reacts with the surface of the substrate, for example, on a wafer. The precursor is often an inorganic material. The second step is a purge or pump step, where the unreacted precursor gas and byproduct are removed, often by an inert gas, usually Nitrogen (N_2) or Argon (Ar). The third step involves co-reactants. The second precursor often involves small molecules that react with the adsorbed molecules. The fourth and final step is also a purge or pump step. After these four steps, one cycle is completed, and one sub-monolayer of the desired material is deposited on the surface of the substrate. Then everything can be repeated to get the desired layer thickness. A significant limitation of the ALD is the time consumption since each cycle consists of four consecutive steps [1].

2.4.2 Alumina Produced in ALD

One of the most common materials in ALD is crystalline alumina (Al_2O_3) [15]. Alumina has been used as a model for other methods because it is very efficient and self-limiting. Alumina can be produced both at higher and lower temperatures. However, it is also shown that growth per cycle (GPC) does not change much when produced at room temperature [34]. ALD with alumina is very conformal and has a minimal surface roughness. The earliest

method used trimethylaluminum (TMA) and water (H_2O) to form alumina on the wafers. Now it is more common to use TMA and ozone (O_3) [15].

As Steven M. George [15] shows, the surface chemistry during ALD with alumina can be described with the following equations, where the last reaction is the overall reaction.

$$\boldsymbol{AlOH + Al(CH_3)_3 \rightarrow AlOAl(CH_3)_2 + CH_4} \quad \textbf{(2.5)}$$

$$\boldsymbol{AlCH_3 + H_2O \rightarrow AlOH + CH_4} \quad \textbf{(2.6)}$$

$$\boldsymbol{2Al(CH_3)_3 + 3H_2O \rightarrow Al_2O_3 + 3CH_4} \quad \textbf{(2.7)}$$

Compared to many other materials, which can be deposited during ALD, alumina has a very high reaction enthalpy. This makes the formation of the alumina very efficient. Repeating the reactions for many cycles shows that the growth rate of alumina is very linear. The thickness of the highly homogeneous film can be measured using different characterization methods. One cycle gives around 1 Å thickness of alumina. It is shown that the GPC decreases at temperatures between 177℃ and 300℃, caused by the loss of aluminum hydroxide (AlOH) and TMA ($AlCH_3$) at higher temperatures [15].

2.5 Chemical Mechanical Polishing (CMP)

The concept of chemical mechanical planarization was invented already in the 1980s, by Klaus D. Beyer [35]. Chemical mechanical polisher (CMP) is one of the best methods to get a smooth and even surface and is a common technique used in the semiconductor [3], and fabrication process of the integrated circuit (IC) industry [36]. Depending on the slurry, pH, grain size, head speed and material, it is possible to get an even surface at the nano level. Unlike ALD and PECVD, which are bottom-up approaches, CMP uses a top-down approach, which means that a surface that is rough and non-uniform can be polished down to a desired homogeneous thickness. When making semiconductors and other MEMS devices, the size and the homogeneity at the nano-level are essential. As A.P. Malshe *et al.* [37] state, polishing and planarization techniques are essential aspects to succeed in getting a material with a uniformed thickness, which can adversely affect its application. Several approaches can be used to achieve a desired thickness of the sample, but many end up with a macro-roughness, which is not desirable [38]. Previous work has used CMP to planarize different substrates, including metals [39], polymers [40], and composites [41]. CMP has advantages because it succeeds in making the surface ultra-smooth with very low damage, few defects, high efficiency, and at a low cost [38][42]. It can also be used on many types of surfaces and even multi-material surfaces [38]. The only disadvantage using CMP is the difficulty to know when the desired amount of material is removed or when the right degree of planarization has been reached.

2.5.1 The CMP Process

CMP uses both mechanical and chemical mechanisms to polish the surface. During the process, the wafer is sliding and rotated in the opposite direction of the pad, while being pressed face-down covered in a slurry with a specific chemical composition. The slurry is between the sample surface and the pad [38]. The CMP is controlled by robotics and software to get exceptional performance. As Jianfeng Luo *et al.* [43] state, the removal rate (RR) depends on both the mechanical and the chemical reactions, but most analyses look separately at the different effects. For example, for metals, the polishing mechanism is most related to the passivation, slurry viscosity, and electron chemical interaction [44]. In Figure 2.8, which is taken from Zhu Honglin *et al.* [45], it is possible to see how the CMP works and some of the different variables that can be changed. There are three main players in the process: the surface to be polished, the pad, and the slurry [38].

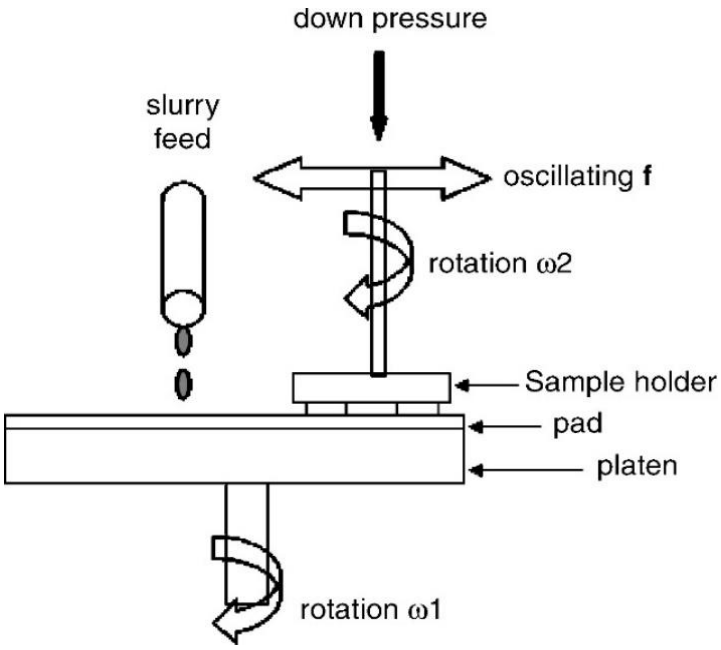

Figure 2.8: Schematic view of the CMP setup [45]

2.5.2 Influence of Input Parameters on Material Removal Rate (MRR)

Mechanical polishing happens due to friction between the wafer and the pad and depends on the material of the pad and the particle percentage in the slurry. Polishing pads can be divided into hard and soft pads, and the pad's hardness will vary as the pad is used [46]. The mechanical interaction between the pad and the wafer has been studied for some time. Researchers have also been looking at the effect of the slurry and its pH [47], pressure [48], head velocity [49], friction force [42], lubrication [50], different pad surfaces [51], and the wafer geometry [52]. It is necessary to understand several chemical and mechanical phenomena to design and develop the CMP [36]. Aspects such as surface kinetics, electrochemical interfaces, hydrodynamics, and so on, are important [35]. Nevertheless, the CMP needs further investigation.

CMP will have two different contact modes. A hydro-dynamical contact mode and a solid-solid mode. As Luo Jianfeng *et al.* [43] explain, there will be a thin fluid film between the wafer and the pad when the applied down pressure is small, and the velocity is high. They are looking at the abrasive particle (nanoscale) compared to the slurry film (microscale), and they state that a lot of the abrasive particles will be inactive. When looking at the chemistry behind the CMP, it is hard to predict the number of particles (active) that affect the RR. As can be seen in Figure 2.9 [53], the polishing pad's roughness will influence the different contact modes during CMP, as the pad's surface is much rougher than the wafer.

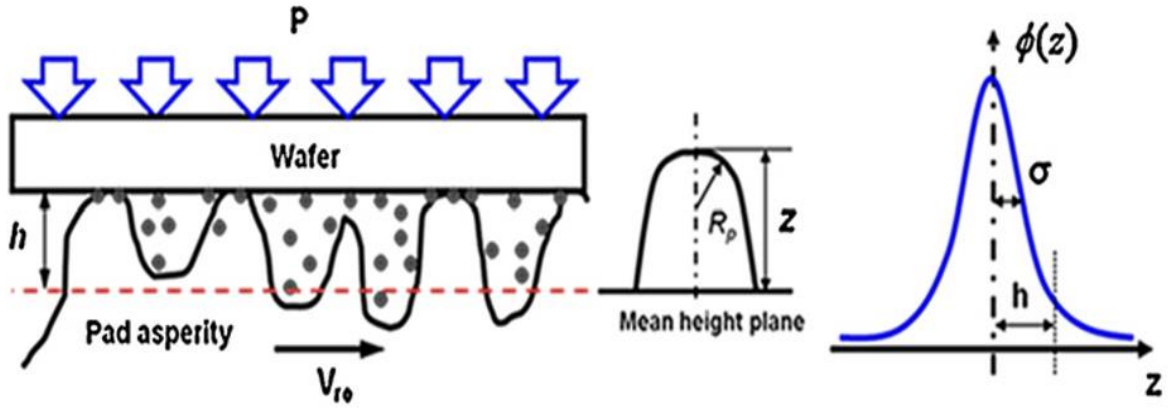

Figure 2.9: Schematic view of the rough pad used in CMP [53]

The chemical polishing is dependent on the slurry and its pH and viscosity, and different slurry systems have been invented [54]. But as M.M Winterkorn *et al.* [3] confirm, the uniformity after CMP is highly dependent on the material which is being polished. What can be seen in Table 2.1 [3] below is that the uniformity is much better for poly-Si compared to alumina and that the polishing rate is much higher for poly-Si compared to alumina.

Table 2.1: Polishing rate and uniformity of poly-Si and alumina after CMP [3]

Material	Poly-Si	Alumina
Polishing rate [nm/s]	3.2-3.8	1.3
Uniformity [%]	2.6	20

Zhang and Busnaina [43] have tried to modify Preston's equation (2.8) for material removal rate (MRR) with CMP because Preston's RR is dependent on many more factors than just the pressure and velocity. Here the P_0 is the downward pressure, V is the relative velocity of the wafer, and K_p is a constant representing the remaining parameters. The revised equation has an additional term, the initial material removal rate $MRR_{initial}$.

Jianfeng Luo *et al.* [43] gives the three following equations. The first is Preston's equation, and the two others are revised from Preston's equation.

$$\boldsymbol{MRR = K_p P_0 V} \quad \textbf{(2.8)}$$

$$\boldsymbol{MRR = K_p P_0 V + MRR_{initial}} \quad \textbf{(2.9)}$$

$$\boldsymbol{MRR = K_p \sqrt{P_0 V}} \quad \textbf{(2.10)}$$

The third equation is taking the normal stress and shear into account. The problem is that all these equations are very rough and not very robust. It is desired to have an equation that gives a linear relationship between the RR and the different parameters. But as Jianfeng Luo *et al.* [43] conclude, it is only possible to have a linear relationship if the pad is much harder than the material being polished. In CMP, it is normal to have a polishing pad made of polymers that are much softer than most other materials. They finally give the following equations that should yield more realistic behavior than the three above:

$$\boldsymbol{MRR_{thickness} = C_4\left(1 - \varphi\left[3 - C_5 P_0^{\frac{1}{6}}\right]\right) V P_0^{\frac{1}{3}}} \quad \textbf{(2.11)}$$

$$\boldsymbol{MRR = \rho_w N Vol_{removed}} \quad \textbf{(2.12)}$$

In the equations ρ_w is the density of water, N is the number of active abrasives, Vol_{removed} is the volume of the material, which was removed by a single abrasive, φ is the probability density function, and C_4 and C_5 are two parameters independent of pressure and velocity. Earlier studies have shown that the size distribution of the particles of the slurry will satisfy a normal distribution φ and that the particles will be spherical [53]. The equations take more parameters into account, for example, wafer- and pad hardness, and the size of the abrasive particles in the slurry. However, the size of particles in the slurry will change during the polishing, as can be seen in Figure 2.10 [44]. This can make the calculation of the MRR very complicated. On the other hand, the equation is still lacking the impact of the slurry flow rate (volume/time), which will affect the MRR [36]. They conclude that the MRR is nonlinear, and that the roughness has a significant influence on the MRR.

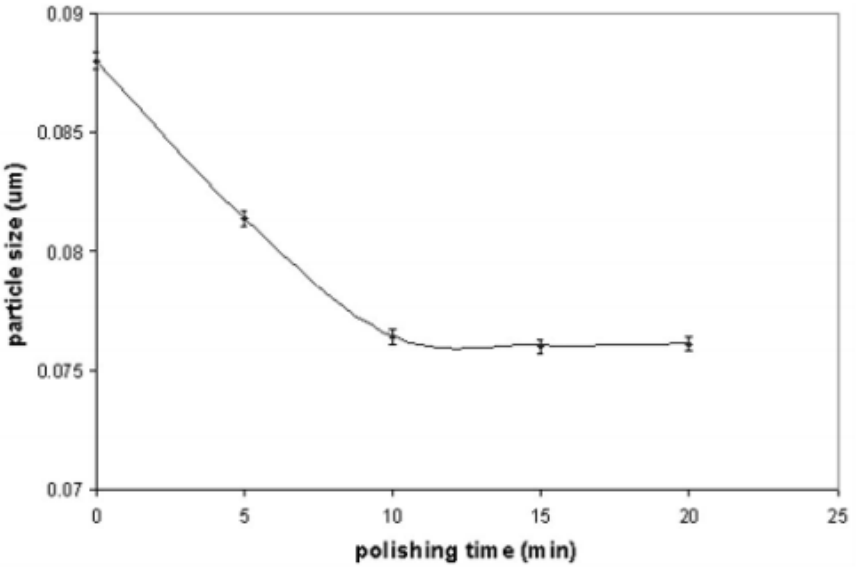

Figure 2.10: Changes in the particle size of the slurry during the CMP time [44]

As mentioned, the MRR is strongly dependent on which material is being polished. The slurry will be chosen depending on the material. As Neville *et al.* [55] state, materials such as silica and alumina will use a slurry which is either acidic or basic. For example, a silica-based slurry can be in a potassium hydroxide solution. B. Mullany and G. Byrne [54] state that it is not only the pH of the slurry that will affect the MRR. A higher friction value associated with a lower viscosity of the slurry yields a higher MRR. Zhu *et al.* [45] tried to see if the RR is dependent on the different crystal orientations. Pre-polished samples of sapphire (Al_2O_3) were used, and the results showed that some orientations have a different RR.

2.5.3 Planarization in Different Applications

As Krishnan *et al.* [35] state, CMP will experience difficulties when the sample has variational pattern density. Trench etches will affect the wall slope and the variation in the oxide and nitride thickness across the wafer. They also headlight that the dishing, erosion, and pattern density will contribute in giving the sample a non-uniform surface. Since the polishing rate is dependent on the surface of the sample, it strongly affects the homogeneity after CMP. Different approaches have been used to try to solve this problem. For example, Davari *et al.* [56] have looked at how it is possible to make a planarization technique that combines reactive ion etching (RIE) and CMP. He manages this by masking and etching to remove the high-density material before CMP. Others have solved the problem by filling up the structure to eliminate the pattern density differences.

On the other hand, hardness, roughness, compressibility, and porosity of the pad will have a significant effect on how the slurry will react with the sample and the slurry transport [57]. Even though the sample is very homogenous after masking and etching, there are still problems resulting from the different pad surfaces. So only parts of the wafer will experience solid-solid interaction due to roughness on the pad's surface, and it will determine how the slurry will travel under the wafer. Different pads will also affect the result and the quality and have a considerable effect on the RR [46].

2.5.4 CMP with Silica

Most studies of silica (SiO_2) are understood via glass polishing, and the main responsible mechanism for removing the silica layer is due to mechanical abrasion and hydration due to an alkaline slurry [53]. Some claim that brittle materials like silicon will etch due to micro-fracture. The CMP will make very small depths of cut (less than 1 μm), and therefore, silicon can be seen as a ductile material [43]. The size of the particles in the slurry will be bigger than the particles that will be removed. Jianfeng Luo *et al.* [43] claim that the assumption of plastic deformation over the whole particle-wafer interface is reasonable. Many researchers have also tried to eliminate the mechanical scratches caused by slurry particles. Therefore, different polishing slurries have been developed [58].

Figure 2.11, taken from Jianfeng Luo *et al.* [43], shows how the MRR is changing with different slurries. Slurry 1 is with an alkaline/cerium-oxide slurry, and slurry 2 is with a conventional alkaline/silica slurry. They aimed to show that their equations are related to

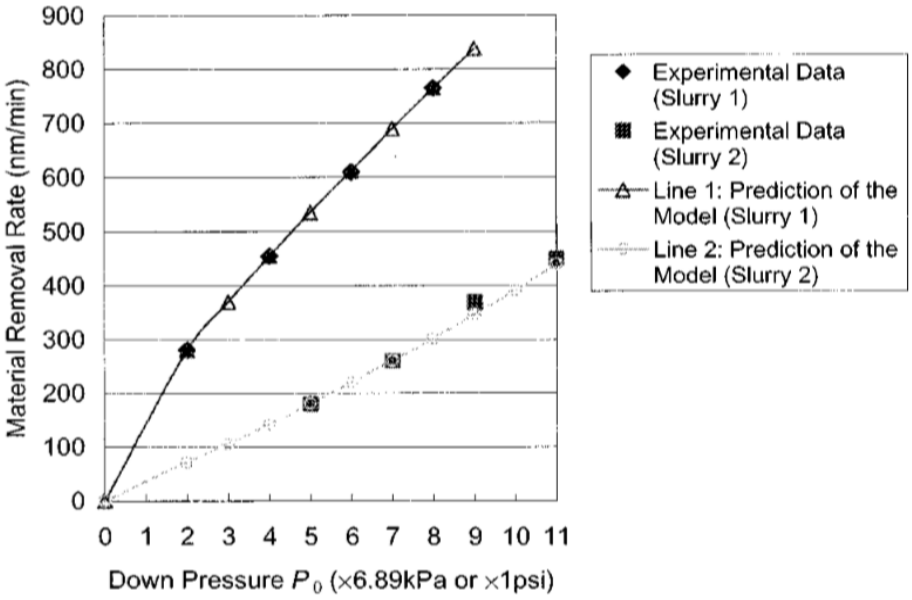

Figure 2.11: MRR versus down pressure with two different slurries [43]

reality, and they state that the results indicate that. Slurry 1 has a higher MRR than slurry 2, and a higher down pressure yields higher MRR.

H.S. Lee *et al.* [53] have also looked at how different slurries will influence the RR on silica wafers. Four types of slurries have been tried. The difference between the slurries was the mean size of the particles (nm). All wafers were polished for 1 minute before they were measured by a reflectometer. As seen in Figure 2.12 [53], the graph shows that there is a relation between the size of the particles and the MRR. The MRR is increased when the particle size is between 13 nm to 61 nm, but from 61 to 118 nm there is a small decrease.

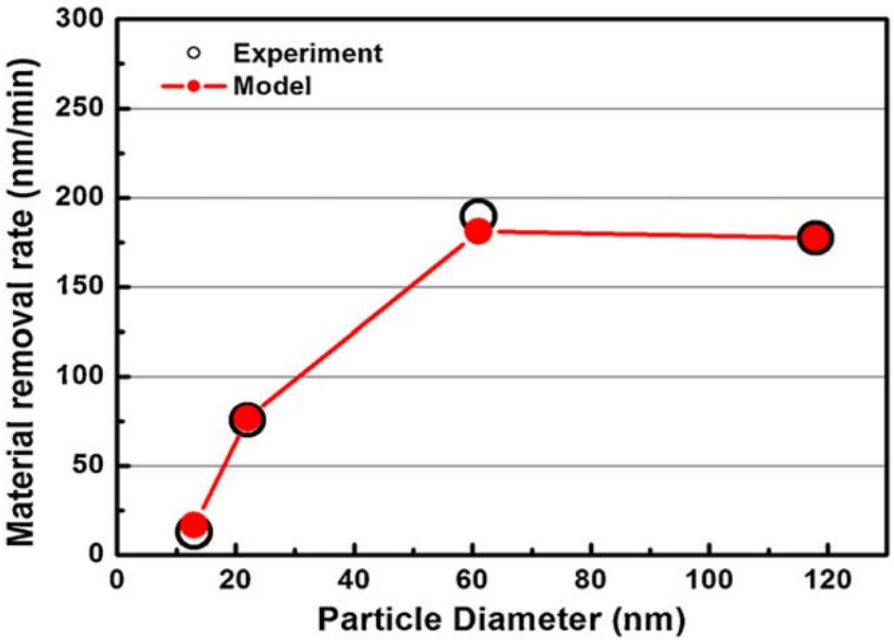

Figure 2.12: Average MRR as a function of average particle size [53]

In Figure 2.13, H.S. Lee *et al.* [53] show that there is a correlation between the particle concentration and the MRR. For silica, the MRR will increase with increasing particle concentration. It is hard to tell if the function is linear or not, but the experimental value is similar to what they have modeled and expected. They have also looked at the uniformity of the wafer after CMP. They conclude that the MRR will be uniform in the center of the wafer, but that the edges will first reduce, then increase in MRR. This can be due to uneven slurry flow and normal contact stress distribution, as seen in Figure 2.14 [53]. This phenomenon is known as the edge ring effect and often occurs after CMP [46].

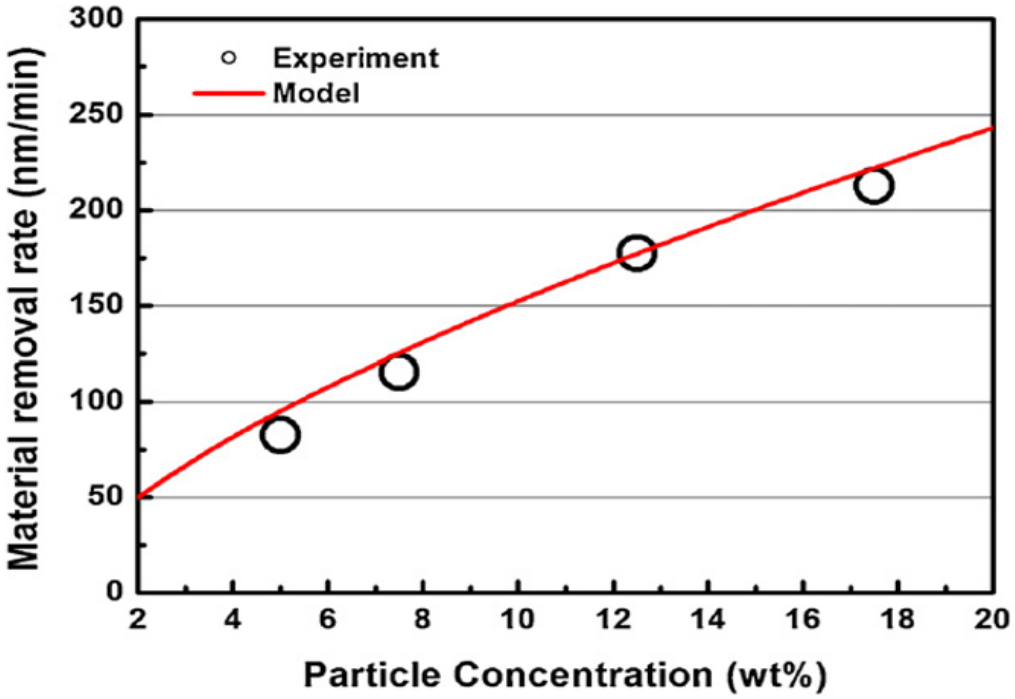

Figure 2.13: Average MRR as a function of particle concentration [53]

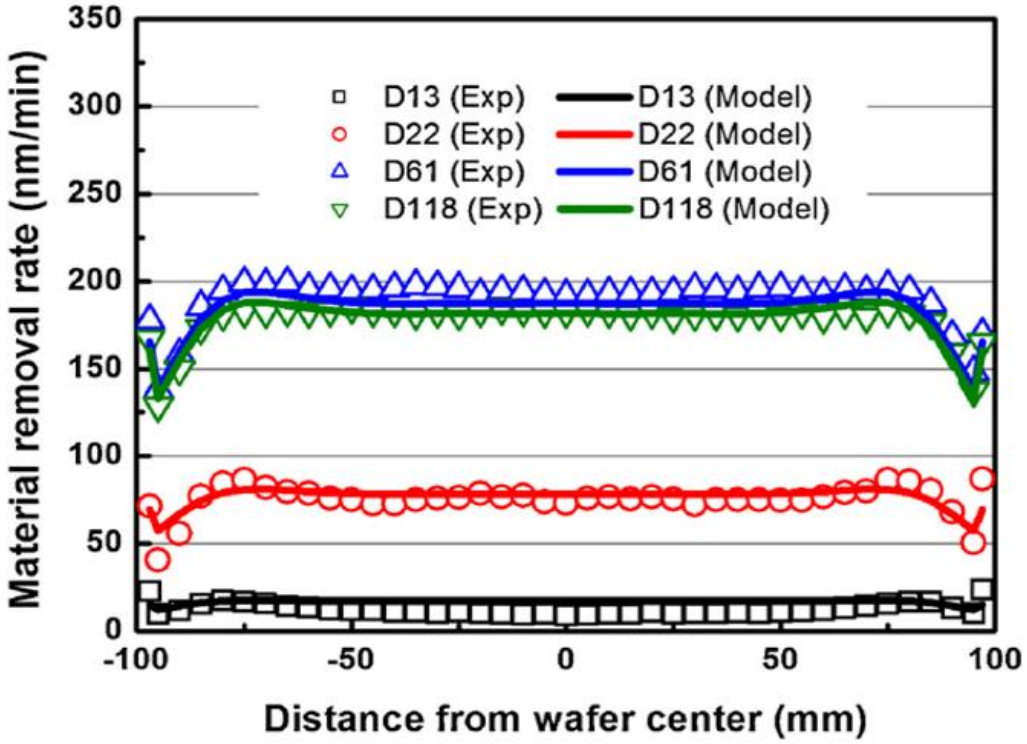

Figure 2.14: MRR distribution for various particle diameters [53]

As stated, the pH affects the MRR. As seen in Figure 2.15 [39], there is a small difference when the pH is between 0 and 9, but when the pH increases further, the solubility of the silica reaches 1000 PPM.

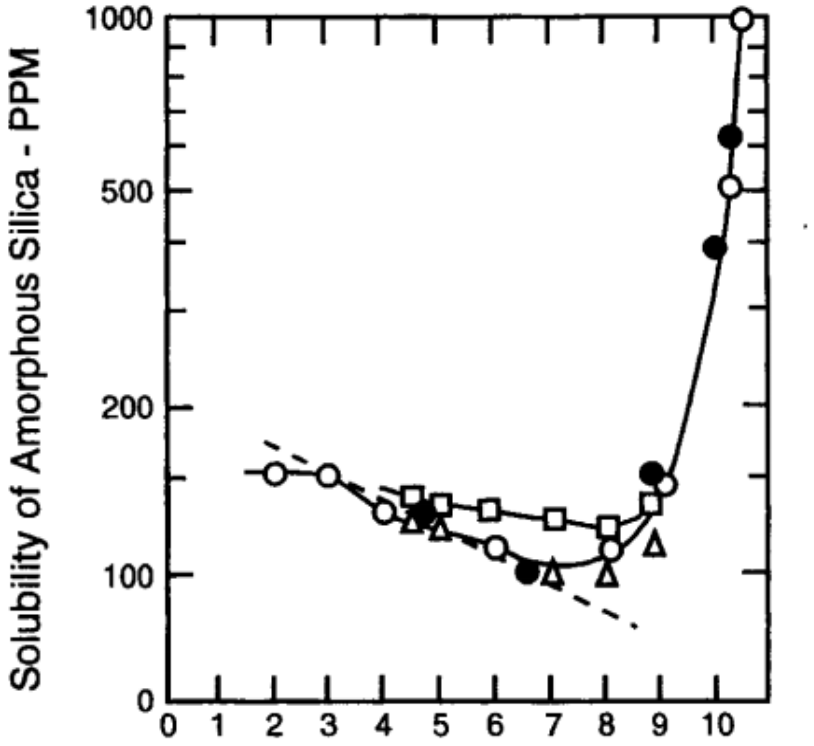

Figure 2.15: The solubility of silica vs. pH [39]

There has also been some research looking at different conditioning temperatures and if that will affect the polishing rate of silica. Nam-Hoon Kim *et al.* [59] state that the RR will increase with increased conditioning temperature, as shown in Figure 2.16 [59]. In this figure, all the wafers were polished for 60 seconds immediately after the different conditioning process were completed. The RR was around 70.0 nm/min when the wafer was conditioned with deionized water (DI-water) at 20℃, and the RR increases up to 168.5 nm/min when the temperature of the DI-water was around 80℃. They explain that this is due to the hydroxyl (OH^-) groups increases in the slurry, which will weaken the oxide surface and make it easier to remove by CMP.

Weidan Li *et al.* [61] have also looked at the polishing pad's effect on the CMP of silica. They state that the pad plays an important role, and by increasing the pads temperature from 40℃ to 80℃, both the oxide RR and planarization efficiency increases. Oliver *et al.* [60] state that the pad is the key to the CMP process, and almost all silica CMP is done with urethane pads, which is quite hard. Harder pads yield surfaces that are more

planarized than with softer pads. But the pad will degrade during use, so the RR will decrease over time [38].

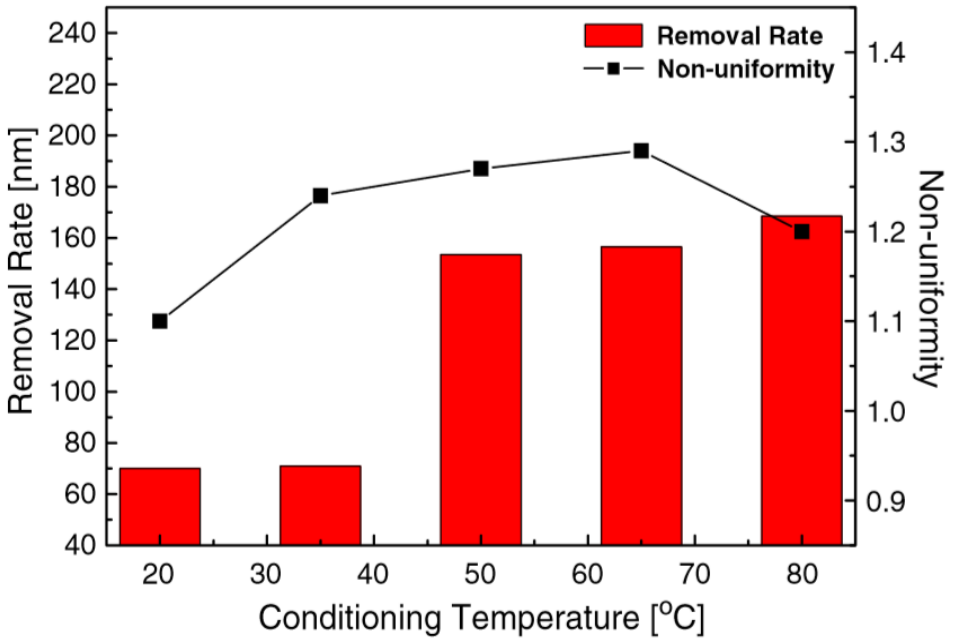

Figure 2.16: Changes in RR due to higher conditioning temperature [61]

2.5.5 CMP with Silicon

There is little literature on how a-Si will be affected during CMP, but already some sources have studied how crystalline Si gets affected, which might be similar to a certain degree. Estragnat *et al.* [44] looked at how the pH affects the RR. As shown in Figure 2.17 [45], the RR increases with increasing pH when a slurry containing alumina is used. If the slurry is only based on DI-water, the RR is 0 nm/min for all pH. The silicon RR with either alpha- or gamma-alumina shows a similar trend. This shows that the RR is dependent on the pH and which slurry is used. They state that the pH will change the surface chemistry of the silicon, which plays a vital role on the RR, and at a lower pH, the surface roughness is lower than at a higher pH value.

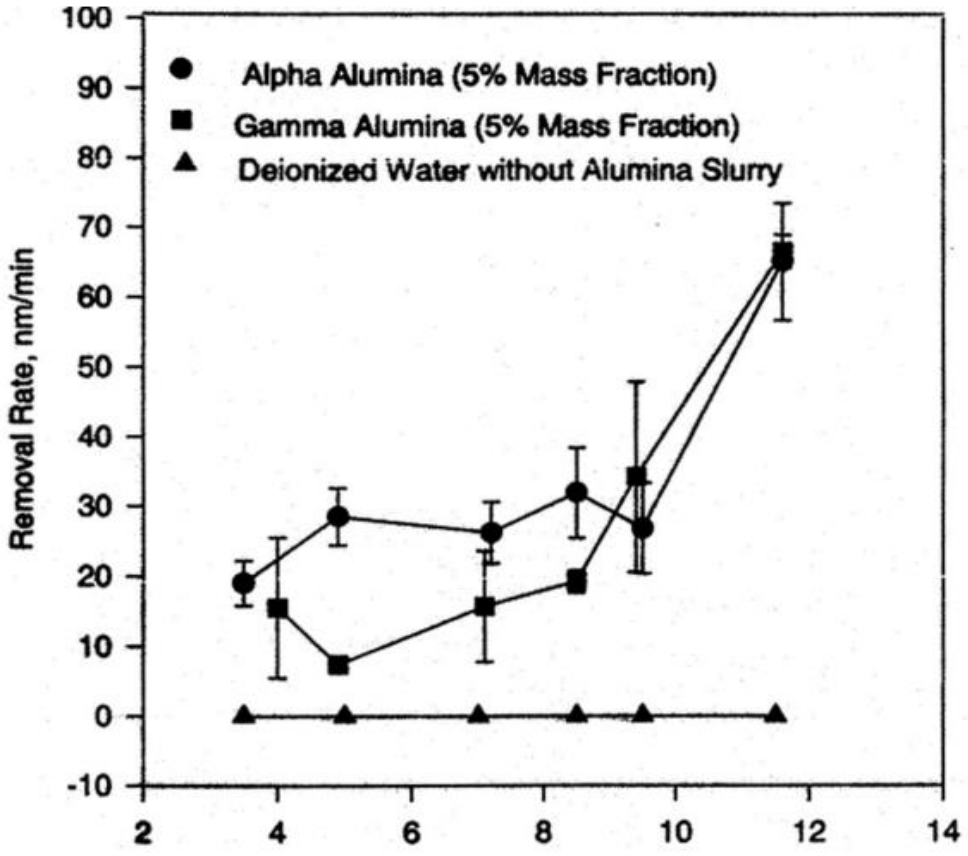

Figure 2.17: RR of silicon at different pH [44]

Yong-Guang Wang *et al.* [36] have another conclusion. They state that the pH does not affect the MRR that much, compared to the slurry flow rate and the oxidizer concentration. The optimal polishing conditions to get a high MRR, up to 161.23 nm/min, includes CMP at a pH of 7, oxidizer concentration of 0.44 wt%, and a slurry flow rate at 71.86 mL/min. They conclude that an increase in pH leads to a decrease in MRR, but due to the chemical solution of silicon the MRR will increases when increasing pH above 11. A higher polishing rate yields a shorter process time, which is desirable. However, if the polishing rate gets too high, it is difficult to control the process [38]. The effect of pH on MRR can be seen in Figure 2.18 [36].

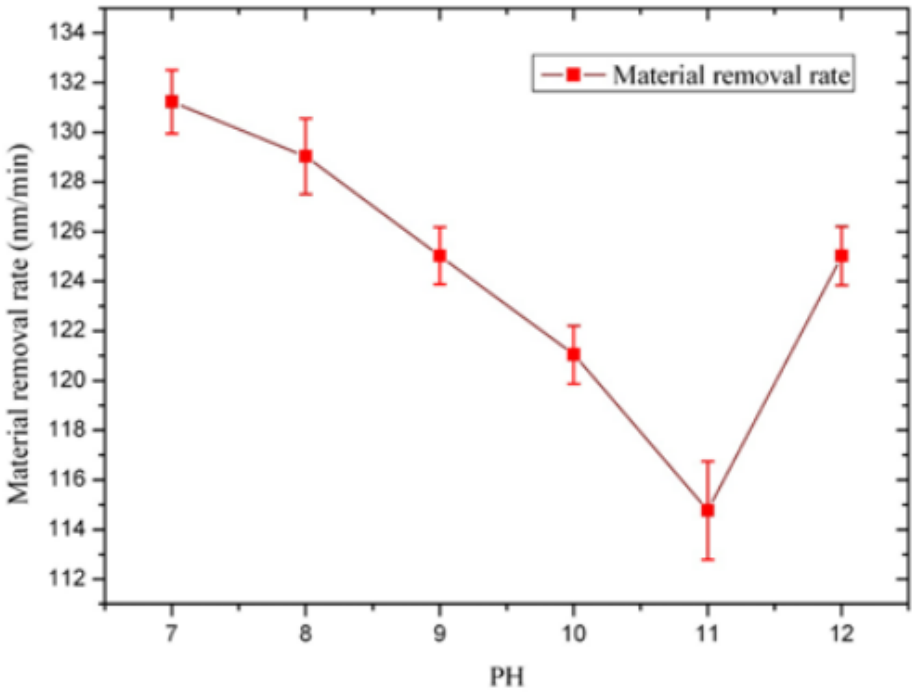

Figure 2.18: The effect of pH on MRR on a silicon wafer [36]

2.5.6 CMP with Alumina

There has also been some earlier investigation of how the RR of alumina can be affected. It is known that aluminum has one big problem with CMP; it can easily be scratched because of its high malleability and softness [38]. J. Hernandez *et al.* [57] have looked at the effect on the alumina RR due to changes in pressure and velocity. It can be seen from Figure 2.19 [57], that the RR depends more on the pressure compared to the velocity. However, according to Preston's equation, it should be a linear RR. As discussed before, Preston's equation is not adequate, and it is necessary to find a better model to calculate the RR.

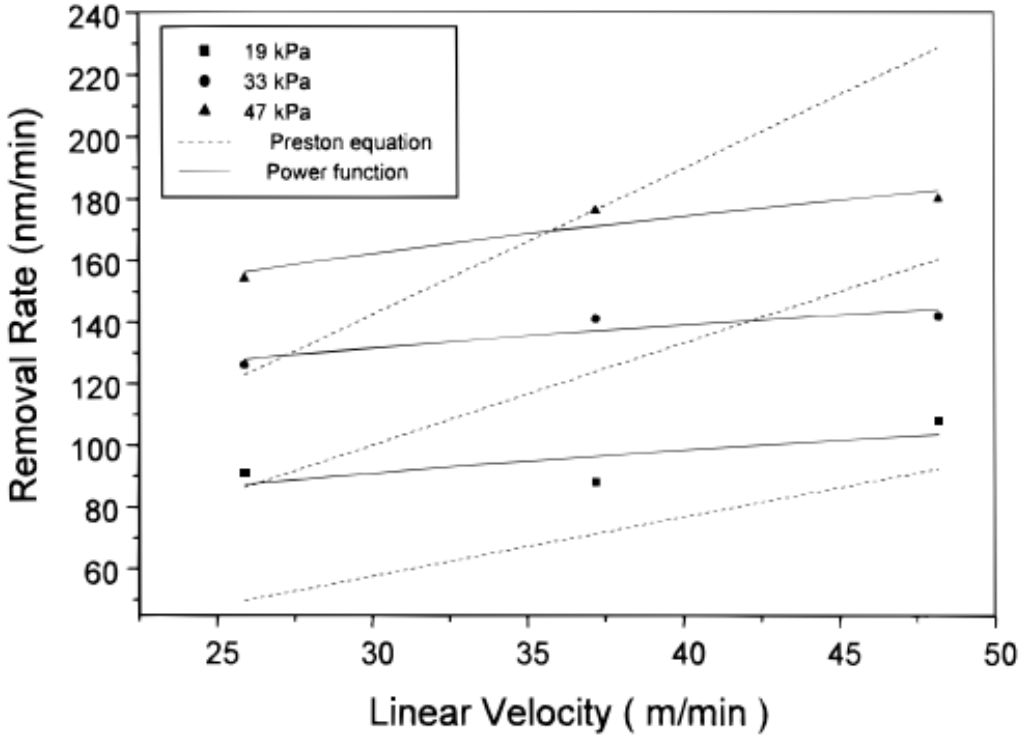

Figure 2.19: Alumina RR against linear velocity [57]

J. Hernandez *et al.* [57] have also looked at how different slurry abrasive concentrations affect the RR and quality of the surface. It is said that the RR drops significantly when the slurry changes from a mixture of alumina particles and hydrogen peroxide (H_2O_2) to a mixture containing only DI-water. In Figure 2.20 [57], the samples that have been polished with a slurry containing alumina particles and H_2O_2 are circled, while the wafers which were polished only with DI-water are not. The samples polished with the slurry that contained alumina particles and H_2O_2 had a RR above 70 nm/min, while the samples polished with just DI-water had a RR below 40 nm/min. Since the pad was not reconditioned between the different samples, it looks like sample 2 had a very high RR compared to samples 3-5. This is just due to particles from the previous sample that are still present in the system.

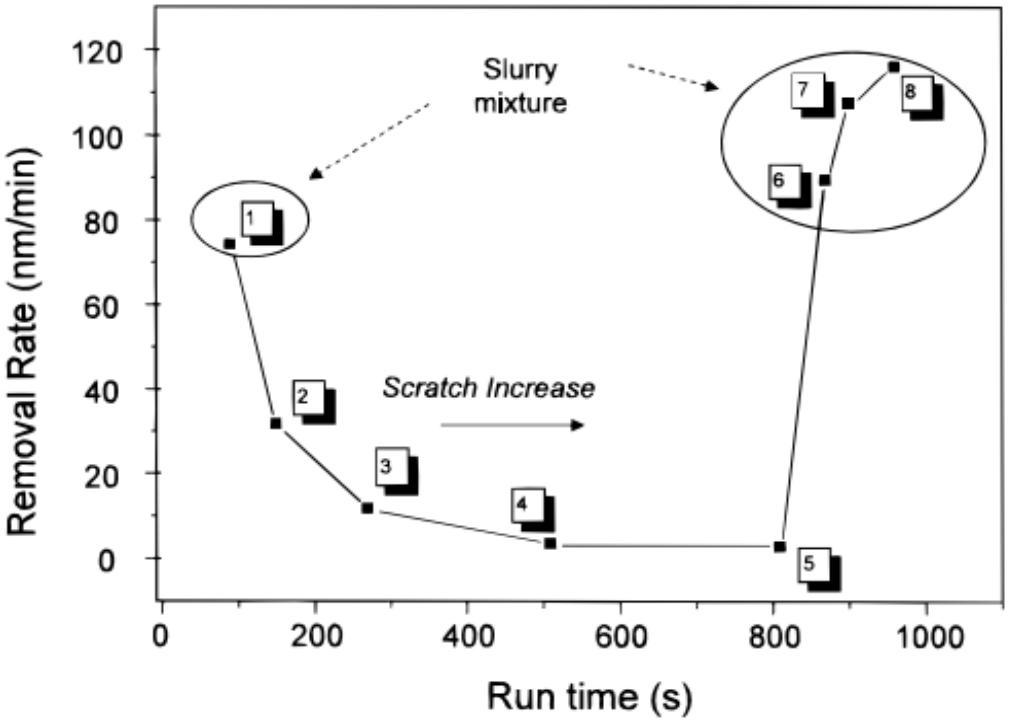

Figure 2.20: Higher slurry concentration will increase the RR of alumina [57]

2.5.7 The CMP at NTNU

The CMP (Alpsitec TOOL E400 E N◦O1) at NTNU is positioned at the PFI lab and is designed to accommodate 2- and 4-inch wafers as well as parts. It has two integrated slurry pumps and software, allowing ten different polishing steps, which can be controlled in the polishing recipe. It is possible to design the recipe and change all the ten steps. Therefore, there is an almost unlimited number of unique processes that can be used. The tool can easily be controlled by the touch screen, where all manual movements and recipe parameters can be changed. The CMP machine can be seen in Figure 2.21.

As seen in chapter 2.5, many parameters can influence the CMP result. In addition to different sample materials, slurry compositions, and polishing pads, many different machine operation choices can be changed. As most researchers have concluded in their scientific papers, the CMP process is not fully understood and needs further investigation, and many of the disadvantages of the CMP are due to the fact that the CMP is a new process that needs optimization [38].

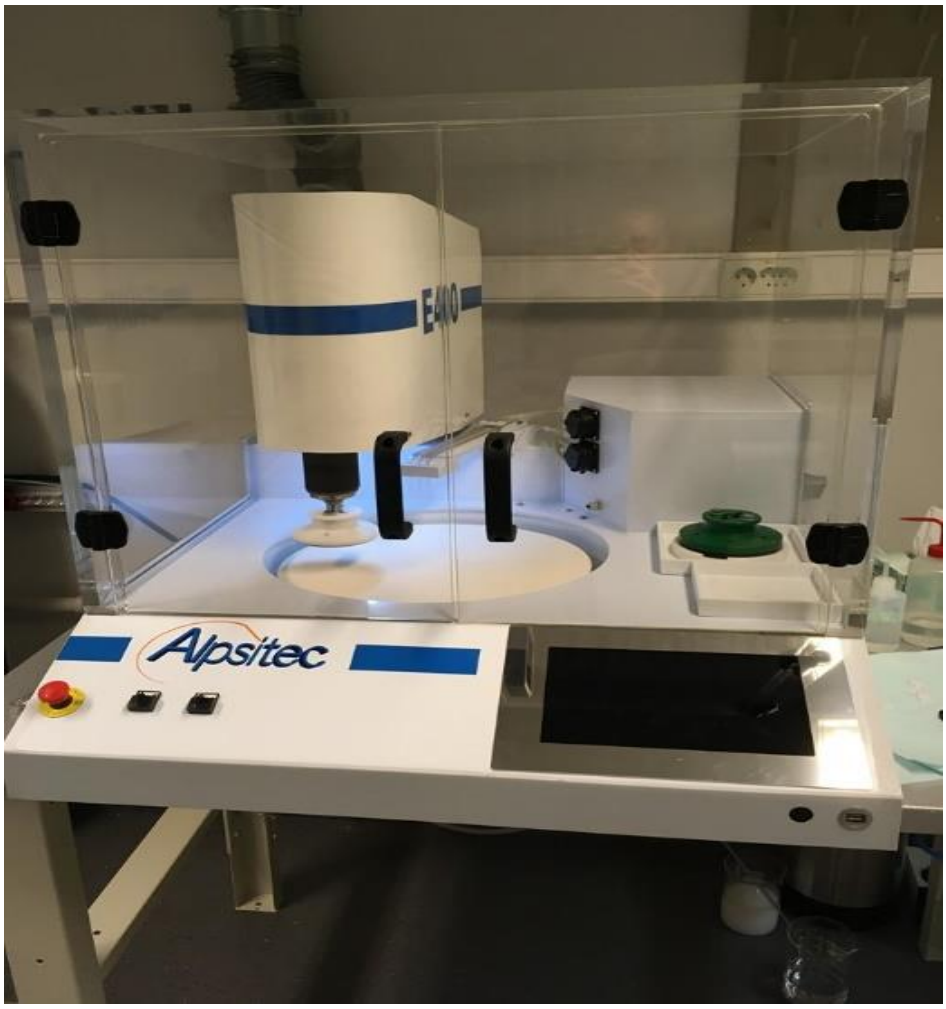

Figure 2.21: The CMP at NTNU

2.6 Lithography

Lithography was invented already in the 1790s when it was used as a cheap method of writing with a stone or metal on a plate. Now lithography is widely used as a micro- and nano-patterning method that can achieve the desired thickness in many semiconductor and nanotechnology applications [2]. By different approaches, materials, and systems, it is possible to make almost anything. There are countless techniques and methods to make nanostructures and nanopatterns, all with some advantages and limitations, but what they all have in common, is that they are based on the same general technical approach, optical or non-optical [61]. They use various masks to transfer different patterns into a reactive polymer film, often called a negative or positive photoresist (PR). An energy source is used for transferring the pattern [62]. The resist will be used to replicate the pattern into the surface underneath and is the radiation-sensitive material needed to make integrated circuits (ICs) devices [2]. Lithography is one of the critical aspects in making smaller devices, and every year new and better methods are being invented [63]. As shown in Figure 2.22 [66], progress in lithography manages to make smaller patterns. Current technology is able to design patters down to just a few nm.

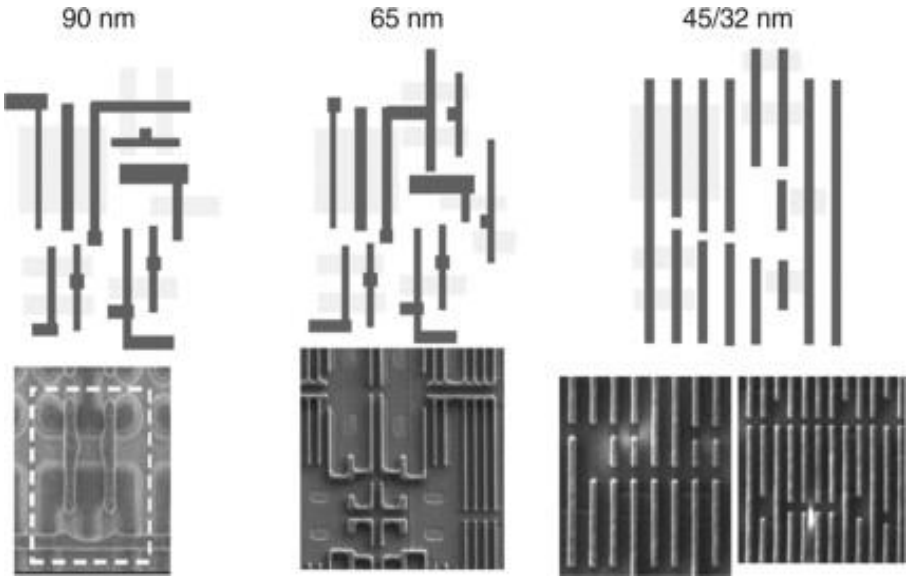

Figure 2.22: Microprocessor design [66]

2.6.1 Photolithography

Photolithography is one of the most used microelectronic fabrication methods, which is due to the high resolution and high volume chip production capacity [64]. It uses UV light to transfer patterns into the surface of the sample. Reaction with the light removes or hardens the resist, and the remaining resist will be used as a protective layer when the sample is etched. As mentioned, it is possible to either use a positive or a negative PR, typically

made of an organic polymer [63]. In Figure 2.23 [2], the basic steps of the process can be seen. First, the sample is spin-coated with either a positive or negative resist. Then light strikes through a mask, such that just some area still contains the resist, depending on the resist material's chemical nature. If the sample is coated with a negative photoresist, it will harden and become insoluble when exposed to radiation. The wafer image will be the opposite of the mask image. While the positive photoresist will be soft and is soluble during radiation. The developer will then remove the exposed resist and the wafer image will be the same as the mask image. Further, when the sample is being etched, the resist will protect the material underneath, so the etch will not reach the underlying substrate. After the etch, the rest of the photoresist is removed by stripping.

It is also normal to have a pre-treatment step before the coating, to bake after the resist is applied (soft bake), after the exposure (post-exposure bake), and after the development step (hard bake). The pre-treatment step is used to achieve a clean surface with good adhesion for the resist, while the baking is used to improve the adhesion between the photoresist and the wafer, to remove most of the solvent or to harden the resist. It is also normal to check the sample between the different steps to ensure that the step was successful either by using a profilometer, reflectometer, SEM, or another characterization method.

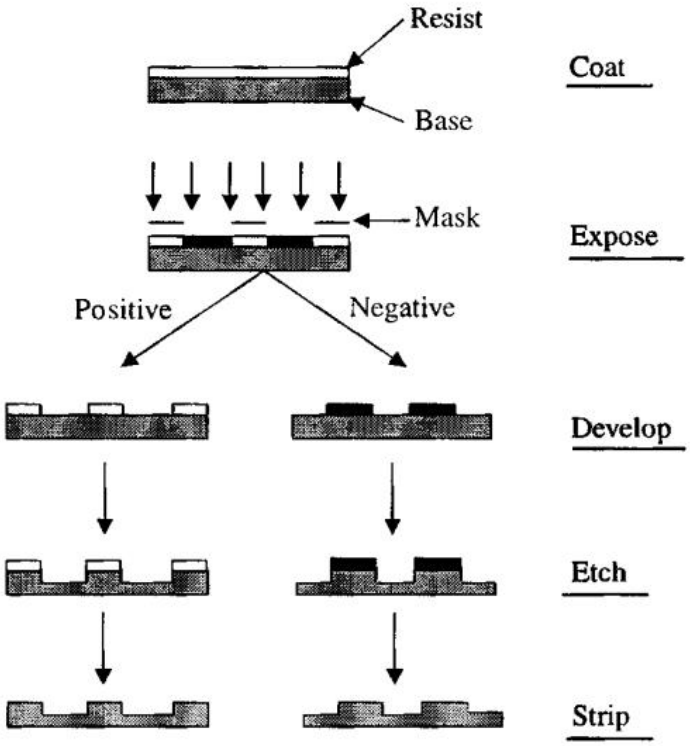

Figure 2.23: Schematic presentation of photolithography [2]

Different approaches in photolithography

There are three different photolithography methods: contact printing, proximity printing, and projection printing. In contact printing, the mask is in contact with the wafer and the photoresist. In proximity printing, there is a gap between the surface of the wafer and the mask, which is a form of "shadow printing" [62]. On the other hand, projection printing uses different lenses to focus the UV light onto the mask. The two first methods are cheaper and more simple, while projection printing is more expensive, but it has several advantages [63], such as high resolution, scanning-free parallel process, wide material sets, and support-structure-free three-dimensional (3D) printing [65]. Basic components of a projection lithography system are shown in Figure 2.24, including the light source, mask, project lens, and substrate [64].

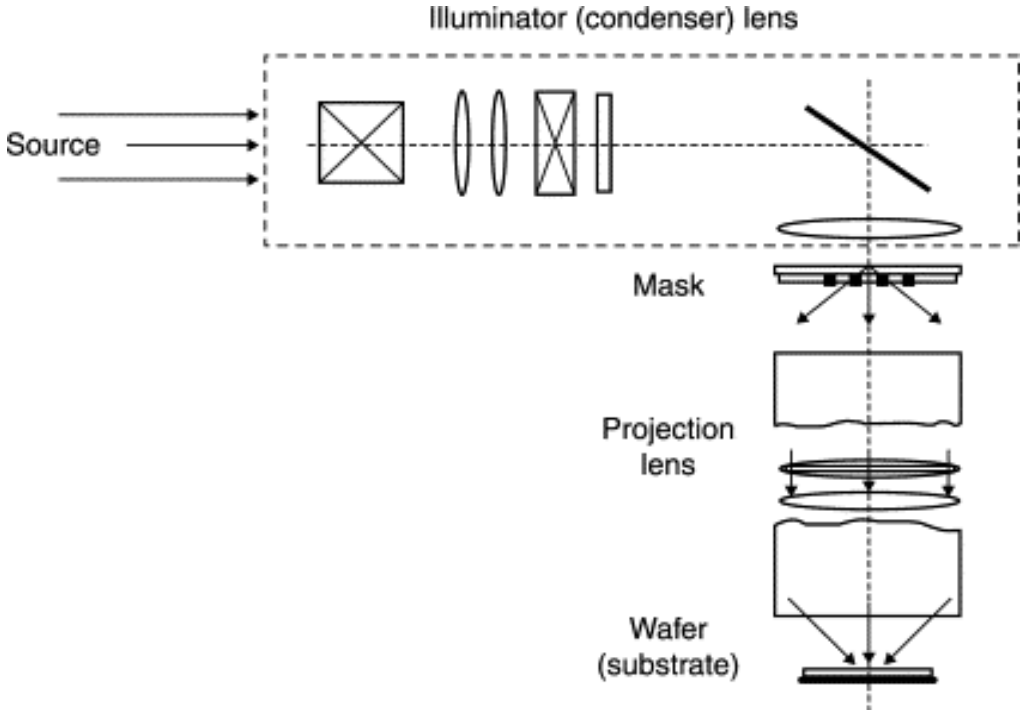

Figure 2.24: Basic components of a projection lithography system [64]

2.6.2 Resolution in Lithography

As mentioned, new and better lithography methods are invented every year. It is desired to find a method that can make smaller patterns with better resolution. That is why people have tried many different exposure sources, which yields different results. The most used sources are UV and deep UV (DUV) [63]. The three strongest emission wavelengths are 436, 405, and 365 nm which are called the g-line, h-line, and i-line, correspondingly [63].

The resolution limit in photolithography is known by the Rayleigh's equation given below [62], where *R* is the resolution, *λ* is the exposure wavelength, *NA* is the numerical aperture of the optical system, and K_1 and K_2 are constants depending on the specific resist material and tool issues. The corresponding depth of focus (DOF) is also given [62]. It is desired to have large enough DOF to produce usable imaging [64].

$$\boldsymbol{R = K_1 * \frac{\lambda}{NA}} \quad \textbf{(2.13)}$$

$$\boldsymbol{DOF = K_2 * \frac{\lambda}{NA^2}} \quad \textbf{(2.14)}$$

Therefore, scientists have tried to improve photolithography resolution by using shorter wavelengths and larger numerical apertures (*NA*). For example, Smith *et al.* [64] explains that Lyman-alpha (121 nm) and Deuterium (160 nm) have very short UV-wavelengths, but their power is too low to be practical. The resolution has a limit, but optical lithography is still far from reaching the end of the road [62]. The DOF needs to be large enough to give usable imaging on the PR layer. In Figure 2.25 [64] the trends of wavelength scaling over the past years are shown. The scaling factor (NA/K_1n) is a measure of resolution with respect to wavelength.

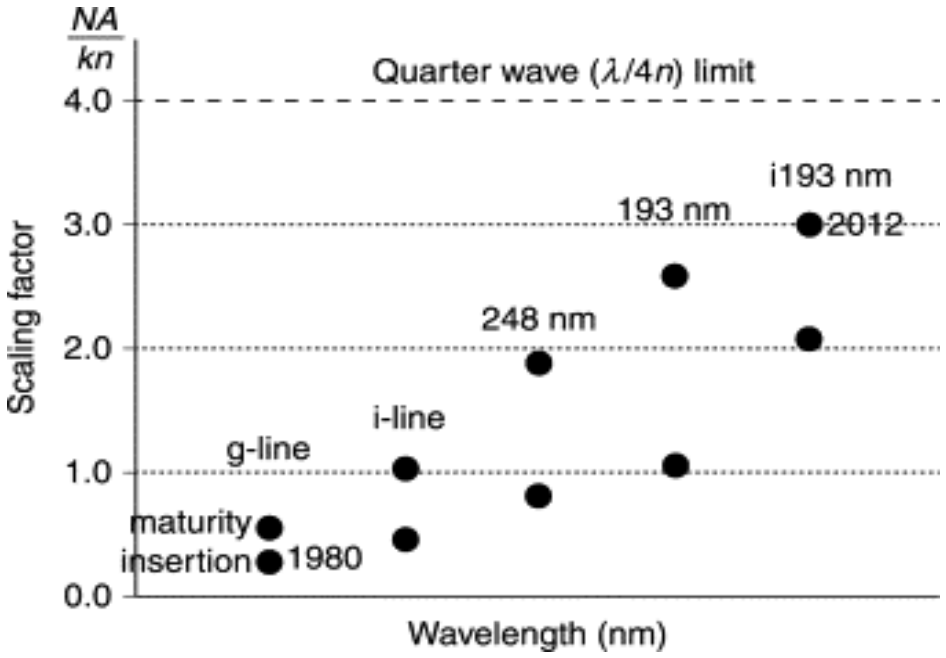

Figure 2.25: Wavelength scaling trends of optical lithography [64]

Extreme ultraviolet (EUV) lithography can replace the 193 nm DUV lithography which is in use today, but it has not been used in high volume production yet [63]. EUV masks require much more work compared to the standard photolithography. That is why they have tried other methods like modifying the illumination, phase-shifting the masks, and using mask correction methods to manage to make nanoscale patterning. Ito *et al.* [62] compare the conventional system with phase shifting and modified illumination, and in Figure 2.26 [62], some basic methods to obtain better resolution are shown.

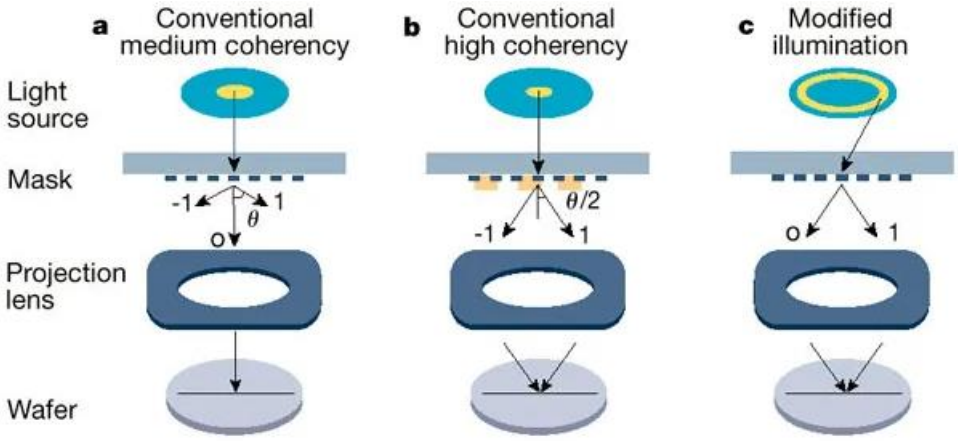

Figure 2.26: Different methods for resolution enhancement [62]

Researchers have also looked at how to develop the mask algorithm to optimize the patterns [66]. Many lithography methods are under development, such as Multi Beam Electron Beam Lithography (MBEBL), soft lithography, Nanoimprint Lithography (NIL), Proximity X-ray lithography, and near-field optical lithography. However, many of these methods are very expensive and not easy to use for prototyping, which is why maskless lithography is favorable [67]. It is also possible to change from the optical lithography technique to another system, but this will require a new infrastructure of tools, materials, and processing, at a substantial cost. However, maybe this is the key to achieving smaller patters in the microelectronics industry without pattern collapse [62][63].

Different photoresists used in lithography

As mentioned, when trying to produce smaller patterns, the resolution depends on the exposure source, and its wavelength, as well as the PR used [63]. It is desired to have a PR that has low volume shrinkage, excellent degradation, good pattern transferability with excellent mechanical and thermal performance [68]. As the size goes down, problems such as photoacid diffusion into the PR's unexposed region, line edge roughness (LER), or

pattern collapse start to be problematic [69]. Most PR's are typically made of organic polymers, and a large number of different types are considered [63]. The different resists are typically grouped into two groups, known as chemically amplified resists (CARs) and nonchemically amplified (non-CA) [63]. The resist is a complex mixture of polymers with a vast range of different properties and presents challenges in modeling the resist's behavior [70]. A lot of different approaches, such as molecular resist [71], inorganic metal oxide material [72], or nanoparticle resist [73], have been investigated to find a new and better PR to succeed in making smaller patterns [74].

2.6.3 Maskless Lithography

Due to the cost of mask fabrication, lack of flexibility, and low productivity, standard optical lithography has not satisfied the industry [75]. Future devices require smaller patterns than the optical lithography can succeed in producing [76]. Maskless lithography is one method to obtain patterns in the nanometer or even atomic-scale precision to succeed in minimizing electronic devices. Digital Micromirror Device (DMD), first conceived in 1977 [77], is one method that is based on maskless lithography, which combines traditional optical lithography with new technology [78]. The DMD works as a virtual mask to write the patterns directly on the surface of the sample, and the mask patterns are generated by computer software [75]. In a DMD lithography system the high-resolution projection lens is one of the most critical components, but the system also consist of a light source, the DMD, a controller (software), and a stage [81][82]. The DMD maskless lithography can achieve both 2D and 3D UV patterning of complex patterns, either performed by layer-by-layer [81] or scanning lithography [82]. In the layer-by-layer method, a motorized stage creates the 2D pattern by on- and off-state mirrors with a substrate that is immersed in a liquid photopolymer [82]. The scanning lithography has the advantages of point-by-point controllability, thereby avoiding unevenness and succeeding in making complicated 3D structures [83]. In Figure 2.27 [75] a system for double-sided microlens and spatial filter array (D-MSFA) for DMD-based maskless lithography can be seen. The system contains a UV illumination system, a DMD, an image projection lens, a D-MSDA, and a three-axis (xyz) scanning stage.

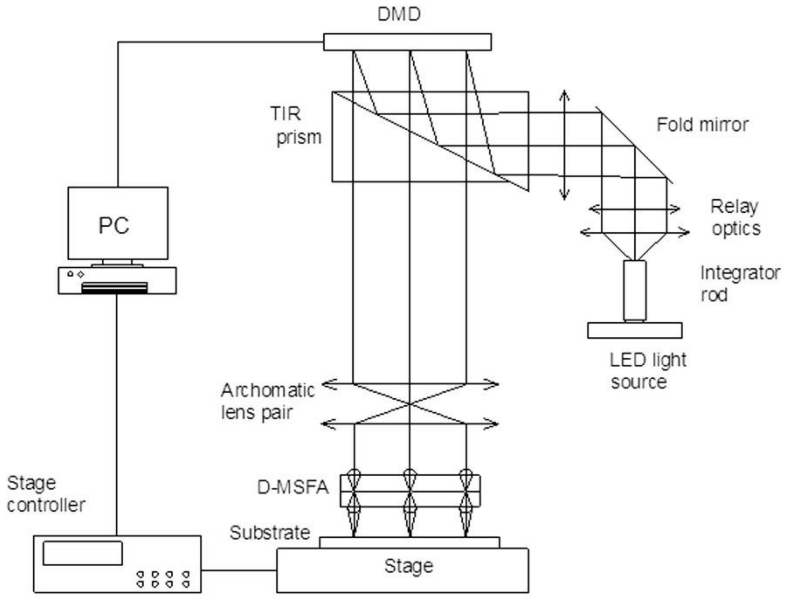

Figure 2.27: DMD-based maskless lithography system [75]

E-beam lithography is also another type of maskless lithography. It is considered to have the highest resolution when using 50-100 keV of primary electrons [63]. Thickness down to a few nm have been fabricated through e-beam lithography [84]. The downside with e-beam lithography is the slow throughput, which limits the high-volume manufacturing. On the other hand, they are still working on developing better methods such as projection e-beam [85], multiple-beam [86], or shape-variable beam [87] to increase the throughput. Until now, the multiple-beam e-beam lithography has the highest potential due to parallelizing the beams that pattern the wafers [63]. There are a number of other lithography methods which are maskless such as, scanning probe lithography (SPL), focus ion beam [88], or nanoprobe maskless lithography [63]. However, all of them have pros and cons, such as high cost, low throughput, or limited patterns [75].

2.6.4 Nanoimprint Lithography

Scientists have also used other methods to succeed reaching the desired thickness. As previously stated, all lithography methods are based on the same principle, but due to various exposure sources, it is possible to get very different results [89]. One example is nanoimprint lithography (NIL), which is one of the most promising techniques with many advantages [90]. It promises high resolution and fast processing speed at a low cost. NIL uses direct mechanical deformation of the resist and can achieve much better resolution than standard photolithography. A schematic view of the NIL process is shown in Figure 2.28 [91].

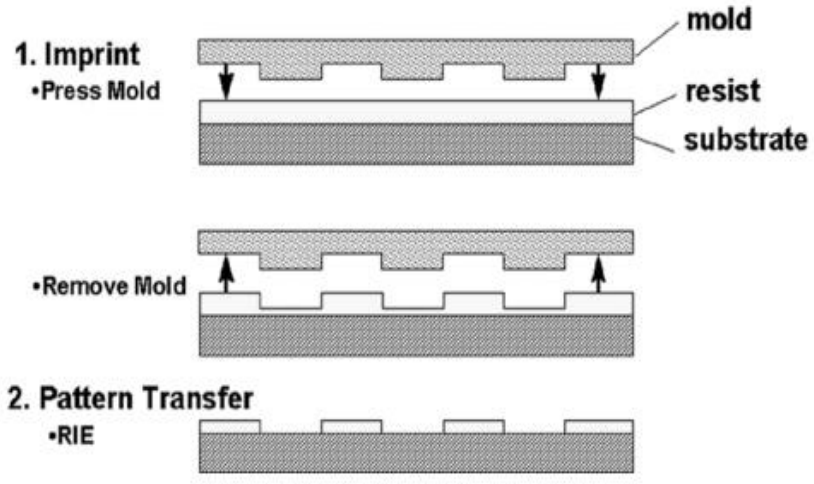

Figure 2.28: Schematic view of a NIL process [91]

The principle of NIL is straightforward. It uses a stamp or mold that has been etched, which contains nanoscale surface-relief features. The mold or stamp can be made of any material, for instance, silicon [92, p. 10], nickel [93], or polymer [94]. The structure will then be transferred due to a combination of capillary force, pressure, and a light source. The NIL method can yield features down to 10 nm in size. NIL receives increasing attention every year due to very high resolution, low cost, and the possibility to operate at room temperature and low pressure [68]. Although NIL is useful for producing patterns with very small structures, the throughput remains impractical low for commercial applications [62] and is still too complex [67].

2.6.5 Planarization in Lithography

As many researchers have figured out, the size and planarization in lithography are two of the major problems. As B. Davari *et al.* [56] state, it is very difficult to achieve control in the nanometer range during the etch step. This is due to the resist viscous flow and shrinkage after cure. They are therefore combining the CMP with lithography to manage planarization in the nanometer range. As shown in Figure 2.29 [56], the CMP achieved planarization of the non-planarized surface [38], and remove spikes that remains after the RIE process. They conclude that, combining RIE and CMP yields excellent planarization of the chip.

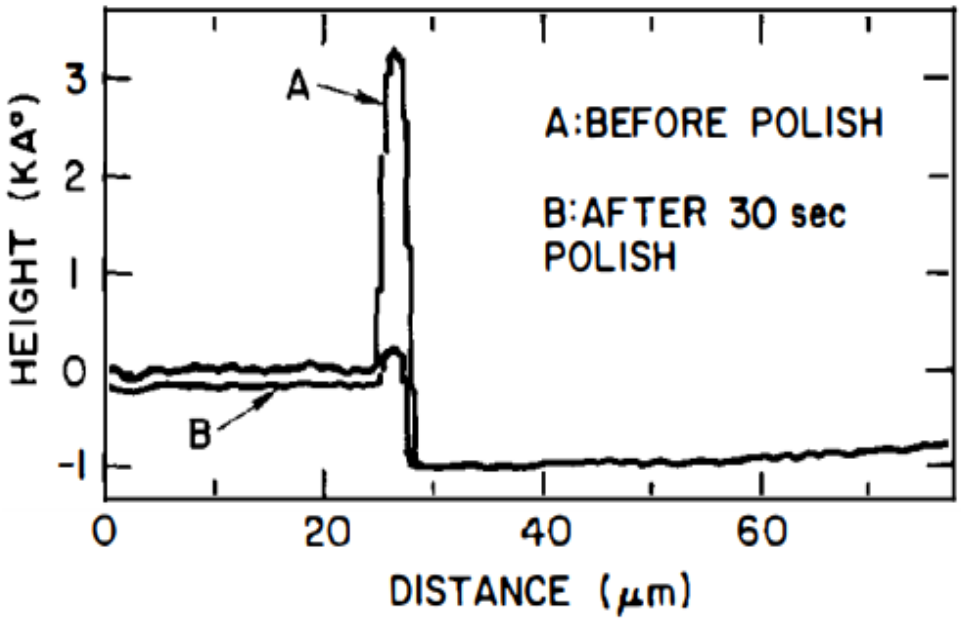

Figure 2.29: The sample before and after CMP [56]

2.7 Ellipsometry

Ellipsometry is a commonly used technique to measure thicknesses and characterize thin films. The technique became important to the semiconductor industry and fabrication of nanostructures used in microelectronics due to its ability to measure layers below 1 nm thickness [95]. It is a contact-less, non-destructive approach using optical measurements to determine the thickness of different films on a plane and reflecting substrate [96]. Ellipsometry measures the relative change in polarization between the incident radiation and the reflected radiation, after it hits the surface, as a function of wavelength [97]. Therefore, the measurements are not dependent on the intensity as long as the absolute intensity is sufficient [98]. The measurements are usually described by the two parameters Δ and ψ, which characterize the change in polarization as the light is reflected from the surface. The ellipsometry uses a model and compares the model to the results. ψ characterizes the amplitude ratio upon reflection, and Δ characterizes the phase shift difference [95]. Ellipsometry has a considerable advantage over other techniques. It not only measures a single amplitude parameter but also manages to fit both phase and polarization amplitude for each measurement. The ellipsometry obtains more information than other techniques [99]. It is also very precise and reproducible. However, ellipsometry can only measure transparent or semi-transparent films. It also has some difficulties to measure ultra-thin films below nanometer-size. Figure 2.30 [95] shows the basics of the ellipsometer.

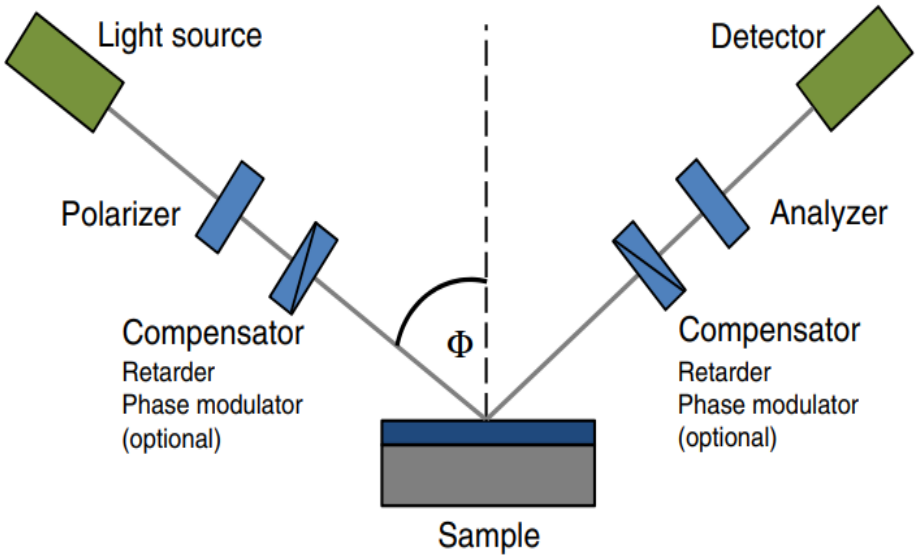

Figure 2.30: Scheme of an ellipsometer [95]

As one can see in Figure 2.31 [3], it is possible with ellipsometry, to map a wafer and see the variation in the film thickness. Here, 55 points on a 4-inch wafer were measured using ellipsometry after a CMP process.

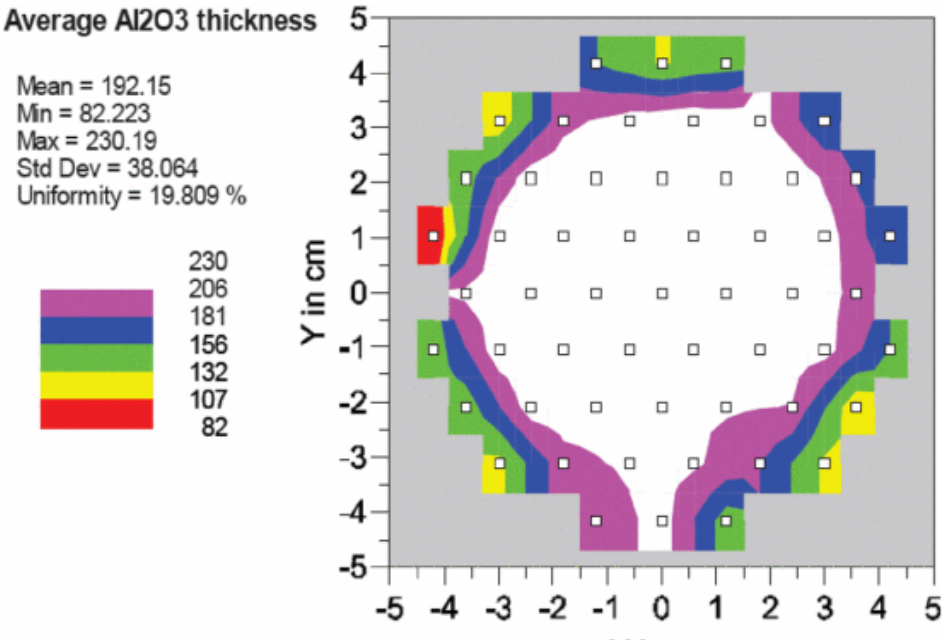

Figure 2.31: Illustration how to map a whole wafer with ellipsometer [3]

2.8 Scanning Electron Microscopy (SEM)

Many microscopes can be used to produce images of samples by scanning the surface with some sort of beam. For instance, optical microscopy (OM) has been on the market for a long time, before being replaced by SEM, due to more accurate technology with increased depth of field and better resolution [100]. SEM was invented in Germany in 1930, and already in 1942, SEM achieved a resolution down to 500 Å [101]. SEM uses electrons to get information about the sample by bombarding the specimen's surface with electrons between 1-40 kV [100]. The main advantage of electron microscopy is the resolution, which is due to the very strong interaction between the emitted electrons and the atoms in the sample [102]. SEM is used for visualization and characterization of surfaces, and there are different signals which can be detected, such as secondary electrons, backscattered electrons, and Auger electrons [103]. These signals can give SEM information about phases, grains, and topography, which makes SEM one of the most common techniques for characterization [104]. A SEM picture of different layers is shown in Figure 2.32 [105].

Compared to ellipsometry, SEM is operated in a vacuum. This is because SEM uses the interaction between the electrons and the atoms in the specimen to get information. If SEM was conducted in air, the interaction with air molecules would influence the results. Typical pressure used in electron microscopes is between 0.1 and 10^{-4} Pa. Since the characterization is done in a vacuum, it is necessary with some sample preparation. For example, the sample needs to be clean from dirt, oil, and fat. The samples also need to be electrically conductive, and they should not be much bigger than $50mm^3$. [101]

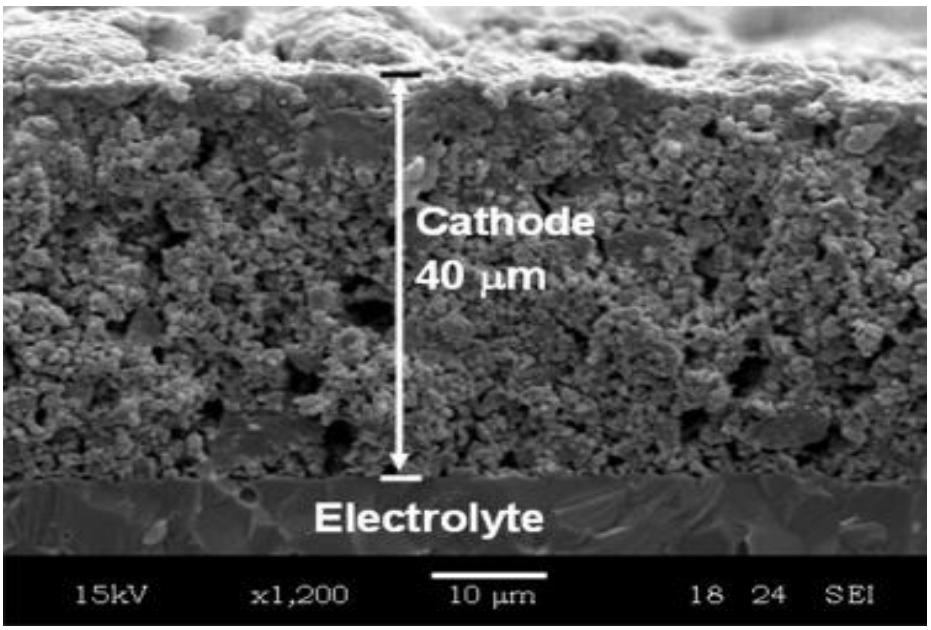

Figure 2.32: SEM picture of a sample [105]

3 Experimental

In this chapter, the experimental steps performed in the project work and thesis are presented. It is desired to find the removal rate (RR) of amorphous silicon (a-Si), alumina (Al_2O_3), and silica (SiO_2), by the chemical mechanical polisher (CMP). Characterization of the removel rate (RR) is done by thickness measurments of the polished layer. It is necessary to find a good model that can be used for thickness measurments in the ellipsometry, before and after CMP. For alumina and silica the reflective constant is well known giving good models and mearsurments accuracy. However, to find a model for a-Si, scanning electron microscopy (SEM) pictures were compared to the ellipsometry measurements. Since a-Si was deposited over an alumina layer, an investigation of the adheisein between the two layers was conducted. The chapter is divided into four subchapters, presenting the experiment, preparing the samples, measuring, and polising in the CMP.

3.1 Experimental Overview

In this project there are many steps to make a tunnel chip which can be used as a holder-chip in transmission electron microscopy (TEM). Since this is a prototyping, the layers need to be tested first in larger sizes before trying to achieve the desired thickness. The two main steps that need more investigation are step 3 and 5, but only step 5 will be investigated. It is also of interest to find the RR of silica and alumina. The different steps are shown in Figure 3.1, made by Stephanie Burgmann.

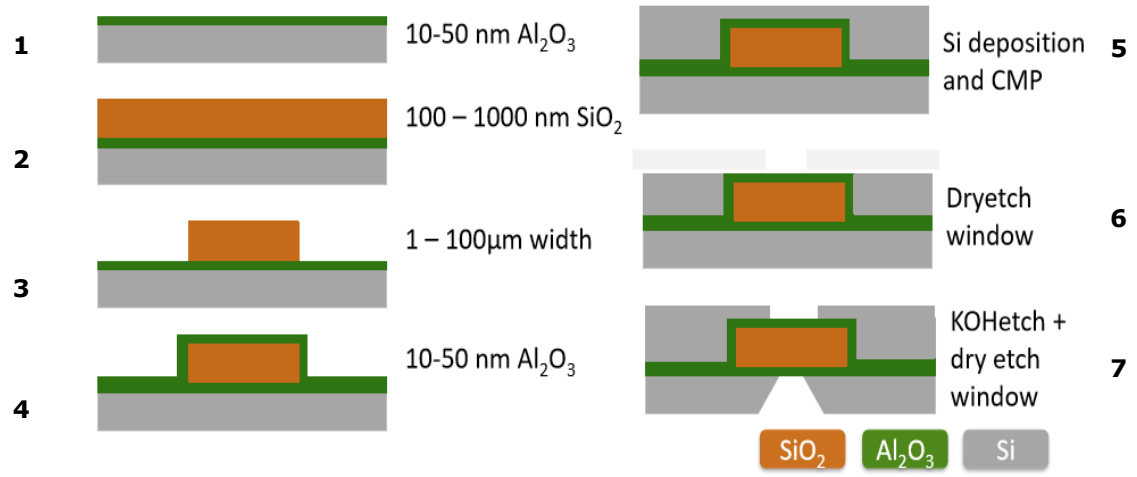

Figure 3.1: Schematic overview of the different steps making the tunnel chip

In the first step, 10-50 nm of alumina is deposited through atomic layer deposition (ALD). In step two, a second layer of 100-1000 nm of silica is deposited with plasma enhanced vapor deposition (PECVD). In the third step, the silica layer is patterned using lithography and dry-etching, leaving a 1-100 µm wide line. To succeed in removing the silica from the sides, but not etch the alumina, basic photolithography can be used. The next step is a new ALD deposition of alumina, and the fifth step is a PECVD deposition with a-Si. In the fifth step, it is desired to use the CMP to planarize the a-Si. The RR of a-Si with the CMP needs to be found so that the CMP can be stopped at the right time. In the last two steps, different etch methods can be used to make windows on the chip.

3.2 Preparation of the Samples

The wafers were all cleaned in the plasma cleaner before depositing the desired thickness of the layers, by either ALD or PECVD. The samples for SEM measurements were cleaved into smaller pieces of around 50mm^2. The samples that will be used in the CMP need to be measured using ellipsometry before and after every experiment, in order to find the RR of the CMP.

3.2.1 Cleaning the Samples

To prepare the wafers for deposition, all contaminates must be removed from the surface. Organic and inorganic contamination can be removed in a plasma cleaner. Since it is desired to get as clean as possible surface and thus achieve good adhesion, both oxygen and argon were used, at 100%. All samples were cleaned for 3 minutes at the highest generation frequency and maximum flow. After the wafers were cleaned, they were either brought to the ALD for depositing alumina, or to the PECVD for depositing silica or a-Si. They were carried around in a plastic carrier given at the NanoLab, and metal tweezer were used to load and unload the samples. Table 3.1 shows the parameters for cleaning the wafers.

Table 3.1: Parameters for cleaning the wafers

Type of wafer	*Gas*	*Generation*	*Flow*	*Time*
Si	Argon and Oxygen	100%	100%	3 min

3.2.2 ALD Deposition

Three experiments were conducted. One for looking at the adhesion between alumina and a-Si, one for comparison between ellipsometry and SEM with the aim of producing a recipe

for ellipsometry, and one for testing alumina in the CMP. To avoid new contamination the cleaned wafers were coated right after the cleaning step. All were made with the standard alumina recipe by NanoLab. The recipe works at 160℃ using water and trimethylaluminum (TMA) as precursors. ALD is a linear process with a deposition rate of 200 cycles per hour. 50 nm of alumina were deposited on the wafers made for testing adhesion, and the wafers made for ellipsometry. 500 cycles yielded a layer thickness of around 50 nm. The alumina wafers made for CMP were coated with around 100 nm layer. Since the machine is very hot it is important to use a metal tweezer and not touch the hot plate with the plastic gloves. Table 3.2 shows the parameters for making the alumina wafers, and Figure 3.2 shows how they are placed in the ALD machine.

Table 3.2: Parameters for alumina deposition

Type of wafer	***Experiment***	***Recipe***	***Cycles***	***Time***
Si	Adhesion a-Si / alumina	Alumina	500	2.25 hours
Si	Recipe for ellipsometry / SEM	Alumina	500	2.25 hours
Si	CMP	Alumina	1000	4.5 hours

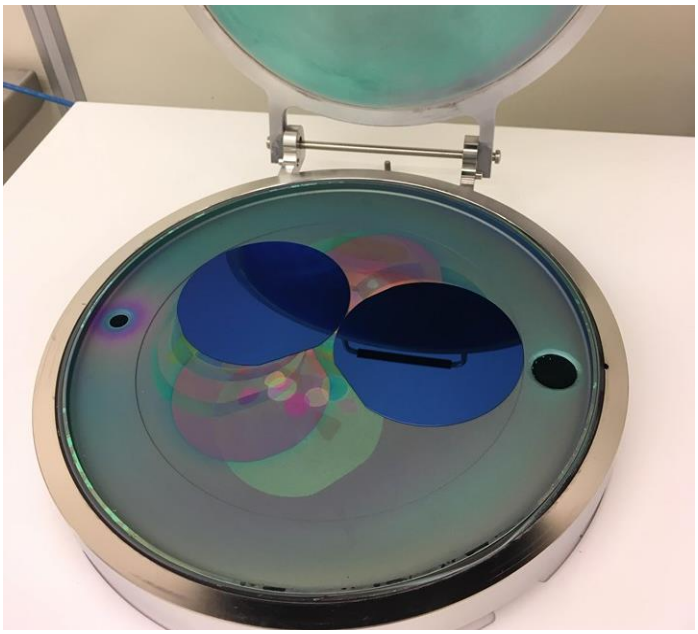

Figure 3.2: The samples in the ALD machine

3.2.3 PECVD Deposition

The PECVD machine is very similar to the ALD. Here, the samples were processed directly after they either were cleaned from the plasma cleaner or received an initial layer from the ALD machine. Table 3.3 shows the parameters for making the layers, and Figure 3.2 shows a wafer placed in the PECVD machine. Due to blisters and bad adhesion when depositing a-Si on alumina [106], different solutions were tested. All wafers made for testing the deposition and measuring of a-Si were done with the Oxford Plasma Technology (OPT) a-Si low-temperature recipe. The regular a-Si recipe is operated at 250 degrees, and usually, a dummy wafer should be run first if another recipe was used before. The wafers tested for adhesion between a-Si and alumina were tested to run immediately after a recipe with OPT SiO_2 was conducted, and different thickness and temperatures were tried. To avoid blisters, low-temperature a-Si were deposited at 180 degrees onto a SiO_2 layer deposited at 300 degrees. The silica wafers made for the CMP were done with the regular SiO_2 (OPT) recipe operating at 300 degrees, where 29 min yields a 2000 nm thick layer.

Table 3.3: Parameters for a-Si and silica deposition

Experiment	***Type of wafer***	***Recipe***	***Time***
Adhesion a-Si / alumina	Si with alumina	a-Si (OPT)	20 min or 34 min
Recipe for ellipsometry / SEM	Si with alumina	a-Si (OPT)	12, 24, 36 and 48 min
CMP	Si	SiO_2 (OPT) + a-Si (OPT)	1 + 45 min
CMP	Si	SiO_2 (OPT)	29 min

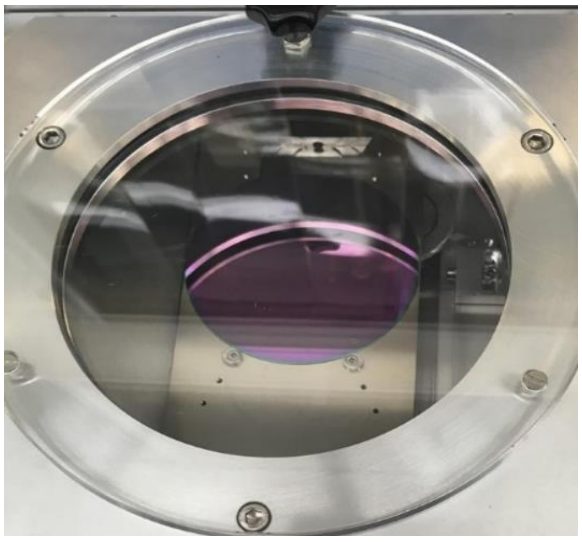

Figure 3.3: Wafer inside the PECVD machine

3.3 Measuring the Wafers

After obtaining a layer on the wafers from ALD, PECVD, or both, it is beneficial to measure the thickness using ellipsometry. However, the a-Si wafers are exceedingly difficult to measure with ellipsometry. This is due to the ellipsometry requiring a recipe that knows approximately how thick the different layers are, and it is necessary to use a recipe designed for the right wafer. So before using the ellipsometer, it should know what type of wafer is being measured and roughly the thickness of the different layers. To acquire the growth-rate (GR) of a-Si at 180 degrees, the wafers also needed to be measured in SEM.

3.3.1 Ellipsometry

When operating the ellipsometry, it is crucial to "Check Alignment" before every measurement. To get a high yield à high intensity, the cross which pops up should be centered, and the intensity should be around 0.6 or higher for the alumina and a-Si wafers and around 0.25 for the silica wafers. This is due to a thicker silica layer compared to the two others, and thus higher adsorption of light in the film. A model called SI_JAW substrate and an interface thickness NTVE_JAW2 of around 2 nm were used on all wafers. To get as low as possible mean square error (MSE), a "fit all" on the "e2 Components" was used. An optimal MSE value should be under 6, but a value under 20 is also good enough. The value is dependent on the thickness and purity of the material and the match of the optical constant. Figure 3.4 shows the setup for the ellipsometry.

Figure 3.4: Setup for the ellipsometry to characterize the samples

The model which was used for the alumina wafers is called CodyLor. This model is applied when measuring layers with a thick layer of alumina (around 100 nm). When the thickness went down after polishing, it was changed to a recipe called Cauchy (around 50 nm). To measure the silica wafers, a recipe called SiO_2 Sellmeier was used. The silica and a-Si wafers had a slightly higher MSE, but under 30, which is deemed as adequate. For the a-Si wafers, a recipe called a-Si parameterized was used.

Table 3.4: Parameters for measuring the silica and alumina wafers

Layer #2	SiO_2 (Sellmeier) Al_2O_3 (CodyLor) Al_2O_3 (Cauchy)	Thickness #2	All Thicker films Thinner films
Layer #1	NTVE_JAW2	Interface thickness	2.0 nm
Substrate	SI_JAW		

Table 3.5: Parameters for measuring the a-Si wafers

Layer #3	a-Si parameterized	Thickness #3	
Layer #2	SiO_2_JAW2	Thickness #2	≈65-70 nm
Layer #1	NTVE_JAW2	Interface thickness	2.0 nm
Substrate	SI_JAW		

Ellipsometry before and after the CMP

Seven points were measured on every wafer, before and after the CMP. A 3D printed 4-inch wafer-holder was used so that the same seven points were measured every time. The seven points which were measured are shown in Figure 3.5. The wafers were always measured with the flat cut facing upwards. The thickness of the layer (in nm) at the seven different points were mapped, as shown in Table 3.6, 3.7, and 3.8. The points correspond to the marks shown in Figure 3.5, and the # indicated which wafer is being measured.

Figure 3.5: The seven points which are measured

Table 3.6: How the a-Si, alumina and silica wafers (when focused on slurry concentration) were mapped

	Thickness of the wafer nr. # with … looking at…						
	#.1 [nm]	#.2 [nm]	#.3 [nm]	#.4 [nm]	#.5 [nm]	#.6 [nm]	#.7 [nm]
without CMP							
CMP 10 sec							
CMP 30 sec							
CMP 60 sec							
CMP 90 sec							

Table 3.7: How the silica wafers (not the one focused on the slurry) were mapped

	Thickness of the wafer nr. # with … looking at…						
	#.1 [nm]	#.2 [nm]	#.3 [nm]	#.4 [nm]	#.5 [nm]	#.6 [nm]	#.7 [nm]
without CMP							
CMP 30 sec							
CMP 90 sec							
CMP 180 sec							
CMP 360 sec							

Table 3.8: How the a-Si wafers were mapped

	Thickness of the wafer nr. # with … looking at…						
	#.1 [nm]	#.2 [nm]	#.3 [nm]	#.4 [nm]	#.5 [nm]	#.6 [nm]	#.7 [nm]
without CMP							
CMP 10 sec							
CMP 30 sec							
CMP 70 sec							
CMP 120 sec							

SEM and ellipsometry to find the thickness layer of a-Si

For finding the a-Si layer thickness, both SEM and ellipsometry were used to compare the results. One wafer was made with 500 cycles of the standard alumina recipe before it was cut into four pieces. Then the four pieces were deposited with a-Si for 12, 24, 36, and 48 min with the regular OPT a-Si recipe at 180 degrees. They were then cut into desired sizes to be measured both in SEM and in ellipsometry for comparison. Using the SEM images a verification of the model for calculating the layer thickness from the ellipsometry measurements was possible.

3.4 Chemical Mechanical Polishing (CMP)

3.4.1 Setup Before CMP

Before using the CMP machine, it is necessary to check that the vacuum works, the right slurry is loaded, and three dummy-wafers are run for three minutes to warm up the machine. Conditioning with the condition-head was used in between every wafer. This is necessary so that the previous wafer will not affect the new one.

3.4.2 Parameters

If one wants to investigate the CMP machine, it is essential to have a standard procedure and change one parameter at a time. The red highlighted text in Tables 3.9 and 3.10 are the only parameters that are changed during the experiment. The parameters used in this project are the step duration, working pressure (WP), backside pressure (BP), and the concentration of the first slurry. The second slurry was not used. It is only step 3 that is changed every time to investigate and map the CMP machine properly. The third step is the actual polishing step, while the others are to adjust the parameters such as wetting, slurry amount, pressure, rotation speed etc., as can be seen in Table 3.9. A new recipe was written for each parameter that was investigated, based on the standard. When the slurry concentration was investigated, the standard recipe was used, as shown in Table 3.9. To change the concentration, the slurry was mixed with DI-water.

Table 3.9: The standard recipe for the CMP for alumina and silica wafers

	Step 1	Step 2	Step 3	Step 4	Step 5
Step duration [s]	10	5	**10**	30	3
Transition duration [s]	2	2	2	0	0
Head speed [rpm]	-30	-20	-42	-60	-60
Plate speed [rpm]	-30	-20	-30	-60	-60
Working pressure [mdaN/cm^2]	-300	200	**300**	200	200
Backside pressure [mdaN/cm^2]	0	0	**300**	60	0
Ring ratio	100 %	100 %	100 %	100 %	100 %
External sweep position [mm]	135	135	135	135	135
Plate DIW	OFF	OFF	OFF	ON	ON
Vacuum	ON	ON	OFF	OFF	ON
Slurry 1 [%]	50	37	37	0	0
Slurry 2 [%]	0	0	0	0	0

Table 3.10: The standard recipe for the CMP for a-Si wafers

	Step 1	Step 2	Step 3	Step 4	Step 5
Step duration [s]	10	2	**10**	2	3
Transition duration [s]	2	2	2	0	0
Head speed [rpm]	-30	-20	-42	-60	-60
Plate speed [rpm]	-30	-20	-30	-60	-60
Working pressure [mdaN/cm^2]	-300	100	**100**	100	0
Backside pressure [mdaN/cm^2]	0	0	**100**	60	0
Ring ratio	100 %	100 %	100 %	100 %	100 %
External sweep position [mm]	135	135	135	135	135
Plate DIW	OFF	OFF	OFF	ON	ON
Vacuum	ON	ON	OFF	OFF	ON
Slurry 1 [%]	50	37	37	0	0
Slurry 2 [%]	0	0	0	0	0

Explanation of the different steps is given in the manual for the tool. The most important parameters for this rapport are listed in Table 3.11 below.

Table 3.11: Explanation of the main parameters in the CMP

Step duration	Define the step duration
Working pressure	Working pressure applied on the wafer per cm^2
Backside pressure	Pressure applied on the back side of the wafer per cm^2
Slurry 1 flow	Activate the slurry pump 1 with the entered flow

3.4.3 Procedure

After the wafers were measured with the ellipsometry, they were first polished for the given time given in Table 3.6, 3.7, and 3.8, with the desired recipe. They were then washed with diluted water before they were put in isopropanol (IPA) in a 1000 mL beaker. After that, the wafers were treated in ultra-sonicated de-ionized water for around 10 minutes. Then they were pulled out and blow-dried with a nitrogen-gun until they were completely dry. The wafers were then measured again with the ellipsometry before they were polished again. The process is repeated in between every time the wafer is removed from the CMP. The beaker with the wafer in IPA in the ion-bath, can be seen in Figure 3.6.

Figure 3.6: The beaker with the wafer in IPA in the bath

3.4.4 A-Si Wafers

Since there are quite many wafers, it is good to have a table over the parameters that are used on each wafer. All the a-Si wafers were done with the standard recipe given in Table 3.10, apart from one parameter, which is highlighted in Table 3.12:

Table 3.12: Parameters for the a-Si wafers in the CMP

A-Si wafers			
Wafer nr.	**Working pressure [mdaN/cm^2]**	**Backside pressure [mdaN/cm^2]**	**Slurry 1**
1	100	100	**1:5**
2	100	100	**1:2**
3	100	100	**1:1**
4	100	100	**1**

3.4.5 Alumina Wafers

All the alumina wafers were done with the standard recipe given in Table 3.9, apart from one parameter, which is highlighted in Table 3.13:

Table 3.13: Parameters for the alumina wafers in the CMP

Alumina wafers			
Wafer nr.	**Working pressure [mdaN/cm^2]**	**Backside pressure [mdaN/cm^2]**	**Slurry 1**
1	300	300	1:9
2	300	300	1:9
3	300	**500**	1:9
4	300	**100**	1:9
5	300	**200**	1:9
6	300	**400**	1:9
7	**100**	300	1:9
8	**200**	300	1:9
9	**300**	300	1:9
10	**400**	300	1:9
11	**500**	300	1:9
12	**400**	300	1:9
13	300	300	**1:4**
14	300	300	**1:5**
15	300	300	**1:5**
16	300	300	**1:7**

3.4.6 Silica Wafers

All the silica wafers were also done with the standard recipe given in Table 3.9, with one parameter changed, which is highlighted in Table 3.14.

Table 3.14: Parameters for the silica wafers in the CMP

Silica wafers			
Wafer nr.	**Working pressure [mdaN/cm^2]**	**Backside pressure [mdaN/cm^2]**	**Slurry 1**
1	300	300	**1:7**
2	300	300	**1:4**
3	300	300	**1:5**
4	300	300	**1:3**
5	300	300	**1:2**
6	**100**	300	1:4
7	**200**	300	1:4
8	**400**	300	1:4
9	**500**	300	1:4
10	300	**100**	1:4
11	300	**200**	1:4
12	300	**400**	1:4
13	300	**500**	1:4

3.4.7 Slurry Mixture

The slurry that was used during the experiment is called "Klebosol 50R50". Klebosol is a brand making colloidal silica with non-agglomerate, non-porous, and spherical particles of silica. The slurry has a huge variety of applications, everything from coatings, catalysis, thermal insulation and metal, and glass polishing. Klebosol 50R50 contains 50% silica with particles in a size of 80 nm. The specific surface area is 50 m^2/g, its density is 1.4, and it has a pH at 9, at a temperature of 20℃. Since the surface area is quite big, it has good reactivity [107]. The pH of the DI-water can be assumed to be around 7. Since different slurry concentrations were made, they will also have different pH and number of particles. The mixtures made with more concentrated slurry will have a higher number of particles and higher pH, while mixtures made of more DI-water will have a lower number of particles and a lower pH.

4 Results

The results of the experiment are shown in this chapter. The results are presented in three subchapters, one for each of the materials: amorphous silicon (a-Si), alumina (Al_2O_3), and silica (SiO_2). The subchapters are divided further between the different experiments and the parameters which were altered.

4.1 A-Si Wafers

Before the a-Si wafers could be used in the chemical mechanical polisher (CMP), they were measured in ellipsometry and in scanning electron microscope (SEM) to get a recipe for the ellipsometry, for further work. It was also necessary with good adhesion between a-Si and the layer underneath to successfully use the wafers in the CMP. A-Si was deposited over alumina with different approaches, to examine the adhesion between the layers. Figure 4.1 is a SEM picture of one of the samples. As one can see, blisters form easily when a-Si is deposited over an alumina layer.

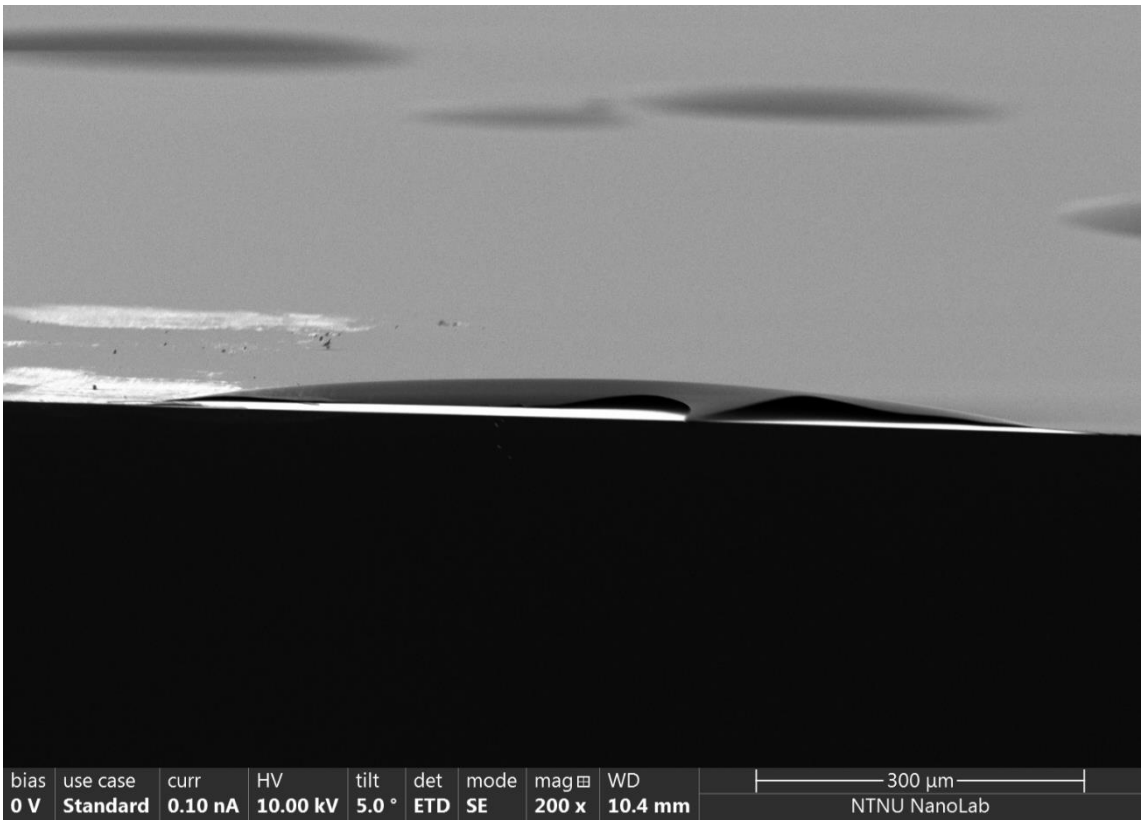

Figure 4.1: SEM picture of a-Si deposited over alumina

4.1.1 Depositing the A-Si

Three different possible solutions were tried to avoid blisters between a-Si and alumina. The solutions consisted of testing different thickness layers and temperatures and running an a-Si recipe immediately after an (OPT) SiO2 recipe.

Different thickness

One possible solution tested to avoid blisters is to deposit thinner or thicker layers of a-Si. In Figure 4.2, two wafers with different thicknesses of a-Si can be seen. The wafer to the left got 20 min of the regular recipe (OPT) a-Si at 250 degrees, while the wafer to the right got 34 min. Longer deposition time yields a thicker layer of a-Si. Both experience many blisters. The wafer made with 20 min recipe is yellow-ish, while the wafer made with 34 min recipe is blue-grey. Both got the a-Si deposition over a 50 nm layer of alumina.

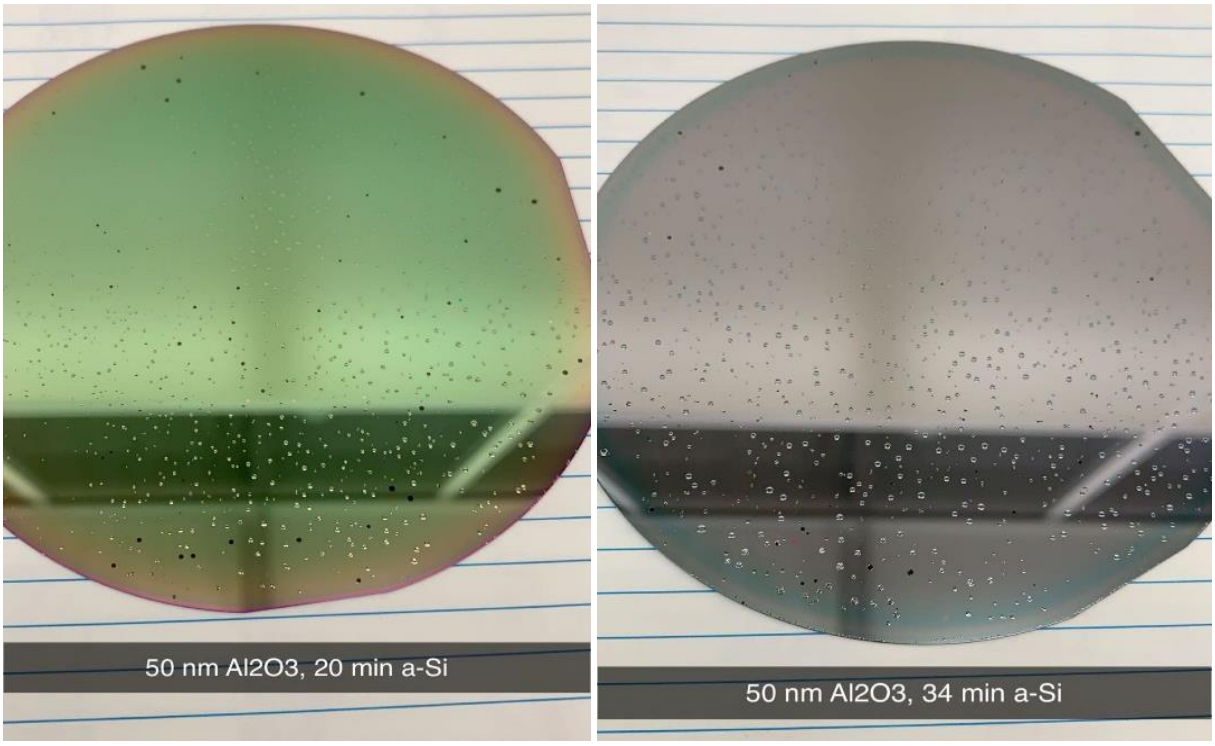

Figure 4.2: Two wafers only difference is the deposition time of a-Si

Different temperatures

One possible solution to the problem of blisters is to deposit a-Si at lower temperatures. Since Figure 4.2 already shows how blisters arise with the regular 250 degrees recipe, two different temperatures are tried. One wafer was run with the recipe at 180 degrees and one at 200 degrees, as shown in Figure 4.3. The wafer made at 200 degrees has a few blisters, while the wafer made at 180 degrees does not have any blister at all. Both wafers got an a-Si deposition over a 50 nm alumina layer.

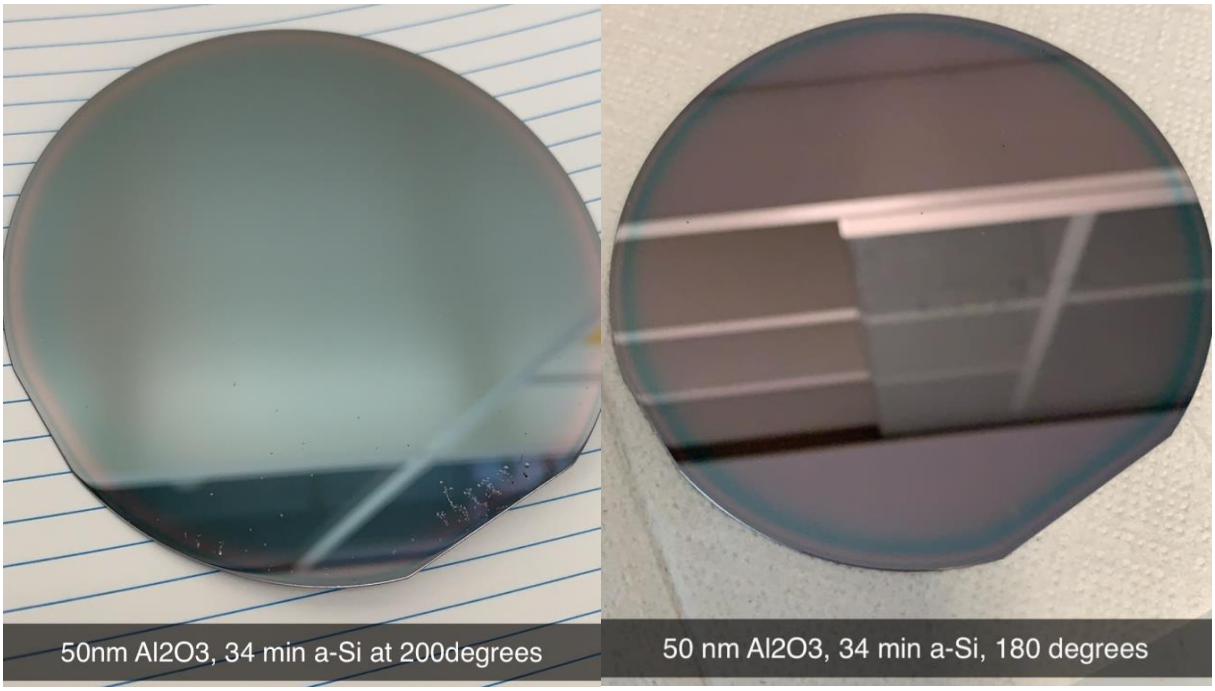

Figure 4.3: Two wafers only difference is the deposition temperature

After (OPT) SiO_2 recipe

Another possible solution to the problem of blisters is to deposit the a-Si recipe after an (OPT) SiO_2 recipe. Figure 4.4 shows two wafers, where both were made with the standard (OPT) a-Si recipe made at 250 degrees, after an (OPT) SiO_2 recipe. The only difference is the deposition time of 20 and 34 min of a-Si, which yields different thicknesses of a-Si. Both wafers have a smooth surface with no blisters on the surface, and both have a 50 nm layer of alumina.

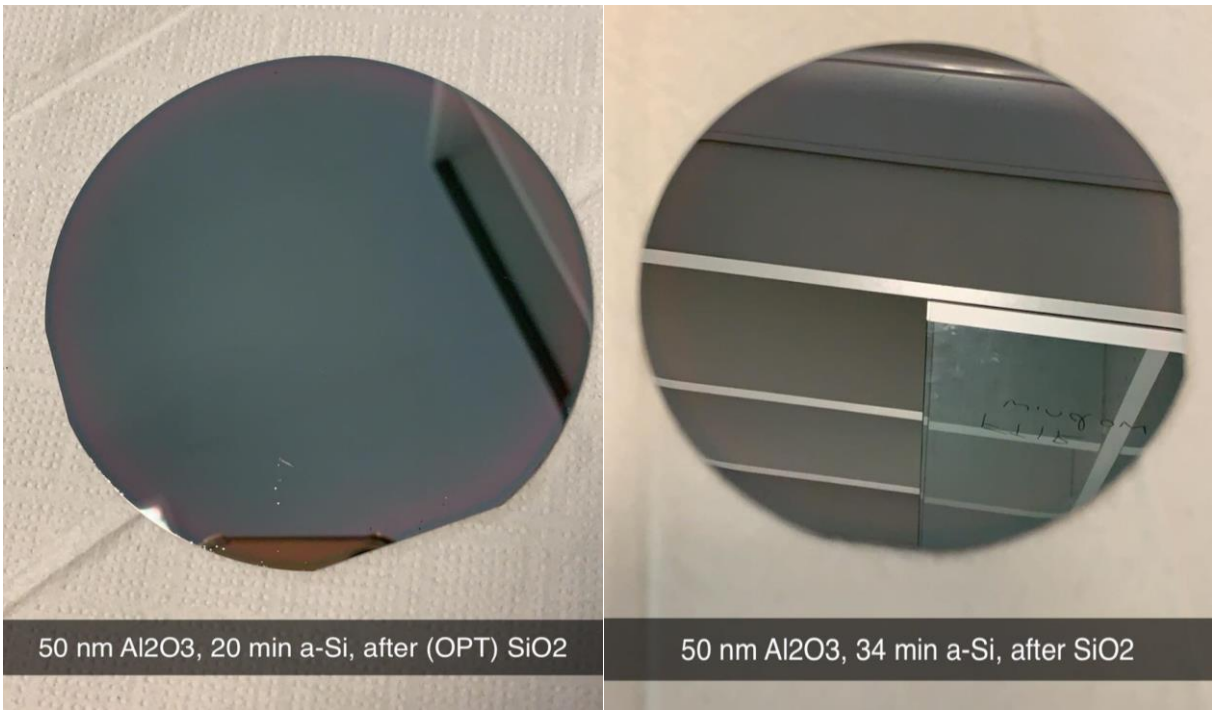

Figure 4.4: Two wafers only difference is the deposition time of a-Si

4.1.2 Measuring the A-Si

As seen in Figure 4.5, SEM and ellipsometry yields very similar measurements. Both show that a higher deposition time yields a thicker layer of a-Si. Since the recipe made with ellipsometry gives very similar results to SEM, the obtained recipe can be used for further work. Table 4.1 gives the values for the thickness of a-Si at the specific deposition time, both measured with SEM and ellipsometry.

Table 4.1: The four samples measured with SEM and ellipsometry

PECVD time [min]	SEM [nm]	Ellipsometry [nm]
12	290.0	280.5
24	516.7	513.8
36	714.9	676.1
48	1065.7	1025.0

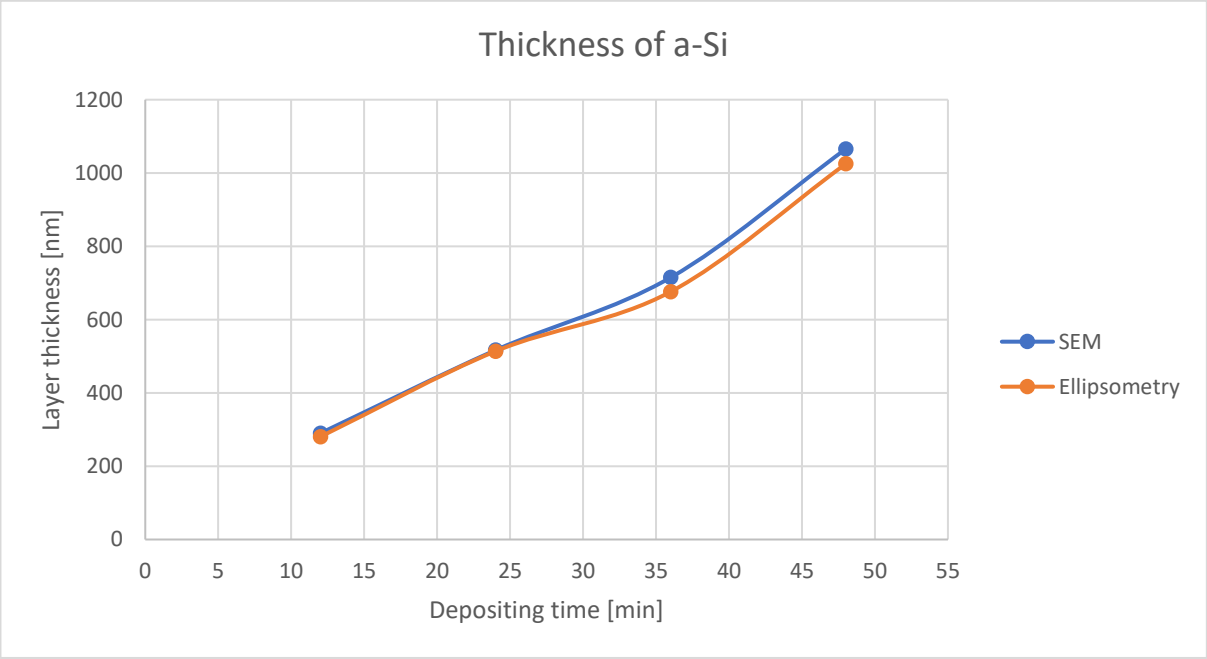

Figure 4.5: The a-Si thickness measured with SEM and ellipsometry

4.1.3 CMP of A-Si with Different Slurry Concentrations

As shown in Figure 4.6, the slurry concentration does affect the amount of material removed (AMR). The higher the slurry concentration, the more material will be removed. Wafer nr. 4 was polished with pure slurry and has achieved the highest amount of material removed after 70 seconds of CMP. Wafer nr. 3 was diluted 1:1 with DI-water and lost a lot of material, while wafer nr. 1 with the most diluted slurry has lost less material. Wafer nr. 1 has lost around 103.7 nm, and wafer nr. 4 has lost around 154.1 nm. As shown in Figure 4.6, wafer nr. 2 loose material very homogeneously, while the others have lost material more non homogeneously.

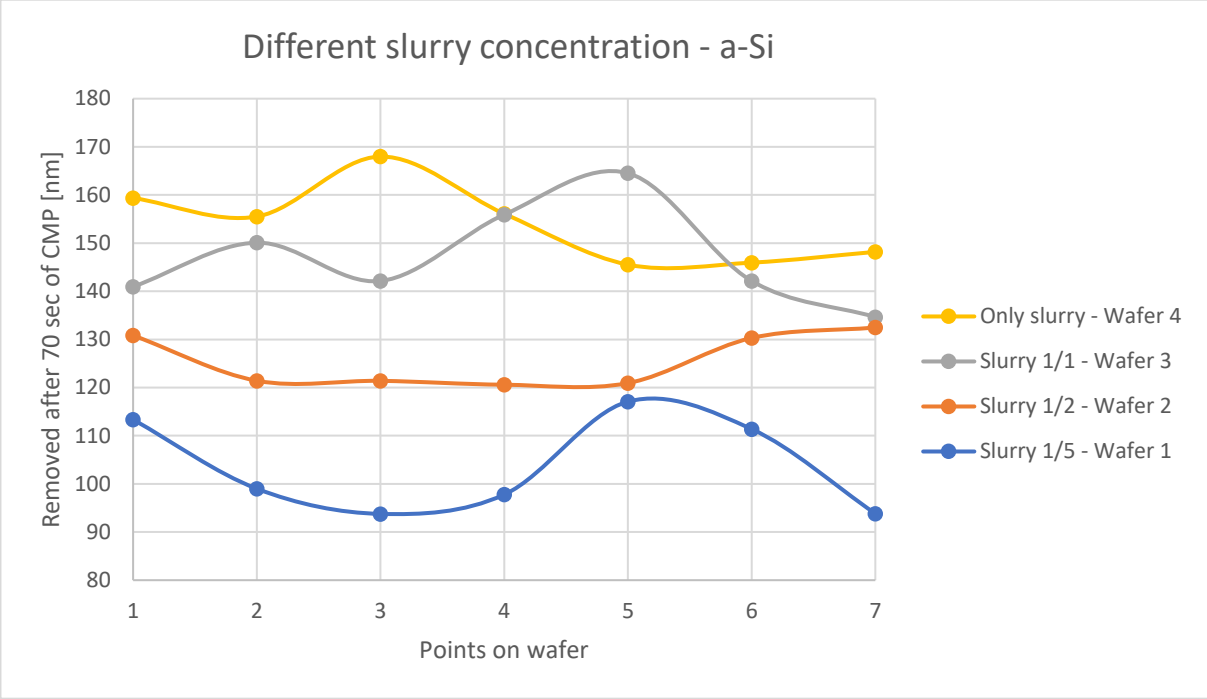

Figure 4.6: How the slurry concentration affects the AMR after 70 seconds of CMP

As can be observed in Figure 4.7, there is a high correlation between the concentration of the slurry, and how much material of the layer is removed during the CMP. Higher slurry concentration gives a higher AMR, and it is possible to see a logarithmic relation. The slope is calculated based on the four values. The R^2 value tells us how much the given equation fits the four points. The closer the value is to 1, the better is the equation. Since the R^2 value is 0.932, it is quite good. Since seven points were measured on each wafer, the mean value was calculated and the standard deviation from the mean was included in the figure at that specific point.

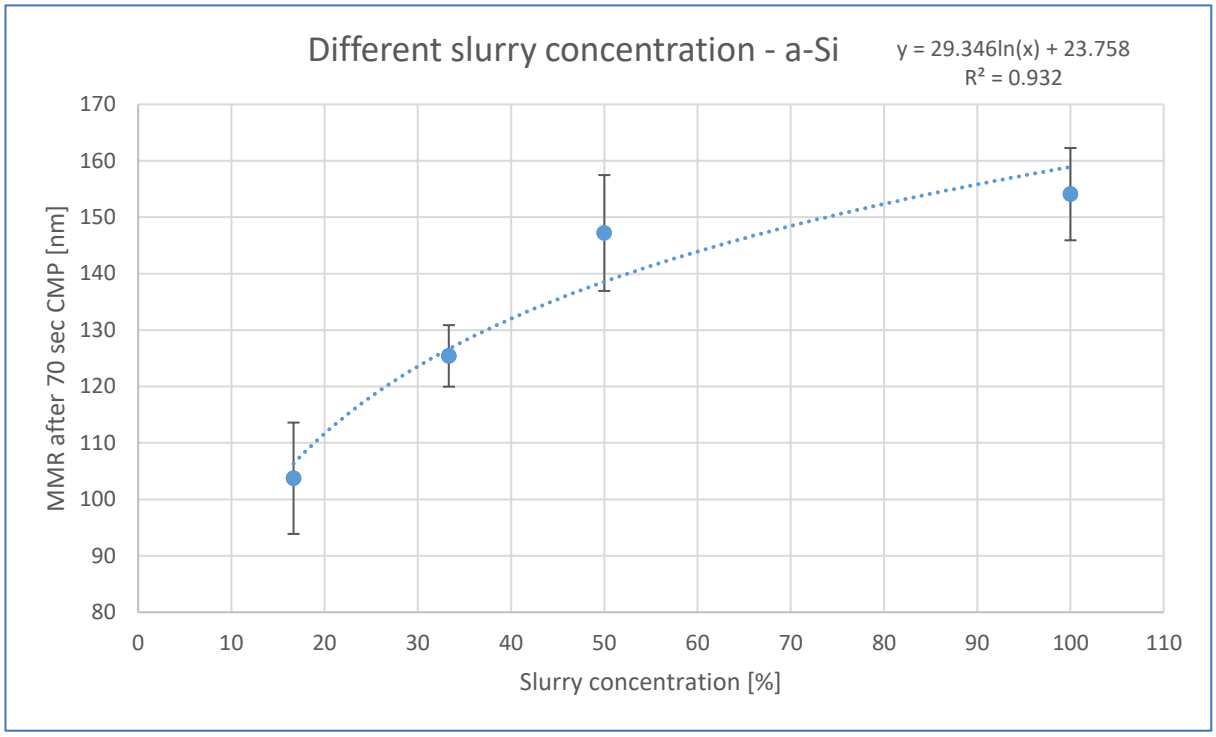

Figure 4.7: Relationship between the concentration of the slurry and MMR after CMP

Table 4.2: The four points given the logarithmic relation

Wafer nr.	Slurries concentration [%]	Mean material removed [nm]	MRR [nm/min]
1	16.67	103.74	62.24
2	33.33	125.42	75.25
3	50.00	147.20	88.32
4	100.00	154.09	92.45

Figure 4.8 shows the roughness of two different wafers after they were polished for 70 seconds. These wafers had the lowest film thickness standard deviation. As shown in the figure, the wafer polished with a slurry concentration 1:2 has a more homogeneous surface. The wafer with slurry 1:2 has a standard deviation of around 6.0 nm while the wafer polished with pure slurry has a standard deviation of around 8.2 nm. It can also be seen that the wafer with the stronger slurry concentration has a smaller thickness of the layer after 70 seconds of polishing compared to the wafer polished with a more diluted slurry.

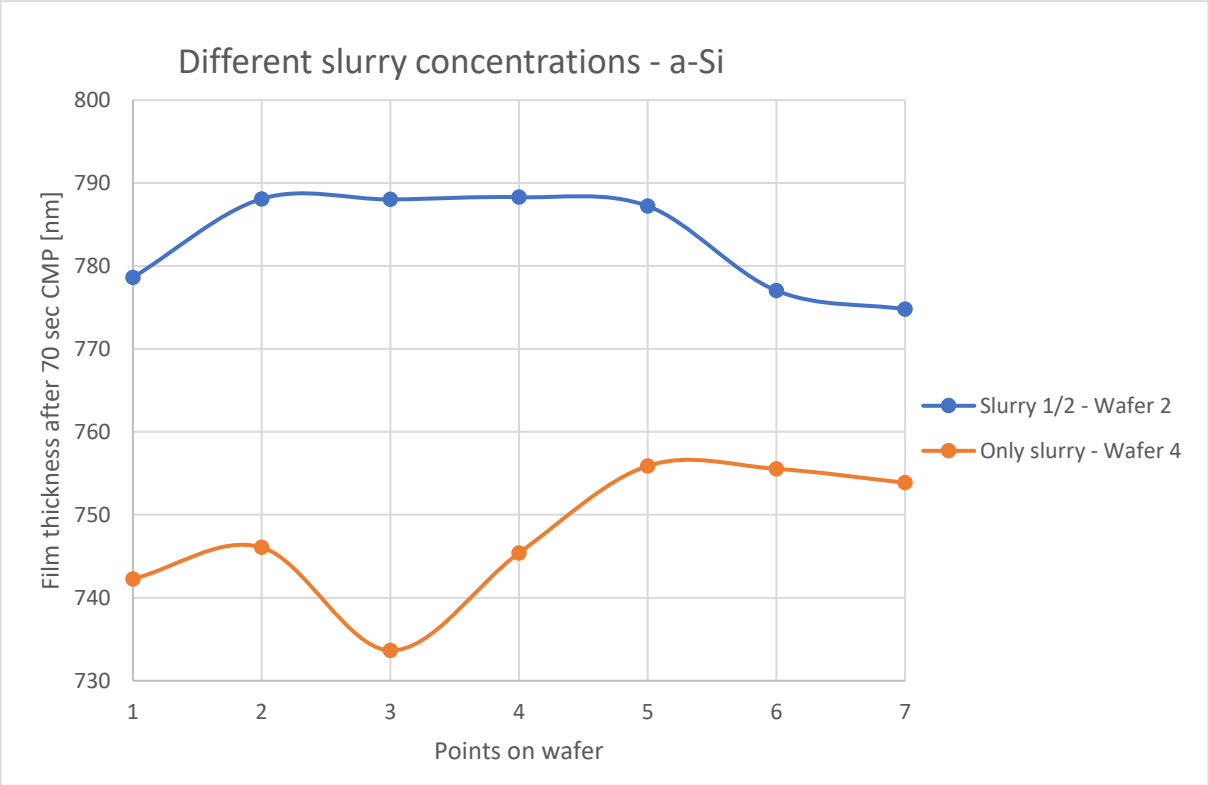

Figure 4.8: The concentration of the slurry influences the surface roughness

4.2 Alumina Wafers

Some of the alumina wafers had very high standard deviation and therefore were not used in the result. Also, one of the wafers broke during the experiment. That is the reason for having more samples than necessary. Since the alumina wafers will only be investigated in the CMP, the subchapters are divided by the different parameters which were focused on: different slurry concentration, backside pressure (BP), and working pressure (WP).

4.2.1 Slurry Concentration

As shown in Figure 4.9, the slurry concentration does affect the AMR. The higher the slurry concentration, the more material will be removed. Wafer nr. 13 was polished with the least diluted slurry and has lost the most material after 30 seconds of CMP. Wafer nr. 9 that had the most diluted slurry has lost less material. Wafer nr. 9 has lost around 22.9 nm, and wafer nr. 13 has lost around 65.2 nm. As seen in Figure 4.9, wafers 9 and 16 loose material very homogeneously, while both wafer 13 and 15 have lost more material in the center than the edges. The amount of material removed (AMR) at the edges of wafers 13 and 15 is almost identical.

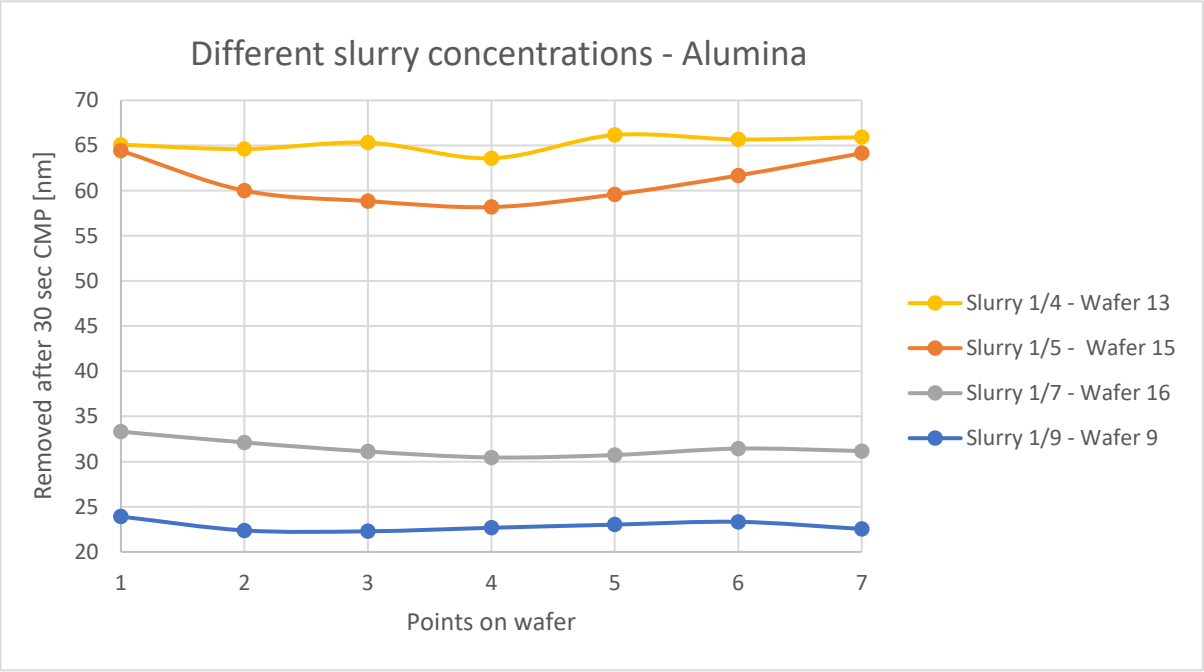

Figure 4.9: How the slurry concentration affects the AMR after 30 seconds of CMP

As shown in Figure 4.10, there is a high correlation between the concentration of the slurry, and how much material of the layer is removed during the CMP. Higher slurry concentration gives a higher MMR, and it is possible to see a linear relation. The slope is calculated based on the four values. Since the R^2 value is 0.977, it is quite good.

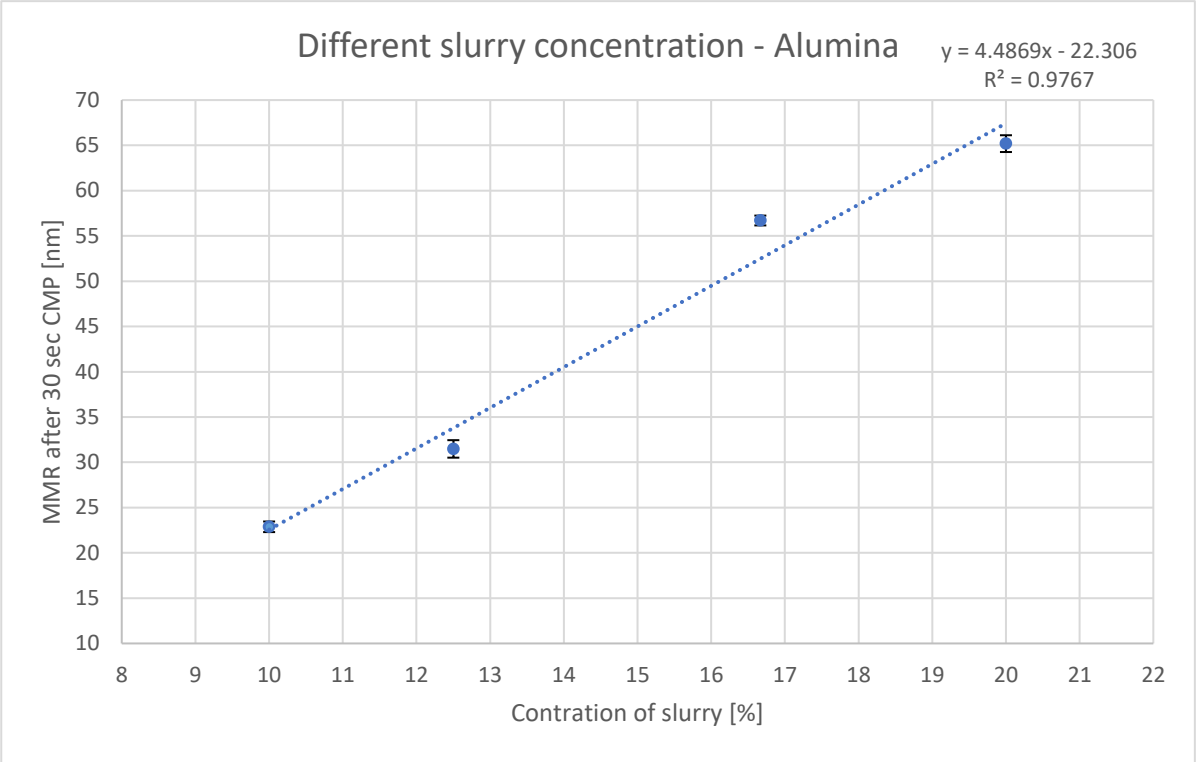

Figure 4.10: Relationship between the concentration of the slurry and MMR after CMP

Table 4.3: The four points given the linear relation

Wafer nr.	Slurries concentration [%]	Mean value of material removed [nm]	MRR [nm/min]
9	10	22.880	45.76
16	12.5	31.480	62.96
15	16.67	56.703	113.41
13	20	65.190	130.38

Figure 4.11 shows the roughness of two different wafers after they were polished for 90 seconds. As shown in the figure, the wafer polished with the higher slurry concentration has a more homogeneous surface. The wafer with slurry 1:9 has a film thickness standard deviation of around 2.00 nm while the wafer with slurry 1:7 has a standard deviation of around 0.78 nm. It is also evident that the wafer with the higher slurry concentration has a smaller layer thickness after 90 seconds of polishing compared to the wafer polished with a more diluted slurry.

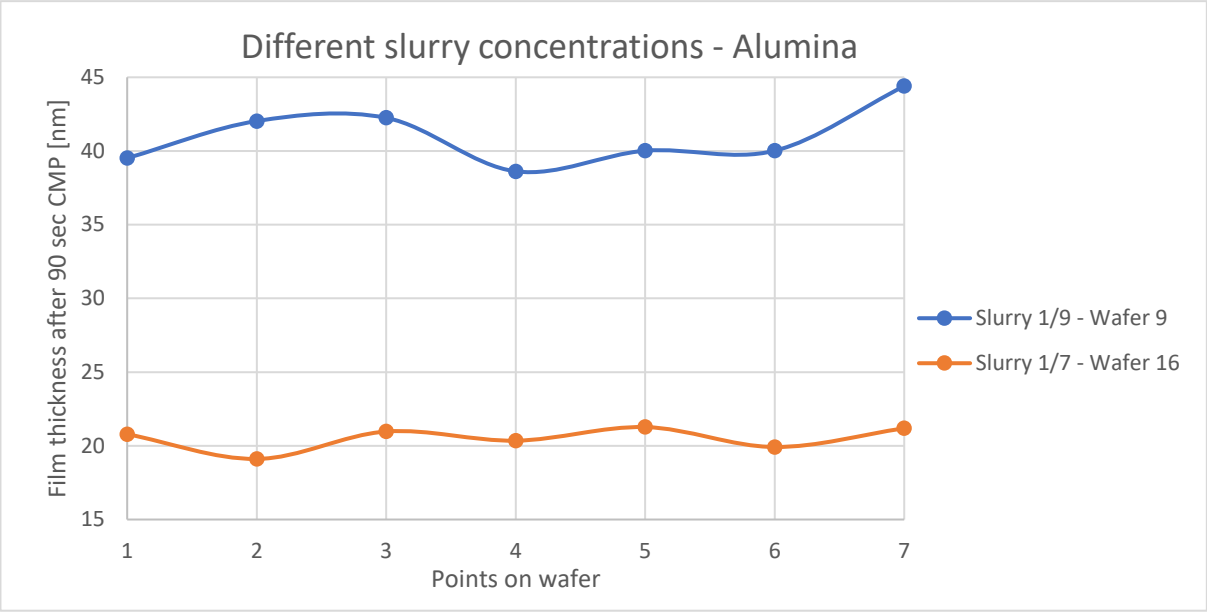

Figure 4.11: The concentration of the slurry influences the surface roughness

Figure 4.12 shows that there is a high correlation between the polishing time and how much material is removed. Both have an approximately linear relation between the time the wafer was polished, and the mean value of material removed. It was found that all wafers, independent of the slurry concentration, WP, and BP have a linear relation between the MRR and the CMP time. Since seven points were measured on each wafer, the mean value was calculated and the standard deviation from the mean was included in the figure at that specific point.

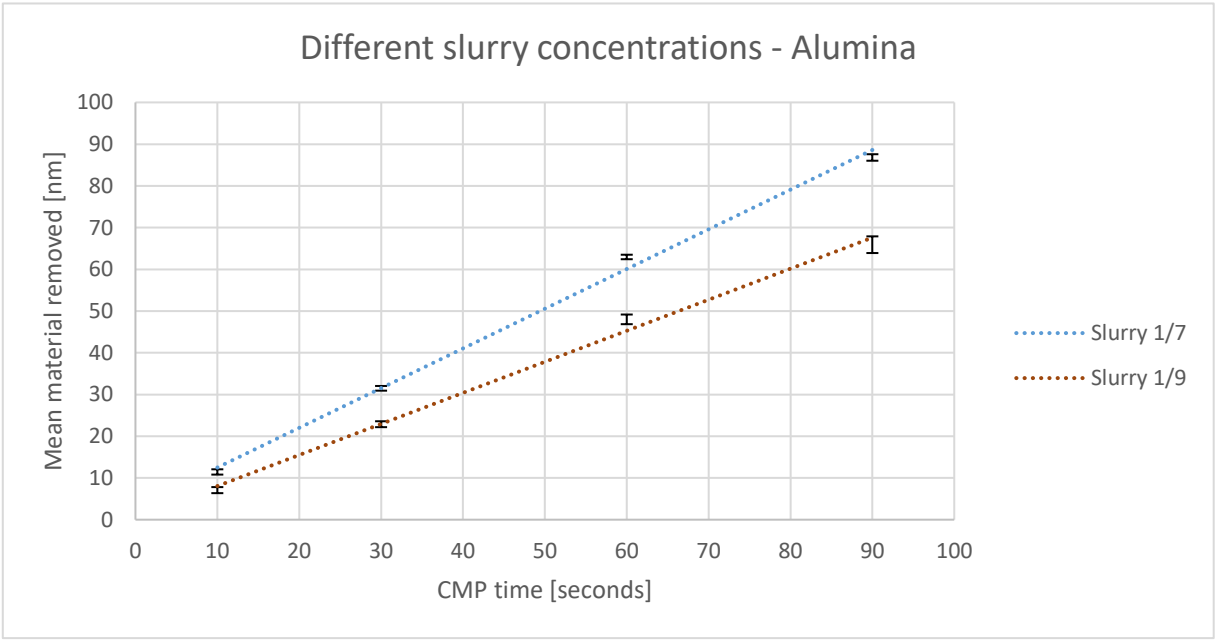

Figure 4.12: The relation between the MMR and the CMP time

4.2.2 Backside Pressure

What is striking in Figure 4.13 is that there is no correlation between the backside pressure (BP), and material removed after 90 seconds. Wafer nr. 6 had a BP of 400 and had a significantly higher removal rate (RR) than the other wafers, and wafer nr. 2 that had a BP of 300, had the lowest RR. The wafers with BP of 400 and 300 also had the highest standard deviations, with a very big variation between how much material was removed at the edges and the center of the wafer. The wafers with BP of 100, 200, and 500 have a more consistent AMR.

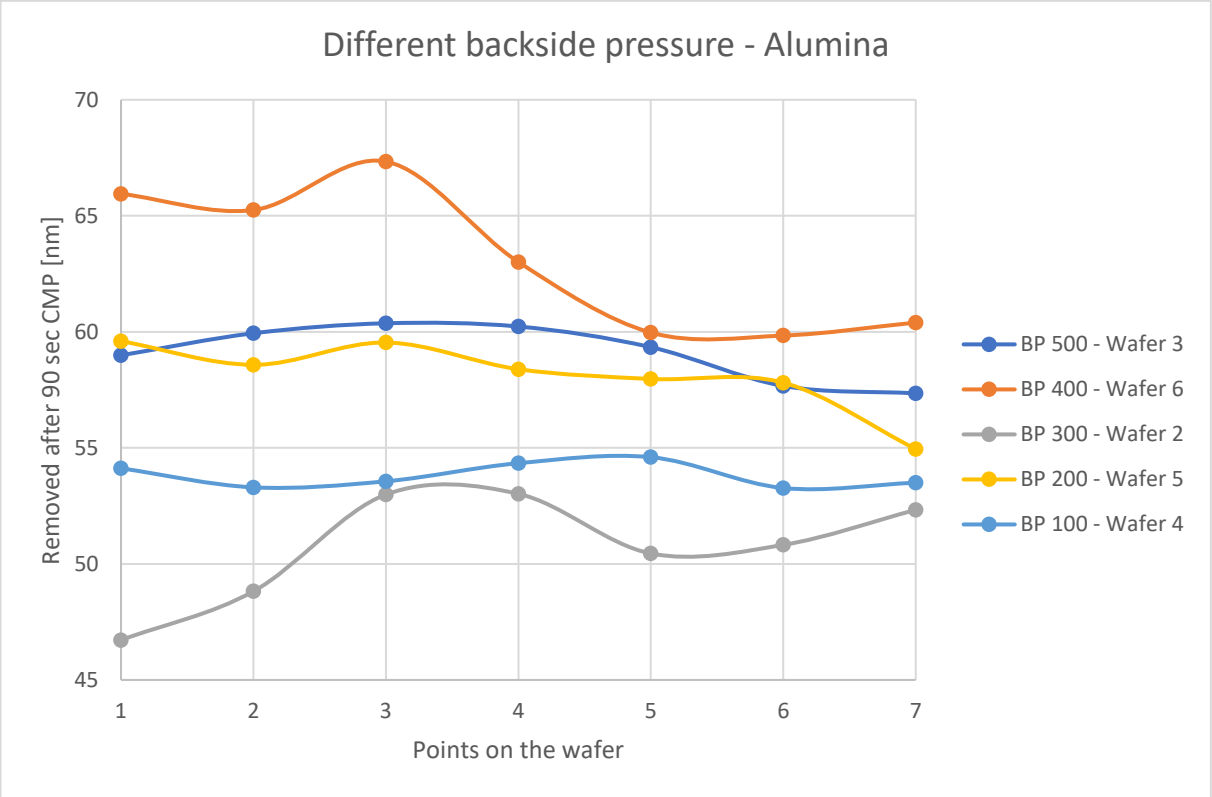

Figure 4.13: How BP affects how much material is removed after 90 seconds of CMP

Figure 4.14 clearly shows that there is no correlation between the BP and the AMR from the wafers. The wafers with BP of 200, 400, and 500 had the highest mean value of material removed after 90 seconds of polishing, while the wafers with 100 and 300 BP had the lowest. The standard deviation is also plotted for each point.

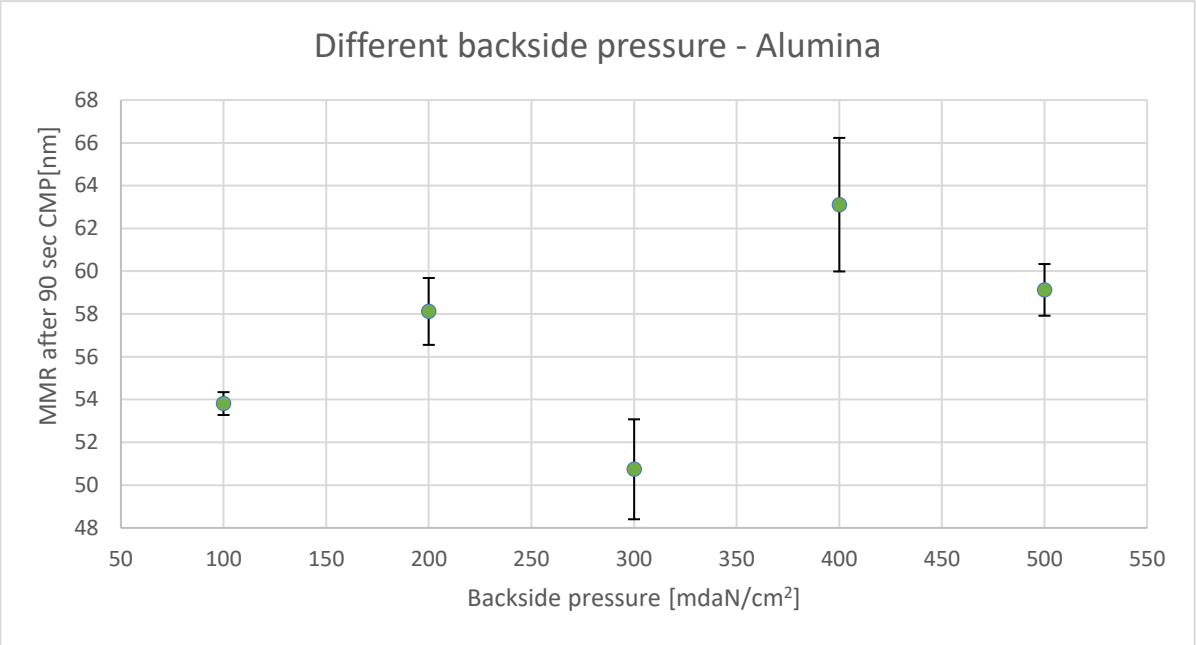

Figure 4.14: No relation between the BP and MMR after 90 seconds of CMP

In Figure 4.15, the two wafers with the most homogenous surface are plotted. Both wafers with BP of 200 and 500 had after 90 seconds of CMP a similar layer thickness, surface roughness and the lowest film thickness standard deviation. The wafer using a BP of 200 has a standard deviation of around 0.86 nm while the wafer using BP of 500 has a standard deviation of around 0.98 nm. What is interesting in the figure is that the thickness of the layer on the edges of the two wafers is quite similar, as well as it being higher at the edges compared to the centers.

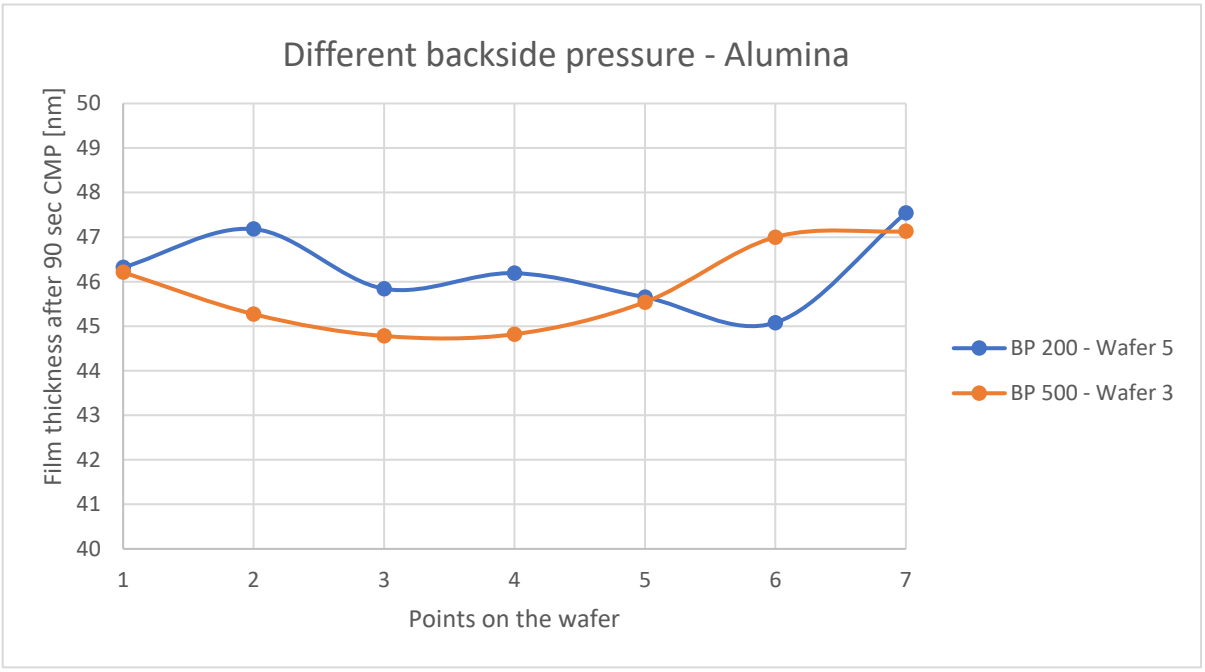

Figure 4.15: The BP influences the surface roughness

4.2.3 Working Pressure

As observed in Figure 4.16, a higher WP will have a higher AMR, except in the samples with a WP of 100 and 200. It can also be seen that changing the WP will have a very small effect on how homogeneous the resulting layer thickness gets.

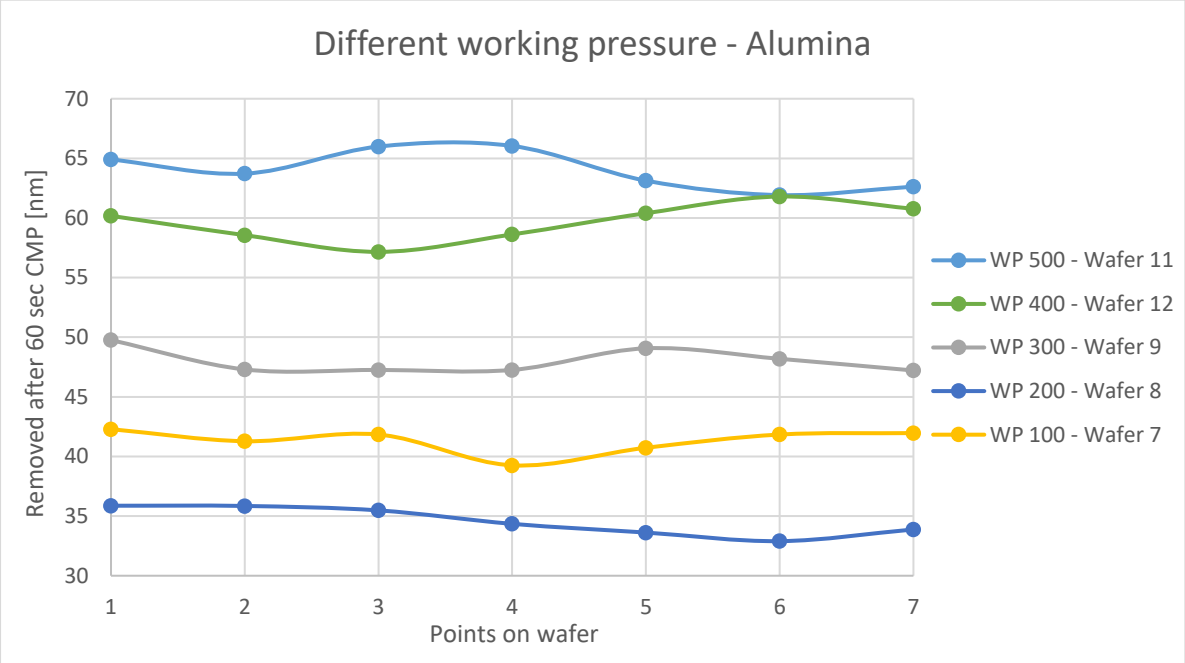

Figure 4.16: How the WP affects how much material is removed after CMP

Higher WP gives a higher mean value of material removed, expect between the 100 and 200. One can observe this in Figure 4.17, as well as the standard deviation at the different WP. They all had a standard deviation of between 1.2 and 1.6 nm. It is hard to tell if the WP will give a linear relation to the MMR. As one can see R^2 is close to 1, but not very close. The different standard deviation has similar values.

Table 4.4: The five points almost making a linear relation

WP [mdaN/cm^2]	Mean value of material removed [nm] / MRR [nm/min]
100	41.31
200	34.56
300	48.01
400	59.64
500	64.05

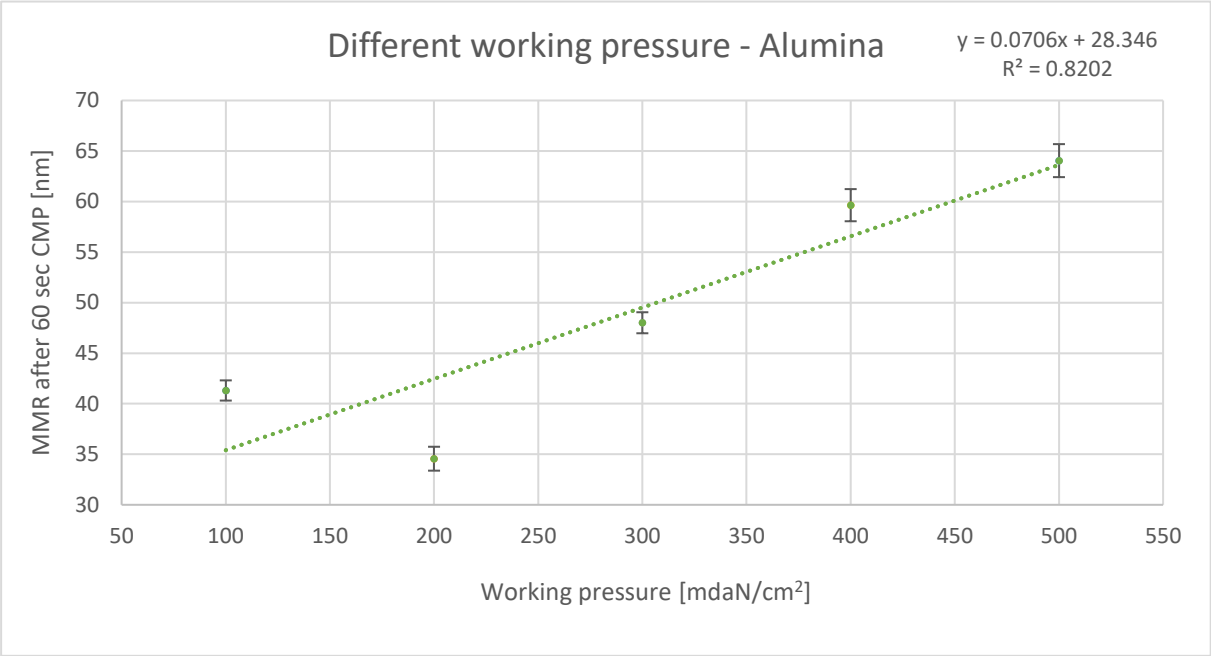

Figure 4.17: Relation between the WP and MMR after 60 seconds of CMP

In Figure 4.18 the two wafers with the most homogenous surface are plotted. Both wafers with WP of 300 and 500 had after 60 seconds of CMP a relatively homogenous surface. Wafer nr. 9 has a film thickness standard deviation of 1.16 nm while wafer nr. 11 has a standard deviation of 1.46 nm. What is interesting in the figure is that the wafer polished with a WP of 500 has a pit in the center of the wafer, while the wafer polished with a WP of 300 has an elevated center.

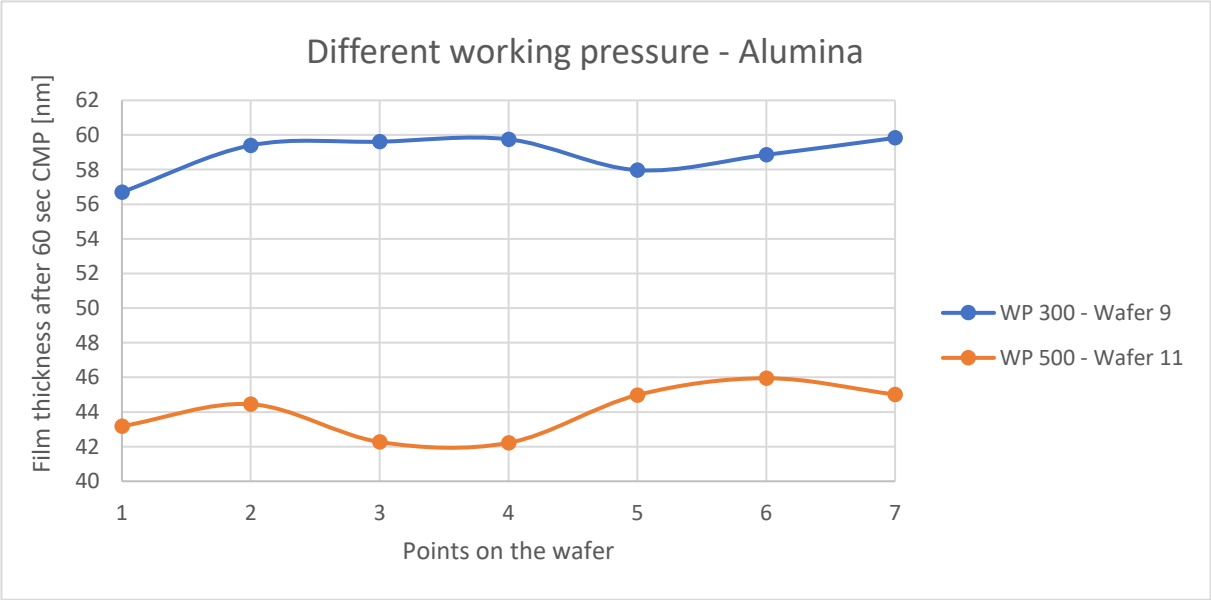

Figure 4.18: Different WP will affect the thickness of the wafer after 60 seconds CMP

4.3 Silica Wafers

4.3.1 Slurry Concentrations

As shown in Figure 4.19, the slurry concentration has a huge impact on the AMR. A more concentrated slurry will remove more silica from the wafer. The wafer polished with a slurry of 1:7 ratio, has a very similar AMR throughout the wafer, after 90 seconds of CMP. Wafers polished with a slurry of 1:5 and 1:3, have a slight difference between AMR at the center compared to the edges.

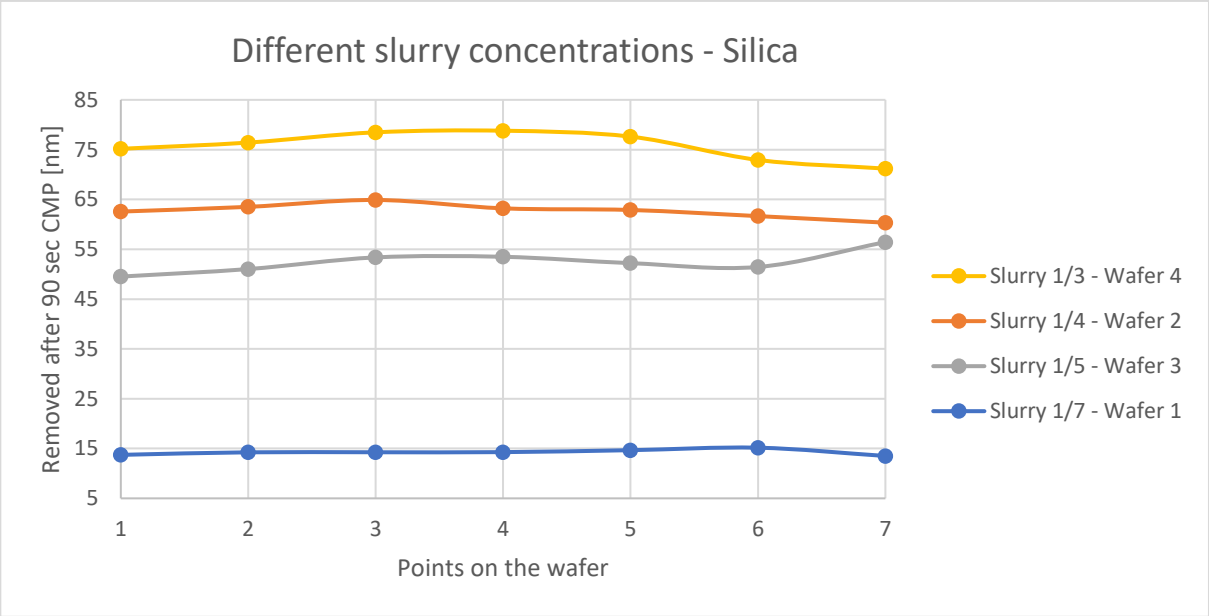

Figure 4.19: How slurry concentrations affects how much material is removed

Figure 4.20 is showing the AMR with different slurry concentrations after 90 seconds of CMP. Here, it is hard to tell if the relation is linear, polynomial, logarithmic, or another function. However, one can observe a clear correlation between slurry concentration and the amount of removed material. Increasing slurry concentration yields a higher MMR. The R^2 value is close to 1, which means that the graph fits almost perfectly to the five points. It was assumed that the graph is following a 3rd degree polynomial.

Table 4.5: The five points giving the polynomial

Wafer nr.	Slurries concentration [%]	Mean material removed [nm]	MRR [nm/min]
1	12.5	14.26	9.51
3	16.67	52.50	35.00
2	20	62.73	41.82
4	25	75.80	50.53
5	33.33	423.57	282.38

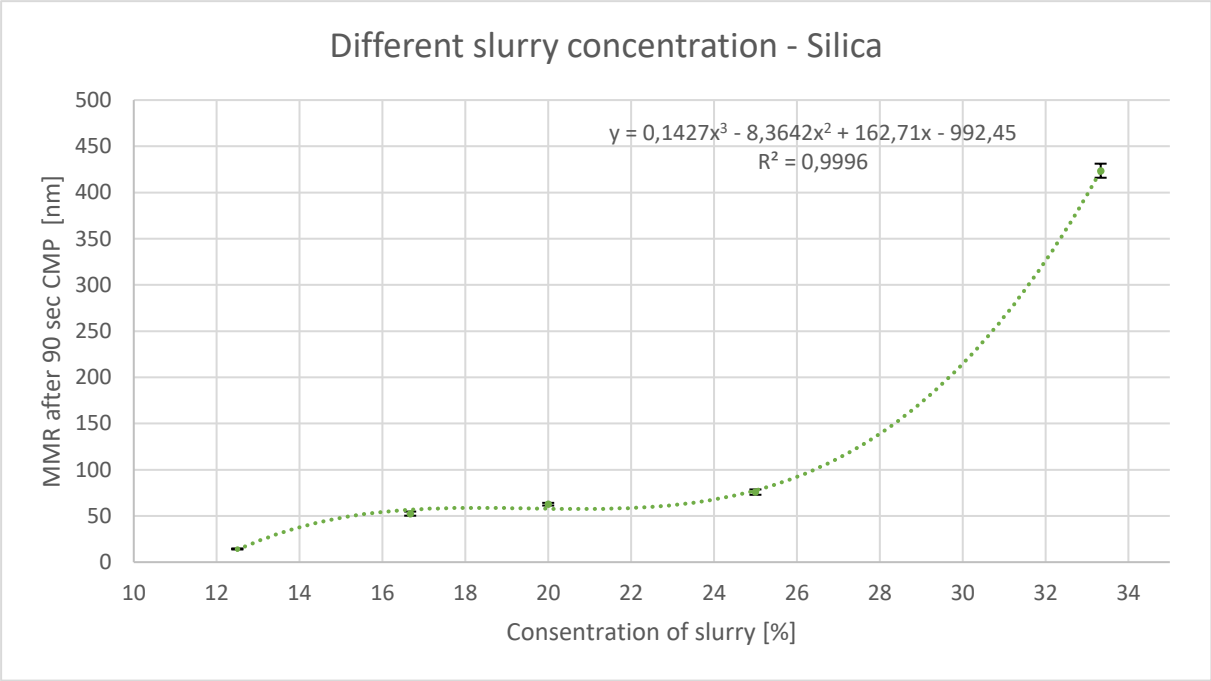

Figure 4.20: The relation between the MMR and slurry concentration

In Figure 4.21, the two wafers with the lowest film thickness standard deviation are plotted. The wafer with slurry 1:7 has a standard deviation of only 1.72 nm while the wafer with slurry 1:5 has a standard deviation of 5.28 nm. This means that both wafers have a relatively homogeneous surface after polishing, especially when the wafer is polished with slurry 1:7.

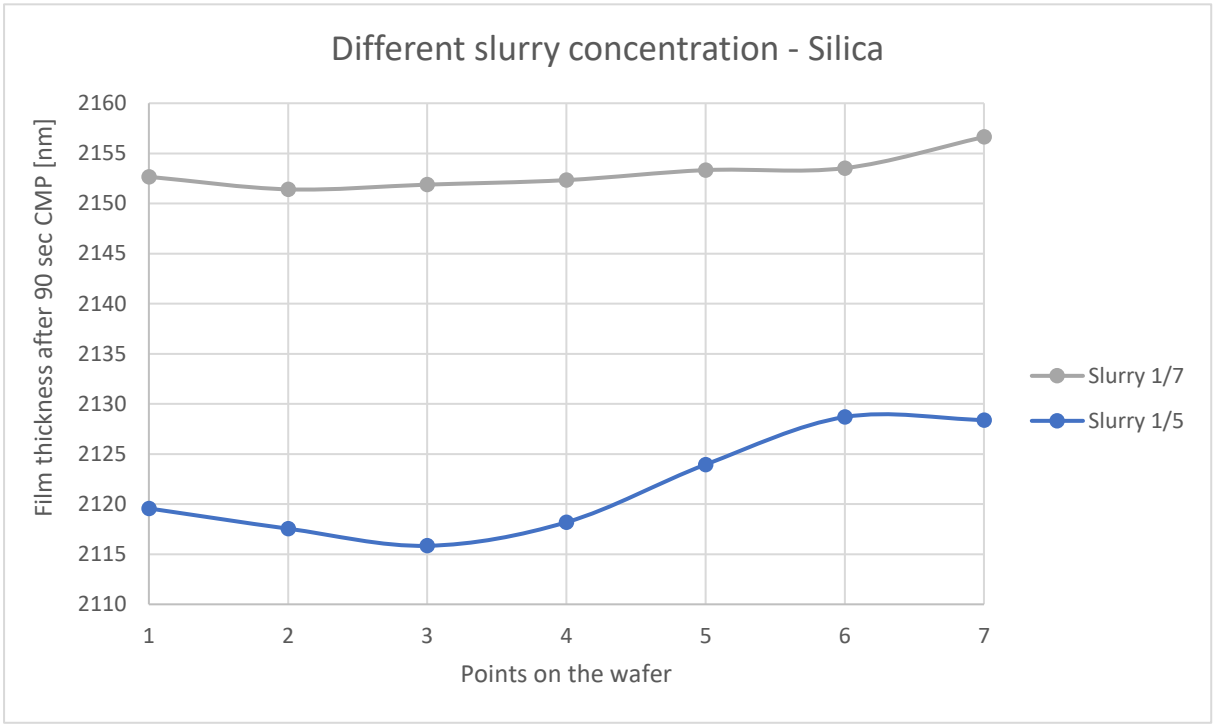

Figure 4.21: Different slurry concentration will affect the surface roughness after CMP

4.3.2 Backside Pressure

What stands out in Figure 4.22 is that there is no correlation between the BP and the AMR. The wafer with BP of 500 had the highest removed material after 360 seconds of CMP. The wafer that had the 2nd highest was the wafer with the BP of 100. It can also be seen very clearly that more material is removed from the center of the wafers compared to the edges.

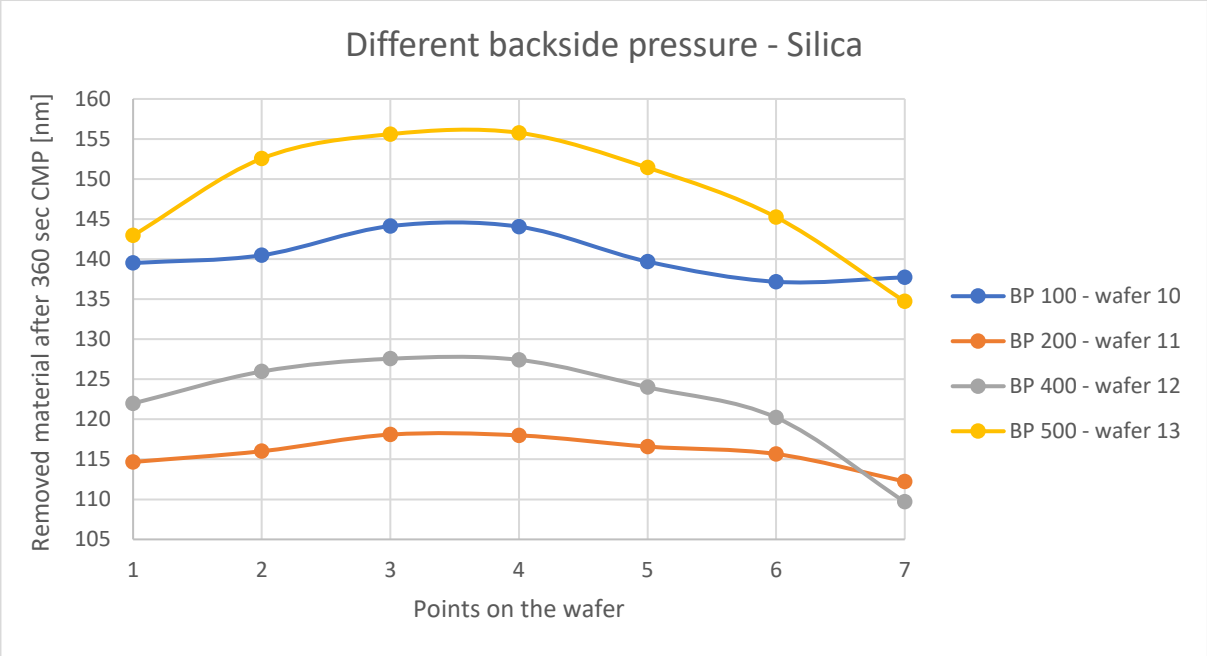

Figure 4.22: BP affects how much material is removed from the surface

In Figure 4.23, the removed material after 360 seconds of CMP is plotted versus the BP. It is hard to say if there is any clear correlation. It is assumed that the graph is following a 2nd degree polynomial. The standard deviation is plotted for each point. As observed, the standard deviation is quite high, so it can be that there is no relation at all between the BP and the MMR. The wafer that was polished with BP of 200 had the lowest MMR, but also the lowest standard deviation.

Table 4.6: The four points making the polynomial

BP [mdaN/cm^2]	Mean value of material removed [nm]	MRR [nm/min]
100	140.39	0.39
200	115.89	0.32
400	122.40	0.34
500	148.32	0.41

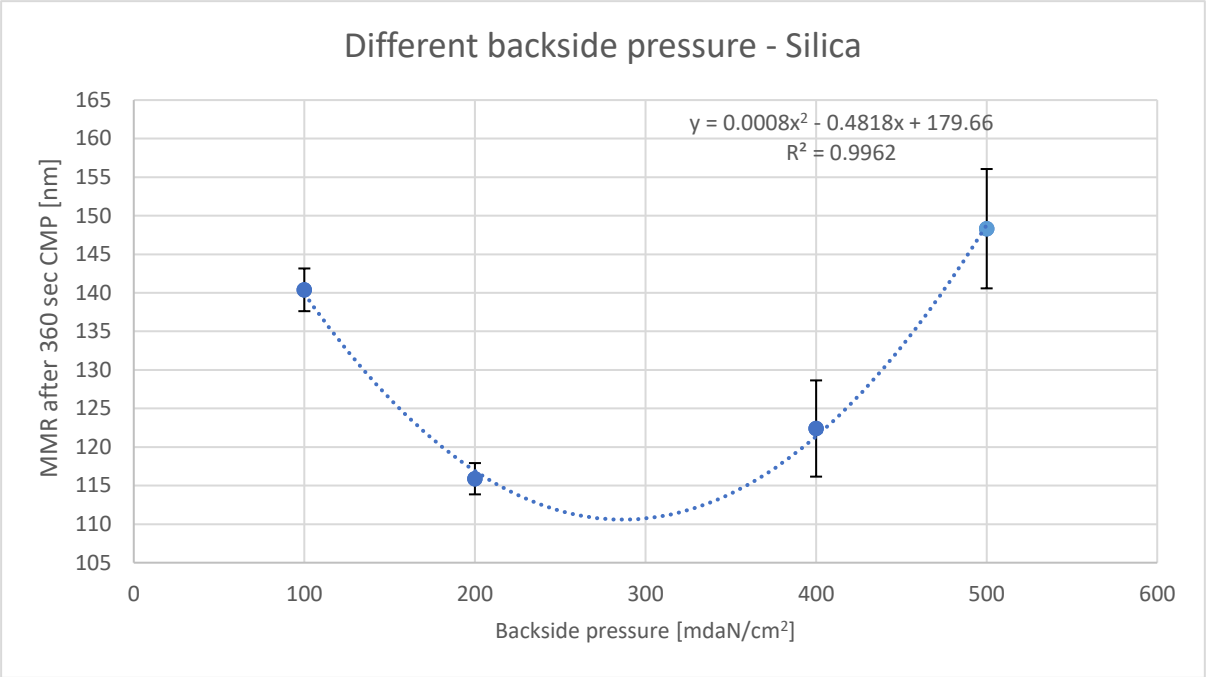

Figure 4.23: The MMR after 360 seconds of CMP at different BP

The two wafers with the smallest film thickness standard deviation are the wafer with the lowest BP and are shown in Figure 4.24. The wafer polished with a BP of 100 has a U-form with a higher film thickness on the edges than the center. The wafer polished with a BP of 200 has a slope from lower MRR on the one side compared to the other. The standard deviation of wafer nr. 10 is 9.35 nm after 360 seconds of CMP, while the standard deviation of the wafer nr. 11 is 7.1 nm.

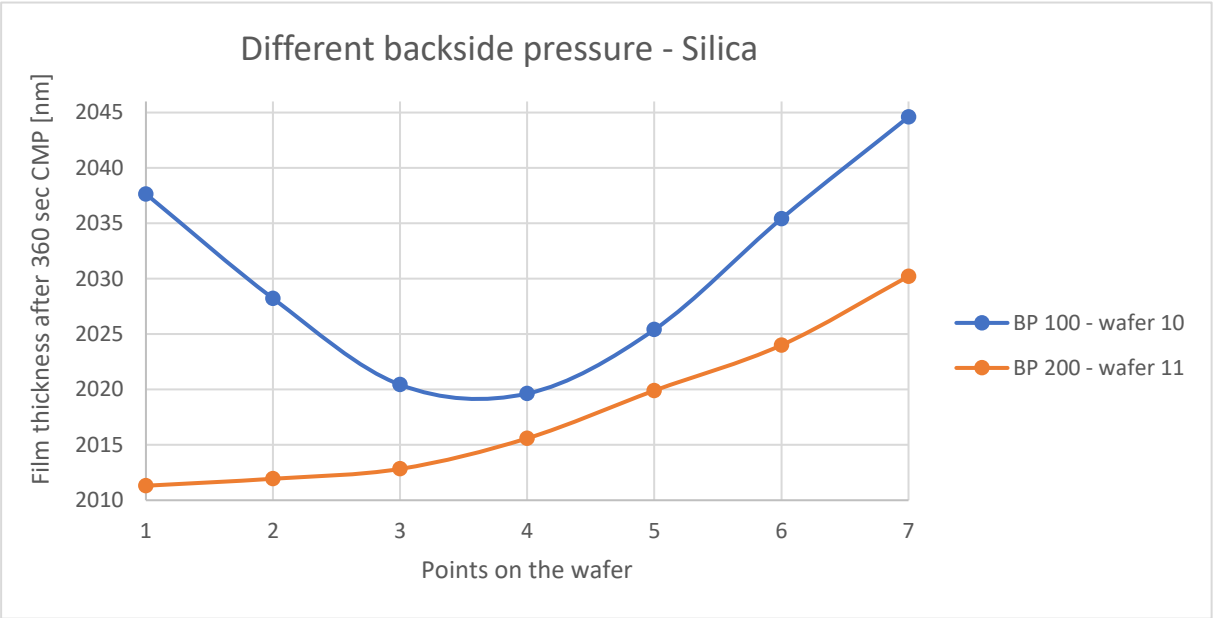

Figure 4.24: Different BP will affect the thickness of the film

4.3.3 Working Pressure

What can be understood from Figure 4.25 is that the higher WP will have a higher AMR after 360 seconds of CMP. The AMR stayed homogeneous when changing the WP, except from the wafer with the WP of 400.

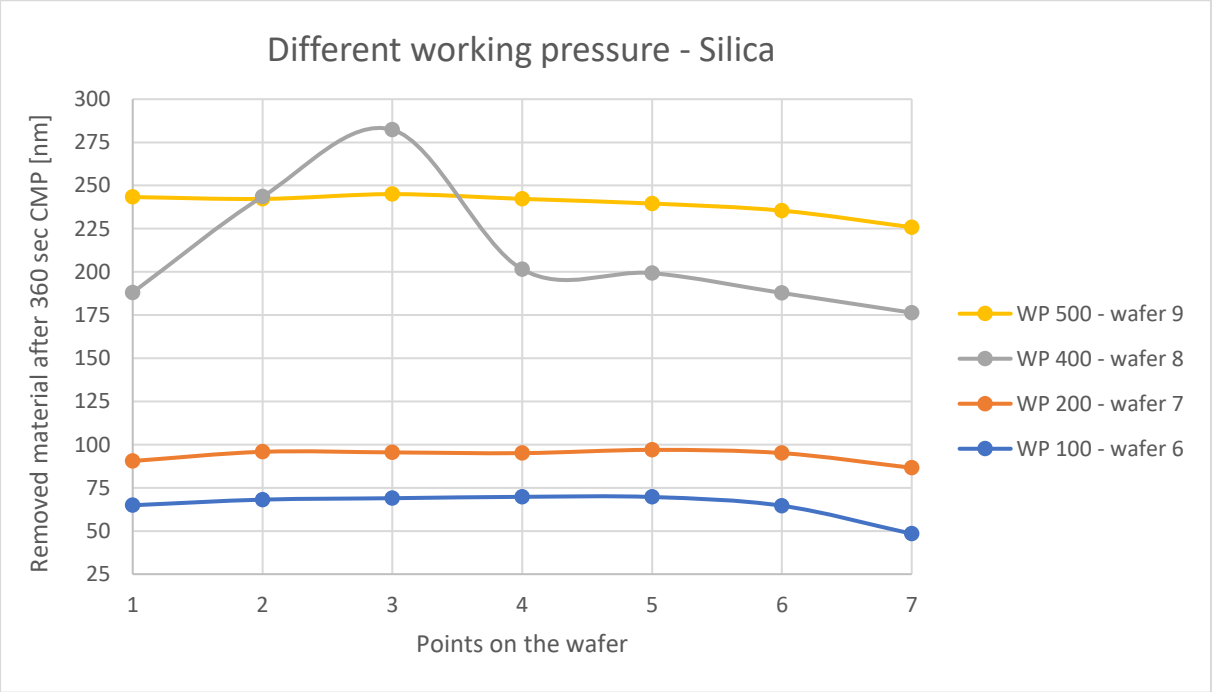

Figure 4.25: Different WP will affect the removed material from the surface

Higher WP gives a higher MMR. As seen in Figure 4.26, the MMR is almost linear. The standard deviation at the different WP is also shown. All had a very low standard deviation expect the wafer with the WP of 400. Since the R^2 is close to 1, it can be assumed that the given equation is a good fit. Table 4.6 gives an almost linear relation.

Table 4.7: The four points given the linear relation

WP [mdaN/cm^2]	Mean material removed [nm]	MRR [nm/min]
100	64.93	0.18
200	93.65	0.26
400	211.27	0.59
500	239.11	0.66

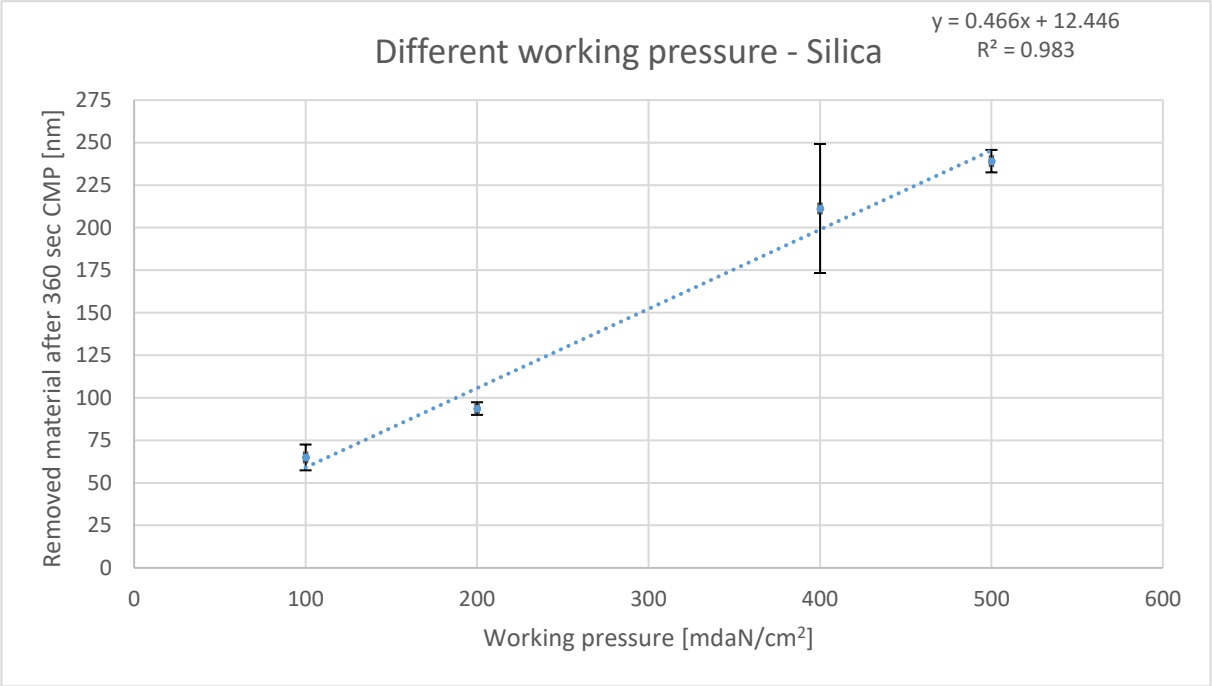

Figure 4.26: A linear relation between the WP and the MMR

The two wafers with the lowest film thickness standard deviation are wafers nr. 7 and 9 and are shown in Figure 4.27. The wafer with a working pressure of 200 has a standard deviation of 8.15 nm, while the wafer with a working pressure of 500 has a standard deviation of 11.94 nm. This means that both wafers have a relative homogeny surface after polishing. They both have a slightly curved shape with more material removed from the center.

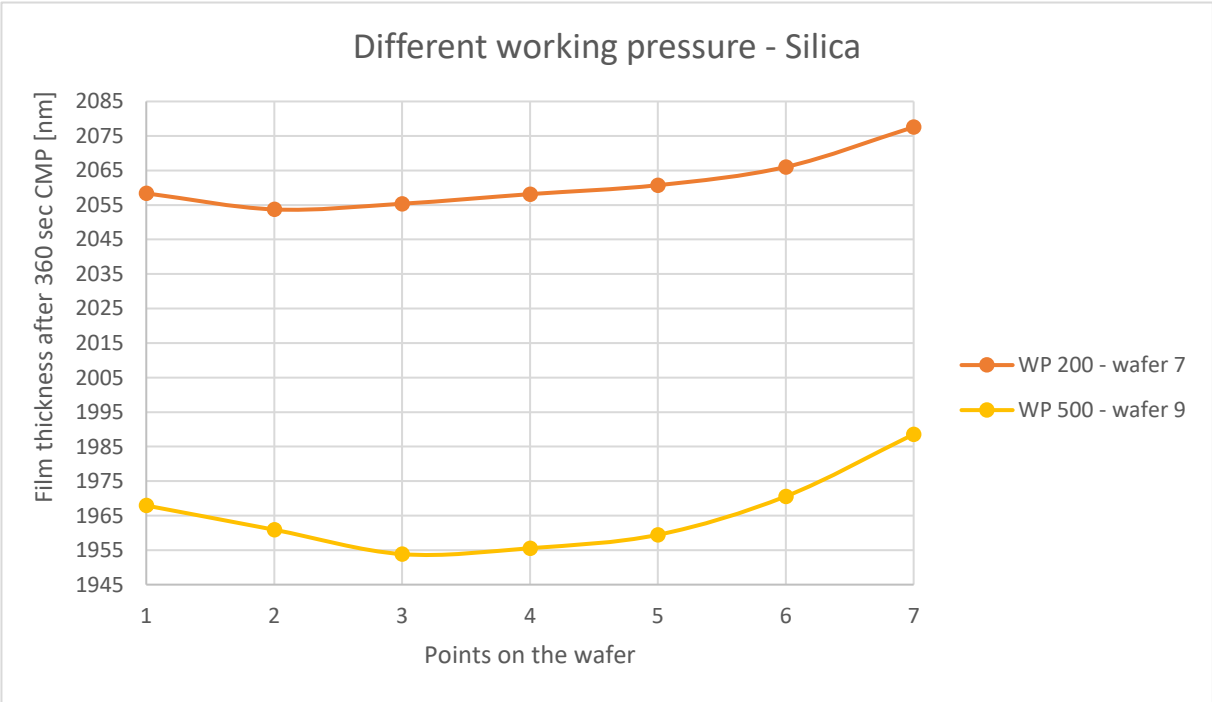

Figure 4.27: The working pressure will affect the film thickness after CMP

5 Discussion

This Chapter will discuss three processes, deposition, measurement, and polishing. How the deposition time, temperature, and recipe will affect the amorphous silicon (a-Si) layer, and how it is possible to avoid blisters on the wafers. How the thickness of the a-Si layer is measured in SEM and ellipsometry, and the most important part, how the CMP will affect the a-Si, silica (SiO_2), and alumina (Al_2O_3) wafers. How changing the slurry concentration, the backside pressure (BP), and working pressure (WP), will affect the wafers. It is clear from the results that changing the different parameters yielded very different outcomes. A focus will be put on the effect these three parameters have on the amount of material removed (AMR), the standard deviation of the AMR, and the standard deviation of the film thickness. The results from the experiment will be compared with the theory presented in chapter 2. The discussion will be presented in three subchapters, one for each of the materials: a-Si, silica, and alumina. The subchapters are divided further between the different experiment and the parameters which were focused on.

5.1 A-Si Wafers

5.1.1 Depositing A-Si

As seen in section 4.1 and Figure 4.2, the number of blisters the wafers received does not change drastically by changing the deposition time. The wafer with a deposition time of 20 min of a-Si has a yellowish color due to the thinner layer of a-Si, while the 34 min wafer is grey-blueish color. Both wafers have black spots and smaller and bigger blisters all over the wafer. Both wafers were made with the same recipe that yielded unsatisfactory results. This can be due to the poor adhesion between the a-Si and the alumina at a temperature of 250 degrees. As stated in Chapter 2, the a-Si changes its properties drastically when the thermal diffusion parameters, like time and deposition temperature in the PECVD vary, and it can be fewer defects if the film thickness increases. It could be that the wafers would have less or more blisters if the deposition time were drastically different, but between the 20 min and 34 min layer, there was almost no difference. The stress value was not measured and could be significantly different.

As shown in Figure 4.3, there are much fewer blisters when the deposition temperature goes down. The wafer made at 200 degrees has blisters just on one edge of the wafer, while the wafer made at 180 degrees has none. It is known that the deposition of a-Si is very complicated and dependent on both physical and chemical interaction and the

deposition surface. In this experiment, all the wafers were deposited with the same power and frequency over a 50 nm alumina layer. The deposition surface should be similar, but the wafer made at 200 degrees in Figure 4.3 has many blisters at the edge. This can be due to contamination after the wafer was cleaned in the plasma cleaner. Also, the metal tweezer used for picking up the wafers can contaminate the surface, which affects the deposition conditions of a-Si.

It is known that a-Si prefer to be deposited over an oxide layer, and when a-Si is deposited over a crystalline material, blisters or hillocks and bad adhesion can appear between the two layers. Since the alumina layer is crystalline, it makes sense that the a-Si layer struggles with adhering. In Figure 4.4, the wafers are made with a SiO_2 recipe that yields smooth surfaces with no blisters independent of the deposition time, although they were made at 250 degrees. In comparison to Figure 4.2, both wafers in Figure 4.4 are blue or grey, and not yellowish. This color difference can be due to better adhesion, which results in a different bonding between a-Si and silica compared to a-Si and alumina.

Since there were much fewer blisters when a-Si was deposited at a lower temperature over an (OPT) SiO_2 layer, this was the preferred approach to manufacture wafers for the CMP experiments. The recipe used was MAYA (OPT) SiO_2 + (OPT) a-Si (180 degrees).

5.1.2 Measuring A-Si

The results show that the SEM and the ellipsometry measurements with the recipe used, yield very similar values. It makes sense that a higher deposition time yields a thicker layer, and as seen from the previous section, the graph is linear. Both SEM and ellipsometry can yield inaccurate measurements. As shown in Figure 2.32, the different layers can be measured in SEM. However, it is complicated to measure in the nanometer size due to a rough surface. As stated in Chapter 2, ellipsometry has a considerable advantage over other techniques because it is not necessary to cut the specimen to a specific size or be used in a vacuum. However, ellipsometry needs a model to measure the layer thickness. This can give inaccurate measurements. Since SEM and ellipsometry with the recipe used yield very similar values, the ellipsometry recipe was used for the CMP measurements.

5.1.3 CMP of A-Si

As shown in Figure 4.6, a higher concentration of the slurry removed more material from the a-Si wafers. Figure 2.18 [36] states that the MRR should decrease with increasing pH, up to a pH around 11. In the experiments, the pH increases with increasing slurry concentration, up to a pH of around 9. Therefore, a-Si will most likely follow the same trend as Estragnat *et al.* [44] explain. The MRR will, in some way, increase with increasing pH. The a-Si wafers had a logarithmic relation between the concentration of the slurry and the amount of material removed (AMR). Since only four different slurries were tested, it is

hard to tell if a less diluted concentration will follow the same logarithmic relation. To achieve a more accurate result, more samples should be tested.

Estragnat *et al.* [44] look at how the pH will influence the MRR, and not how more particles will influence the MRR, which happens in the experiment when the slurry is less diluted. In Figure 4.8, the two wafers with the film thickness lowest standard deviation are plotted. Wafer nr. 2 is polished with a slurry concentration of 33% and had a significantly lower film thickness standard deviation than the other wafers. It can be that this is random, or that this yielded the best slurry option for polishing the a-Si wafers. Wafer nr. 2 had a standard deviation of around 0.99 nm before CMP, and it increased to 6.0 nm after CMP. Nevertheless, the film thickness standard deviation increased for all the wafers after polishing with the CMP.

5.2 Alumina Wafers

Since the alumina wafers are only investigated in the CMP, the subchapters are divided by the different parameters which were focused on: different slurry concentration, backside pressure (BP), and working pressure (WP).

5.2.1 Slurry Concentrations

As expected, the slurries with higher concentrations removed more material from the alumina wafers. As shown in Figure 4.10, the alumina wafers had a very linear relation between the concentration of the slurry and the MMR. As Hernandez *et al.* [57] also show in Figure 2.20, the slurry concentration will affect the removal rate (RR) on alumina wafers. Their results show that the RR of alumina increases from 40 nm/min with only DI-water to 70 nm/min with a slurry containing alumina particles and H_2O_2. As shown in Table 4.3, the MRR from this experiment increased from 45.76 nm/min with a slurry concentration of 10% to an MRR of up to 130.38 nm/min with a slurry concentration of 20%. The calculated linear equation between the four points is not perfect, but the R^2 value is still very high. The equation shows that the MRR would be negative if the slurry concentration is 0%, which is impossible. Since only four different slurries were tested, it is hard to tell if a higher concentration follows the same trend. To achieve a more accurate result, a slurry concentration of 0% and 100% could be tested and added to the results, to obtain a start- and endpoint. Also, to achieve more accurate results, more samples should be polished, and the slurry mixture should be mixed with high precision using better equipment to achieve accurate results.

After deposition in the ALD, the wafers have a very homogeneous layer of alumina. However, after the CMP, the surface was rougher and more inhomogeneous. As shown in Figure 4.11, after 90 seconds of polishing, the wafers with a slurry concentration of 1:7

and 1:9 had a standard deviation of 0.78 nm and 2.0 nm, respectively. These standard deviations are still very low, and it is possible to say that the wafers are relatively homogenous.

5.2.2 Backside Pressure

As shown in Figure 4.14, the BP does not influence the MMR significantly. However, the BP does influence the planarization of the wafer, as seen in Figure 4.15. In essence, the BP applied is there to stabilize the wafer in the wafer holder to achieve a planar surface. It influences the air cushion between the polishing head and the wafer. A large air cushion can result in an uneven result due to the wafer being able to glide more, while a small air cushion can result in a tilted attack angle.

Moreover, as shown in Chapter 2, the CMP has two different contact modes. This also means that a higher BP not necessarily yields a higher MRR. This is because it will be more complicated for the fluid to move under the wafer if it is in a tilted position. Preston's equation for MRR only takes the downward pressure and velocity into account. However, as Luo *et al.* [43] conclude, it is only possible if the pad is much harder than the material being polished. Many researchers talk about active and inactive abrasives when they try to calculate the MRR. It can be that either if the BP gets too high or too low, the inactive abrasives increase. To find the optimal BP, more wafers should be tested.

As shown in Figure 4.14, different BP gives different MMR standard deviations. It looks like the samples polished with BP at 300 and 400 have a standard deviation value much higher than the other wafers. However, the value is still very low. After 90 seconds of polishing with BP of 300 and 400, they have a standard deviation of 2.3 nm and 3.1 nm, respectively. While the wafer polished with a BP of 100 had a standard deviation at 0.534 nm. It can be that the BP does affect the AMR or the standard deviation, but to verify that more samples should be polished. However, Figure 4.15 shows the two wafers with the lowest film thickness standard deviation. These two wafers had the most homogenous surface after CMP. In conclusion, the best fit in terms of planarization result had a BP of 200 mdaN/cm^2.

5.2.3 Working Pressure

Compared to the BP, the WP has a stronger influence on the MRR. This is due to the WP creating the main pressure on the wafer when it is polished. As shown in Figure 4.17, the MMR increases when the WP is increased. As Hernandez *et al.* [57] show in Figure 2.19, the RR is more dependent on the pressure compared to the velocity. One can notice from the results that the sample polished at a WP of 100 mdaN/cm^2 has a higher MMR during the CMP, than the sample done at 200. The wafer with a WP of 100 lost 41.31 nm after polishing for 60 seconds compared to the wafer polished with a WP of 200 which lost 34.56 nm. This could be due to an error in the experiment, or it can be that the material removed

is not linearly dependent on the WP but is slightly more polynomic. To possibly achieve the right relation between the WP and the MMR, many more samples should be used. As mentioned earlier, the slurry concentration influences the MRR, so it is crucial to have a very similar slurry concentration when the WP is investigated.

It can also be seen that independent of the WP, the sample surface is relatively homogeneously. After ALD, the standard deviation of the layer is between 0.2 nm and 1.48 nm. After polishing for 60 seconds, the standard deviation is between 1.16 nm and 1.48 nm. These numbers are still very low. As shown in Figure 4.18, it is unclear if the wafers will have a pit or a cliff in the middle of the sample. To get a more accurate result, more wafers should be polished.

5.3 Silica Wafers

Since the silica wafers are only investigated in the CMP, the subchapters are divided by the different parameters which were focused on: different slurry concentration, backside pressure (BP), and working pressure (WP).

5.3.1 Slurry Concentrations

As expected, a higher concentration of slurry removed more material on the silica wafers. As shown in Figure 4.20, the silica wafers had a polynomial relation between the concentration of the slurry and the MMR. As Jianfeng Luo *et al.* also shows in Figure 2.11 [43], the slurry concentration will affect the film's removal rate. Figure 2.13 [53] shows that the relation is almost linear depending on the particle concentration, but it is only looking at a particle concentration between 6 and 18. By ignoring the last and first values from the plot in Figure 4.20, the graph would appear more linear. To be sure if there is a linear or polynomial relation between the concentration of the slurry and the MMR, more samples should be investigated.

As shown in Figure 4.19, the surface roughness is minimal, and the MMR standard deviation in Figure 4.20 is almost impossible to see. The wafer with the lowest film thickness standard deviation is the wafer polished with the slurry concentration 1:7 (12.5%). It should be mentioned that the PECVD machine does not make an entirely homogeneously film with silica. The wafer polished with the slurry concentration 1:7 had a standard deviation of 1.63 nm before it was polished, while the other wafers had a standard deviation of more than 6 nm before the CMP. To show a tighter correlation between standard deviation and slurry concentration, more wafers should be tested.

5.3.2 Backside Pressure

The BP does not significantly influence the MMR, but the best fit in terms of planarization result had a BP of 200 mdaN/cm^2. As shown in Figure 4.23, it looks like the graph has a high MMR either when the BP is low or high. It can be that the different contact-modes changes depending on the BP. The wafers will either have a higher contact with the slurry or with the pad, which increases the MMR. The value of R^2 is also close to 1, so it seems like the BP is following a 2nd degree polynomial with the lowest value of MMR at 300 mdaN/cm^2.

In Figure 4.23, the wafers with a higher BP have a higher MMR standard deviation than the wafers polished with a lower BP. One can also see in Figure 4.24, the two wafers polished with the lowest BP had the lowest film thickness standard deviation. This can be due to uneven slurry flow under the wafers when the pressure gets too high. To be sure if the BP either influences the MMR or the film thickness standard deviation, more wafers should be tested.

5.3.3 Working Pressure

From Figure 4.26, higher WP will give a higher MMR. Compared to the BP, the WP has a more linear relation to the material removed from the film. This can be due to the same reason as with the alumina wafers. Hernandez *et al.* [57] say that the WP influences the MRR much more than the velocity. The R^2 value in Figure 4.26 shows that the correlation is very good between WP and MMR. To check if this trend will continue, more samples should be investigated.

In Figure 4.26, the wafer polished with a WP at 400 mdaN/cm^2 has a higher MMR standard deviation than the other wafers. This can be due to impurities before or after the CMP or due to an uneven slurry flow under the wafer. However, it can also be due to the CMP process is reducing the roughness of the material surface. However, Figure 4.27 shows the two wafers with the lowest film thickness standard deviation. These two wafers had the most homogenous surface after CMP. In conclusion, the best fit in terms of planarization result had a BP of 200 mdaN/cm^2.

6 Conclusion

In this thesis, one can see that the different parameters will influence the adhesion between amorphous silicon (a-Si) and alumina (Al_2O_3). To battle this, the deposition time, deposition temperature, and deposition of silica (SiO_2) before a-Si were tried. The experiment showed that the deposition time did not change how many blisters the wafer received but lowering the temperature and having a silica layer underneath helped to achieve better adhesion between the two layers. The a-Si wafers for the CMP experiments, were then made with a new recipe that combines 1-minute of (OPT) SiO_2 before a 45-minute layer of (OPT) a-Si deposited at 180 degrees.

It was shown that the different parameters will influence the CMP machine and will influence the homogeneity and removal rate (RR) of the a-Si, silica, and alumina films on the wafers. Many parameters can be changed, but the parameters investigated in this paper were the slurry concentration, duration time, backside pressure (BP), and working pressure (WP). Due to Covid-19, backside pressure and working pressure were not investigated for the a-Si wafers.

All the wafers were profoundly affected by the slurry concentration. Higher slurry concentration gives a higher material removal rate (MRR). The a-Si wafers have a logarithmic relation, while the alumina wafers have a linear relation, and the silica wafers have a more polynomial relation. It is hard to tell if there is any relation between the slurry concentration and the film thickness standard deviation. For the a-Si wafers, a slurry concentration of 33% is recommended, while for silica and alumina, a more diluted slurry is recommended for lower standard deviation. If one needs to remove more material, a higher slurry concentration can be used.

From the BP experiments, no clear indication of any relation between the BP and the material removal rate (MRR) was found. The alumina wafers had the highest amount of material removed (AMR) with the BP at 200 and 400, while the silica wafers had the highest AMR with BP at 100 and 500. However, both silica and alumina showed that higher BP give a higher film thickness standard deviation. This can happen because the slurry does not manage to travel evenly under the wafer. Lower BP is recommended for lower standard deviation.

On the other hand, higher working pressure yields a higher AMR, both with silica and alumina. With the alumina, the working pressure did not influence the film thickness standard deviation, and all the wafers had a relatively low surface roughness. On the other

hand, with silica, one of the wafers had a much higher standard deviation than the others. At a working pressure of 400, the standard deviation was more than double the value the other wafers had. If one needs high MRR and low standard deviation, a working pressure of 500 should be used.

The relation between the MMR and the time the wafer is polished is linear, independent of the slurry concentration, backside pressure, and working pressure. This is true for all the silica and alumina wafers, and the a-Si wafers polished with different slurry concentrations. However, to see if there is a higher correlation between the AMR, film thickness standard deviation, and slurry concentration, backside pressure, or working pressure, more samples should be investigated.

7 Further Work

In this project, only one wafer was tested for each specific parameter value. More wafers should be tested to achieve better results, and slurry concentrations should be measured more accurately. In addition, different backside pressures and working pressures on the amorphous silicon (a-Si) wafers should be investigated. The presented work can also be extended by trying to planarize 3D structures and see if the materials have the same removal rate as the more homogeneous surfaces as done in this thesis. Moreover, a more detailed measurement of the roughness of the surfaces before and after CMP can be conducted by utilizing a 3D ellipsometry. At last, one can test the influence of other types of slurries on the MMR and the surface homogeneity.

8 References

[1] H. C. M. Knoops, S. E. Potts, A. A. Bol, and W. M. M. Kessels, "27 - Atomic Layer Deposition," in *Handbook of Crystal Growth (Second Edition)*, Second Edition., T. F. Kuech, Ed. Boston: North-Holland, 2015, pp. 1101–1134.

[2] G. Cao and Y. Wang, *Nanostructures and Nanomaterials*, 2nd ed., vol. 2.

[3] M. M. Winterkorn, A. L. Dadlani, Y. Kim, J. Provine, and F. B. Prinz, "ETCH 'sandbox': Controlled release dimensions through atomic layer deposition etch stop with trench refill and polish," in *2015 Transducers - 2015 18th International Conference on Solid-State Sensors, Actuators and Microsystems (TRANSDUCERS)*, Jun. 2015, pp. 2272–2275, doi: 10.1109/TRANSDUCERS.2015.7181415.

[4] T. C. Isabell, P. E. Fischione, C. O'Keefe, M. U. Guruz, and V. P. Dravid, "Plasma Cleaning and Its Applications for Electron Microscopy," *Microsc. Microanal.*, vol. 5, no. 2, pp. 126–135, Mar. 1999, doi: 10.1017/S1431927699000094.

[5] J. A. Wilson and A. J. Craven, "Improving the analysis of small precipitates in HSLA steels using a plasma cleaner and ELNES," *Ultramicroscopy*, vol. 94, no. 3, pp. 197–207, 2003, doi: https://doi.org/10.1016/S0304-3991(02)00265-6.

[6] D.-S. Ko, Y. M. Park, S.-D. Kim, and Y.-W. Kim, "Effective removal of Ga residue from focused ion beam using a plasma cleaner," *Ultramicroscopy*, vol. 107, no. 4, pp. 368–373, Apr. 2007, doi: 10.1016/j.ultramic.2006.09.004.

[7] G. P. Canal, H. Luna, L. F. Ruchko, and R. M. O. Galvão, "Design and characterization of an RF plasma cleaner," *Braz. J. Phys.*, vol. 40, no. 1, pp. 108–114, Mar. 2010, doi: 10.1590/S0103-97332010000100015.

[8] "LIMS - [Plasma Cleaner]."

http://ntnu.norfab.no/WebForms/Equipment/EquipmentView.aspx?toolId=38 (accessed Nov. 07, 2019).

[9] "Plasma Cleaning." http://www.plasmaetch.com/plasma-cleaning.php (accessed Nov. 04, 2019).

[10] T. C. Isabell and P. E. Fischione, "Applications of Plasma Cleaning for Electron Microscopy of Semiconducting Materials," *MRS Online Proc. Libr. Arch.*, vol. 523, ed 1998, doi: 10.1557/PROC-523-31.

[11] K. Wasa and S. Hayakawa, "Handbook of sputter deposition technology," 1992, Accessed: May 05, 2020. [Online]. Available:

http://inis.iaea.org/Search/search.aspx?orig_q=RN:24004571.

[12] J.-O. Carlsson and P. M. Martin, "Chapter 7 - Chemical Vapor Deposition," in *Handbook of Deposition Technologies for Films and Coatings (Third Edition)*, Third Edition., P. M. Martin, Ed. Boston: William Andrew Publishing, 2010, pp. 314–363.

[13] L. M. Hoyos-Palacio *et al.*, "Compounds of carbon nanotubes decorated with silver nanoparticles via in-situ by chemical vapor deposition (CVD)," *J. Mater. Res. Technol.*, vol. 8, no. 6, pp. 5893–5898, Nov. 2019, doi: 10.1016/j.jmrt.2019.09.062.

[14] L. Cai, Q. Xu, W. Lu, R. Tu, T. Goto, and S. Zhang, "Growth mechanism of porous 3C–SiC films prepared via laser chemical vapor deposition," *Ceram. Int.*, Mar. 2020, doi: 10.1016/j.ceramint.2020.03.217.

[15] S. M. George, "Atomic Layer Deposition: An Overview," *Chem. Rev.*, vol. 110, no. 1, pp. 111–131, Jan. 2010, doi: 10.1021/cr900056b.

[16] J. Wang *et al.*, "Homoepitaxy of Ge on ozone-treated Ge (1 0 0) substrate by ultra-high vacuum chemical vapor deposition," *J. Cryst. Growth*, vol. 507, pp. 113–117, Feb. 2019, doi: 10.1016/j.jcrysgro.2018.11.003.

[17] Y. Zhu, L. Cheng, B. Ma, Y. Liu, and L. Zhang, "New route to synthesize ZrB2 coatings by reactive chemical vapor deposition method using Zr-BCl3-H2-Ar reagents," *Surf. Coat. Technol.*, vol. 337, pp. 209–216, Mar. 2018, doi: 10.1016/j.surfcoat.2018.01.021.

[18] "(PDF) Amorphous and Microcrystalline Silicon Solar cells: Modeling, Materials and Device Technology," *ResearchGate*.

https://www.researchgate.net/publication/288877900_Amorphous_and_Microcrystalline_Silicon_Solar_cells_Modeling_Materials_and_Device_Technology?channel=doi&linkId=5692861108aee91f69a6fedd&showFulltext=true (accessed May 09, 2020).

[19] "LIMS - [PECVD]."

http://ntnu.norfab.no/WebForms/Equipment/EquipmentView.aspx?toolId=33 (accessed Nov. 07, 2019).

[20] H. S. Nalwa, *Handbook of Thin Films*. California, USA: Elsevier, 2002.

[21] Y. T. Kim, D. S. Kim, and D. H. Yoon, "PECVD SiO2 and SiON films dependant on the rf bias power for low-loss silica waveguide," *Thin Solid Films*, vol. 475, no. 1, pp. 271–274, Mar. 2005, doi: 10.1016/j.tsf.2004.07.044.

[22] G. Subhash, P. Hittepole, and S. Maiti, "Mechanical properties of PECVD thin ceramic films," *J. Eur. Ceram. Soc.*, vol. 30, no. 3, pp. 689–697, Feb. 2010, doi: 10.1016/j.jeurceramsoc.2009.09.020.

[23] J. C. Rostaing, F. Coeuret, J. Pelletier, T. Lagarde, and R. Etemadi, "Highly homogeneous silica coatings for optical and protective applications deposited by PECVD at room temperature in a planar uniform distributed electron cyclotron resonance plasma reactor.," *Thin Solid Films*, vol. 270, no. 1, pp. 49–54, Dec. 1995, doi: 10.1016/0040-6090(96)80068-X.

[24] S. Guha, J. Yang, D. L. Williamson, Y. Lubianiker, J. D. Cohen, and A. H. Mahan, "Structural, defect, and device behavior of hydrogenated amorphous Si near and above the onset of microcrystallinity," *Appl. Phys. Lett.*, vol. 74, no. 13, pp. 1860–1862, 1999, doi: 10.1063/1.123693.

[25] Y. Y. Ong, B. T. Chen, F. E. H. Tay, and C. Iliescu, "Process Analysis and Optimization on PECVD Amorphous Silicon on Glass Substrate," *J. Phys. Conf. Ser.*, vol. 34, pp. 812–817, Apr. 2006, doi: 10.1088/1742-6596/34/1/134.

[26] J. P. Conde, P. Alpuim, and V. Chu, "Hot-wire thin-film transistors on PET at 100 °C," *Thin Solid Films*, vol. 430, no. 1, pp. 240–244, Apr. 2003, doi: 10.1016/S0040-6090(03)00115-9.

[27] J. Joseph, S. G. Singh, and S. R. K. Vanjari, "Ultra-smooth e-beam evaporated amorphous silicon thin films – A viable alternative for PECVD amorphous silicon thin films for MEMS applications," *Mater. Lett.*, vol. 197, pp. 52–55, Jun. 2017, doi: 10.1016/j.matlet.2017.03.158.

[28] Y. Q. Fu, J. K. Luo, S. B. Milne, A. J. Flewitt, and W. I. Milne, "Residual stress in amorphous and nanocrystalline Si films prepared by PECVD with hydrogen dilution," *Mater. Sci. Eng. B*, vol. 124–125, pp. 132–137, Dec. 2005, doi: 10.1016/j.mseb.2005.08.104.

[29] C.-K. Chung, M.-Q. Tsai, P.-H. Tsai, and C. Lee, "Fabrication and characterization of amorphous Si films by PECVD for MEMS," *J. Micromechanics Microengineering*, vol. 15, no. 1, pp. 136–142, Oct. 2004, doi: 10.1088/0960-1317/15/1/021.

[30] A. B. Afif, A. L. Dadlani, S. Burgmann, P. Köllensperger, and J. Torgersen, "Atomic layer deposition of perovskites—Part 1: Fundamentals of nucleation and growth," *Mater. Des. Process. Commun.*, vol. 2, no. 1, p. e114, 2020, doi: 10.1002/mdp2.114.

[31] A. Giaccherini *et al.*, "Operando SXRD of E-ALD deposited sulphides ultra-thin films: Crystallite strain and size," *Appl. Surf. Sci.*, vol. 432, pp. 53–59, Feb. 2018, doi: 10.1016/j.apsusc.2017.07.294.

[32] O. Graniel, M. Weber, S. Balme, P. Miele, and M. Bechelany, "Atomic layer deposition for biosensing applications," *Biosens. Bioelectron.*, vol. 122, pp. 147–159, 2018, doi: https://doi.org/10.1016/j.bios.2018.09.038.

[33] P. R. Chalker, "Photochemical atomic layer deposition and etching," *Surf. Coat. Technol.*, vol. 291, pp. 258–263, 2016, doi:

https://doi.org/10.1016/j.surfcoat.2016.02.046.

[34] R. L. Puurunen and W. Vandervorst, "Island growth as a growth mode in atomic layer deposition: A phenomenological model: Journal of Applied Physics: Vol 96, No 12," Sep. 08, 2004. https://aip.scitation.org/doi/10.1063/1.1810193 (accessed Nov. 08, 2019).

[35] M. Krishnan, J. W. Nalaskowski, and L. M. Cook, "Chemical Mechanical Planarization: Slurry Chemistry, Materials, and Mechanisms," *Chem. Rev.*, vol. 110, no. 1, pp. 178–204, Jan. 2010, doi: 10.1021/cr900170z.

[36] Y.-G. Wang, Y. Chen, and Y.-W. Zhao, "Chemical mechanical planarization of silicon wafers at natural pH for green manufacturing," *Int. J. Precis. Eng. Manuf.*, vol. 16, no. 9, pp. 2049–2054, Aug. 2015, doi: 10.1007/s12541-015-0266-z.

[37] A. P. Malshe, B. S. Park, W. D. Brown, and H. A. Naseem, "A review of techniques for polishing and planarizing chemically vapor-deposited (CVD) diamond films and substrates," *Diam. Relat. Mater.*, vol. 8, no. 7, pp. 1198–1213, 1999, doi: https://doi.org/10.1016/S0925-9635(99)00088-6.

[38] J. M. Steigerwald, S. P. Murarka, and R. J. Gutmann, *Chemical Mechanical Planarization of Microelectronic Materials*, 1st ed. John Wiley & Sons, Ltd, 1997.

[39] D. Roy, "3 - Electrochemical techniques and their applications for chemical mechanical planarization (CMP) of metal films," in *Advances in Chemical Mechanical Planarization (CMP)*, S. Babu, Ed. Woodhead Publishing, 2016, pp. 47–89.

[40] J. M. Neirynck, G.-R. Yang, S. P. Murarka, and R. J. Gutmann, "The addition of surfactant to slurry for polymer CMP: effects on polymer surface, removal rate and underlying Cu," *Thin Solid Films*, vol. 290–291, pp. 447–452, Dec. 1996, doi: 10.1016/S0040-6090(96)09033-5.

[41] G. C. C. Yang and C.-J. Li, "Tubular TiO2/Al2O3 composite membranes: preparation, characterization, and performance in electrofiltration of oxide-CMP wastewater," *Desalination*, vol. 234, no. 1, pp. 354–361, Dec. 2008,

doi: 10.1016/j.desal.2007.09.104.

[42] Z. Shi, Z. Jin, X. Guo, S. Yuan, and J. Guo, "Insights into the atomistic behavior in diamond chemical mechanical polishing with OH environment using ReaxFF molecular dynamics simulation," *Comput. Mater. Sci.*, vol. 166, pp. 136–142, 2019, doi: https://doi.org/10.1016/j.commatsci.2019.05.001.

[43] Jianfeng Luo and D. A. Dornfeld, "Material removal mechanism in chemical mechanical polishing: theory and modeling," *IEEE Trans. Semicond. Manuf.*, vol. 14, no. 2, pp. 112–133, May 2001, doi: 10.1109/66.920723.

[44] E. Estragnat, G. Tang, H. Liang, S. Jahanmir, P. Pei, and J. M. Martin, "Experimental investigation on mechanisms of silicon chemical mechanical polishing," *J. Electron. Mater.*, vol. 33, no. 4, pp. 334–339, Apr. 2004, doi: 10.1007/s11664-004-0140-8.

[45] H. Zhu, L. A. Tessaroto, R. Sabia, V. A. Greenhut, M. Smith, and D. E. Niesz, "Chemical mechanical polishing (CMP) anisotropy in sapphire," *Appl. Surf. Sci.*, vol. 236, no. 1, pp. 120–130, 2004, doi: https://doi.org/10.1016/j.apsusc.2004.04.027.

[46] G. Byrne, B. Mullany, and P. Young, "The Effect of Pad Wear on the Chemical Mechanical Polishing of Silicon Wafers," *CIRP Ann.*, vol. 48, no. 1, pp. 143–146, Jan. 1999, doi: 10.1016/S0007-8506(07)63151-5.

[47] J. Guo *et al.*, "Study on the polishing mechanism of pH-dependent tribochemical removal in CMP of CaF2 crystal," *Tribol. Int.*, vol. 150, p. 106370, Oct. 2020, doi: 10.1016/j.triboint.2020.106370.

[48] N. Suzuki, Y. Hashimoto, H. Yasuda, S. Yamaki, and Y. Mochizuki, "Prediction of polishing pressure distribution in CMP process with airbag type wafer carrier," *CIRP Ann.*, vol. 66, no. 1, pp. 329–332, Jan. 2017, doi: 10.1016/j.cirp.2017.04.088.

[49] S.-W. Park, C.-B. Kim, S.-Y. Kim, and Y.-J. Seo, "Design of experimental optimization for ULSI CMP process applications," *Microelectron. Eng.*, vol. 66, no. 1, pp. 488–495, Apr. 2003, doi: 10.1016/S0167-9317(02)00932-2.

[50] Y. Huang, D. Guo, X. Lu, and J. Luo, "A lubrication model between the soft porous brush and rigid flat substrate for post-CMP cleaning," *Microelectron. Eng.*, vol. 88, no. 9, pp. 2862–2870, Sep. 2011, doi: 10.1016/j.mee.2011.02.113.

[51] R. Yim *et al.*, "Chemical/mechanical balance management through pad microstructure in CMP," *Microelectron. Eng.*, vol. 195, pp. 36–40, Aug. 2018, doi: 10.1016/j.mee.2017.12.002.

[52] S.-Y. Kim and Y.-J. Seo, "Correlation analysis between pattern and non-pattern wafer for characterization of shallow trench isolation–chemical–mechanical polishing (STI–CMP) process," *Microelectron. Eng.*, vol. 60, no. 3, pp. 357–364, Apr. 2002, doi: 10.1016/S0167-9317(01)00694-3.

[53] H. S. Lee, H. D. Jeong, and D. A. Dornfeld, "Semi-empirical material removal rate distribution model for SiO2 chemical mechanical polishing (CMP) processes," *Precis. Eng.*, vol. 37, no. 2, pp. 483–490, Apr. 2013,

doi: 10.1016/j.precisioneng.2012.12.006.

[54] B. Mullany and G. Byrne, "The effect of slurry viscosity on chemical–mechanical polishing of silicon wafers," *J. Mater. Process. Technol.*, vol. 132, no. 1, pp. 28–34, Jan. 2003, doi: 10.1016/S0924-0136(02)00205-4.

[55] M. Neville, C.-H. Hung, and M. A. Lucarelli, "CHEMICAL MECHANICAL POLISHING SLURRY FOR METAL LAYERS," p. 16.

[56] B. Davarik *et al.*, "A new planarization technique, using a combination of RIE and chemical mechanical polish (CMP)," in *International Technical Digest on Electron Devices Meeting*, Dec. 1989, pp. 61–64, doi: 10.1109/IEDM.1989.74228.

[57] J. Hernandez *et al.*, "Chemical Mechanical Polishing of Al and SiO2 Thin Films: The Role of Consumables," *J. Electrochem. Soc.*, vol. 146, no. 12, pp. 4647–4653, Jan. 1999, doi: 10.1149/1.1392688.

[58] B. Gao, W. Zhai, Q. Zhai, and M. Zhang, "Novel polystyrene/CeO2-TiO2 multicomponent core/shell abrasives for high-efficiency and high-quality photocatalytic-assisted chemical mechanical polishing of reaction-bonded silicon carbide," *Appl. Surf. Sci.*, vol. 484, pp. 534–541, 2019, doi: https://doi.org/10.1016/j.apsusc.2019.04.037.

[59] N.-H. Kim, P.-J. Ko, G.-W. Choi, Y.-J. Seo, and W.-S. Lee, "Chemical mechanical polishing (CMP) mechanisms of thermal SiO2 film after high-temperature pad conditioning," *Thin Solid Films*, vol. 504, no. 1, pp. 166–169, May 2006, doi: 10.1016/j.tsf.2005.09.089.

[60] M. R. Oliver, *Chemical-Mechanical Planarization of Semiconductor Materials*. Springer Science & Business Media, 2013.

[61] M. Feldman, *Nanolithography, The Art of Fabricating Nanoelectronic and Nanophotonic Devices and Systems*. 2014.

[62] T. Ito and S. Okazaki, "Pushing the limits of lithography," *Nature*, vol. 406, no. 6799, Art. no. 6799, Aug. 2000, doi: 10.1038/35023233.

[63] R. A. Lawson and A. P. G. Robinson, "Chapter 1 - Overview of materials and processes for lithography," in *Frontiers of Nanoscience*, vol. 11, A. Robinson and R. Lawson, Eds. Elsevier, 2016, pp. 1–90.

[64] B. W. Smith, "1 - Optical projection lithography," in *Nanolithography*, M. Feldman, Ed. Woodhead Publishing, 2014, pp. 1–41.

[65] D. Han, C. Yang, N. X. Fang, and H. Lee, "Rapid multi-material 3D printing with projection micro-stereolithography using dynamic fluidic control," *Addit. Manuf.*, vol. 27, pp. 606–615, May 2019, doi: 10.1016/j.addma.2019.03.031.

[66] Rosenbluth, Alan, Bukofsky, Scott, Hibbs, Michael, Lai, and Kafai, Molless, Antoinette, et al., "Optimum mask and source patterns to print a given shape," p. 18, 2001.

[67] M. Hofmann *et al.*, "Mix-and-match lithography and cryogenic etching for NIL template fabrication," *Microelectron. Eng.*, vol. 224, p. 111234, 2020, doi: https://doi.org/10.1016/j.mee.2020.111234.

[68] M. Zhang, S. Jiang, Y. Gao, J. Nie, and F. Sun, "Design of a disulfide bond-containing photoresist with extremely low volume shrinkage and excellent degradation ability for UV-nanoimprinting lithography," *Chem. Eng. J.*, vol. 390, p. 124625, Jun. 2020, doi: 10.1016/j.cej.2020.124625.

[69] B. L. Sharp, H. L. Narcross, L. M. Tolbert, and C. L. Henderson, "Positive-tone crosslinked molecular resist based on acid-catalyzed depolymerization," *J. Vac. Sci. Technol. B*, vol. 35, no. 6, p. 06GE03, Nov. 2017, doi: 10.1116/1.4991904.

[70] J. Dai, S. W. Chang, A. Hamad, D. Yang, N. Felix, and C. K. Ober, "Molecular Glass Resists for High-Resolution Patterning," *Chem. Mater.*, vol. 18, no. 15, pp. 3404–3411, Jul. 2006, doi: 10.1021/cm052452m.

[71] R. A. Lawson, L. M. Tolbert, T. R. Younkin, and C. L. Henderson, "Negative-tone molecular resists based on cationic polymerization," in *Advances in Resist Materials and Processing Technology XXVI*, Apr. 2009, vol. 7273, p. 72733E, doi: 10.1117/12.814455.

[72] C. K. Ober, H. Xu, V. Kosma, K. Sakai, and E. P. Giannelis, "EUV photolithography: resist progress and challenges," in *Extreme Ultraviolet (EUV) Lithography IX*, Mar. 2018, vol. 10583, p. 1058306, doi: 10.1117/12.2302759.

[73] M. Trikeriotis *et al.*, "A new inorganic EUV resist with high-etch resistance," vol. 8322, p. 83220U, Mar. 2012, doi: 10.1117/12.916384.

[74] R. A. Lawson *et al.*, "Optimizing performance in cross-linking negative-tone molecular resists," in *Advances in Patterning Materials and Processes XXXII*, Mar. 2015, vol. 9425, p. 94250A, doi: 10.1117/12.2086007.

[75] D.-H. Dinh, H.-L. Chien, and Y.-C. Lee, "Maskless lithography based on digital micromirror device (DMD) and double sided microlens and spatial filter array," *Opt. Laser Technol.*, vol. 113, pp. 407–415, May 2019,

doi: 10.1016/j.optlastec.2019.01.001.

[76] M. Schulz, "The end of the road for silicon?," *Nature*, vol. 399, no. 6738, Art. no. 6738, Jun. 1999, doi: 10.1038/21526.

[77] C. Gong and T. Hogan, "CMOS compatible fabrication processes for the digital micromirror device," *IEEE J. Electron Devices Soc.*, vol. 2, no. 3, pp. 27–32, 2014, doi: 10.1109/JEDS.2014.2309129.

[78] C. Peng, Z. Zhang, J. Zou, and W. Chi, "A high-speed exposure method for digital micromirror device based scanning maskless lithography system," *Optik*, vol. 185, pp. 1036–1044, May 2019, doi: 10.1016/j.ijleo.2019.04.009.

[79] Q.-K. Li, Y. Xiao, H. Liu, H.-L. Zhang, J. Xu, and J.-H. Li, "Analysis and correction of the distortion error in a DMD based scanning lithography system," *Opt. Commun.*, vol. 434, pp. 1–6, Mar. 2019, doi: 10.1016/j.optcom.2018.10.042.

[80] D.-H. Lee, "Optical System with 4 ㎛ Resolution for Maskless Lithography Using Digital Micromirror Device," *J. Opt. Soc. Korea*, vol. 14, no. 3, pp. 266–276, 2010, doi: 10.3807/JOSK.2010.14.3.266.

[81] Y. Lu, G. Mapili, G. Suhali, S. Chen, and K. Roy, "A digital micro-mirror device-based system for the microfabrication of complex, spatially patterned tissue engineering scaffolds," *J. Biomed. Mater. Res. A*, vol. 77A, no. 2, pp. 396–405, 2006, doi: 10.1002/jbm.a.30601.

[82] K. Totsu, K. Fujishiro, S. Tanaka, and M. Esashi, "Fabrication of three-dimensional microstructure using maskless gray-scale lithography," *Sens. Actuators Phys.*, vol. 130–131, pp. 387–392, Aug. 2006, doi: 10.1016/j.sna.2005.12.008.

[83] M. J. Madou, *Manufacturing Techniques for Microfabrication and Nanotechnology*. CRC Press, 2011.

[84] S. Hari, T. Verduin, P. Kruit, and C. W. Hagen, "A study of the reproducibility of electron beam induced deposition for sub-20 nm lithography," *Micro Nano Eng.*, vol. 4, pp. 1–6, Sep. 2019, doi: 10.1016/j.mne.2019.04.003.

[85] Y. Sohda *et al.*, "Recent progress in cell-projection electron-beam lithography," *Microelectron. Eng.*, vol. 67–68, pp. 78–86, Jun. 2003, doi: 10.1016/S0167-9317(03)00062-5.

[86] Y. Lin, B. Yu, Y. Zou, Z. Li, C. J. Alpert, and D. Z. Pan, "Stitch aware detailed placement for multiple E-beam lithography," *Integration*, vol. 58, pp. 47–54, Jun. 2017, doi: 10.1016/j.vlsi.2017.02.004.

[87] D. Wang, J. Zhang, H. Wang, and Y. Xia, "Variable shape or variable diameter flattop beam tailored by using an adaptive weight FFT-based iterative algorithm and a phase-only liquid crystal spatial light modulator," *Opt. Commun.*, vol. 285, no. 24, pp. 5044–5050, Nov. 2012, doi: 10.1016/j.optcom.2012.08.081.

[88] J. E. E. Baglin, "Ion beam nanoscale fabrication and lithography—A review," *Appl. Surf. Sci.*, vol. 258, no. 9, pp. 4103–4111, Feb. 2012,

doi: 10.1016/j.apsusc.2011.11.074.

[89] A. H. Atabaki *et al.*, "Integrating photonics with silicon nanoelectronics for the next generation of systems on a chip," *Nature*, vol. 556, no. 7701, Art. no. 7701, Apr. 2018, doi: 10.1038/s41586-018-0028-z.

[90] C. Zhang *et al.*, "Printed photonic elements: nanoimprinting and beyond," *J. Mater. Chem. C*, vol. 4, no. 23, pp. 5133–5153, 2016, doi: 10.1039/C6TC01237J.

[91] L. J. Guo, "Nanoimprint Lithography: Methods and Material Requirements," *Adv. Mater.*, vol. 19, no. 4, pp. 495–513, 2007, doi: 10.1002/adma.200600882.

[92] S. Y. Chou, P. R. Krauss, W. Zhang, L. Guo, and L. Zhuang, "Sub-10 nm imprint lithography and applications," *J. Vac. Sci. Technol. B Microelectron. Nanometer Struct. Process. Meas. Phenom.*, vol. 15, no. 6, pp. 2897–2904, Nov. 1997, doi: 10.1116/1.589752.

[93] Y. Hirai, S. Harada, S. Isaka, M. Kobayashi, and Y. Tanaka, "Nano-Imprint Lithography Using Replicated Mold by Ni Electroforming," *Jpn. J. Appl. Phys.*, vol. 41, no. 6S, p. 4186, Jun. 2002, doi: 10.1143/JJAP.41.4186.

[94] J. P. Rolland, R. M. Van Dam, D. A. Schorzman, S. R. Quake, and J. M. DeSimone, "Solvent-resistant photocurable liquid fluoropolymers for microfluidic device fabrication [corrected]," *J. Am. Chem. Soc.*, vol. 126, no. 8, pp. 2322–2323, Mar. 2004, doi: 10.1021/ja031657y.

[95] M. Losurdo *et al.*, "Spectroscopic ellipsometry and polarimetry for materials and systems analysis at the nanometer scale: state-of-the-art, potential, and perspectives," *J. Nanoparticle Res.*, vol. 11, no. 7, pp. 1521–1554, Oct. 2009, doi: 10.1007/s11051-009-9662-6.

[96] P. Kaspar *et al.*, "Characterization of Fe2O3 thin film on highly oriented pyrolytic graphite by AFM, Ellipsometry and XPS," *Appl. Surf. Sci.*, vol. 493, pp. 673–678, 2019, doi: https://doi.org/10.1016/j.apsusc.2019.07.058.

[97] T. Galy, M. Marszewski, S. King, Y. Yan, S. H. Tolbert, and L. Pilon, "Comparing methods for measuring thickness, refractive index, and porosity of mesoporous thin films," *Microporous Mesoporous Mater.*, vol. 291, p. 109677, 2020, doi: https://doi.org/10.1016/j.micromeso.2019.109677.

[98] K. Pedersen, "Ellisometry," *2004*, p. 138.

[99] B. J. Glasgow, "Ellipsometry of human tears," *Ocul. Surf.*, vol. 17, no. 2, pp. 341–346, 2019, doi: https://doi.org/10.1016/j.jtos.2019.02.008.

[100] R. Hernando, J. L. Fernández-Marchena, J. C. Willman, A. Ollé, J. M. Vergès, and M. Lozano, "Exploring the utility of optical light microscopy versus scanning electron microscopy for the quantification of dental microwear," *Quat. Int.*, May 2020, doi: 10.1016/j.quaint.2020.05.022.

[101] J. Hjelen, *Scanning elektron-mikroskopi*. NTH: Metallurgisk institutt, 1989.

[102] B. J. Inkson, "2 - Scanning electron microscopy (SEM) and transmission electron microscopy (TEM) for materials characterization," in *Materials Characterization Using Nondestructive Evaluation (NDE) Methods*, G. Hübschen, I. Altpeter, R. Tschuncky, and H.-G. Herrmann, Eds. Woodhead Publishing, 2016, pp. 17–43.

[103] M. de Assumpção Pereira-da-Silva and F. A. Ferri, "1 - Scanning Electron Microscopy," in *Nanocharacterization Techniques*, A. L. Da Róz, M. Ferreira, F. de Lima Leite, and O. N. Oliveira, Eds. William Andrew Publishing, 2017, pp. 1–35.

[104] J. I. Martín-Viveros and A. Ollé, "Use-wear and residue mapping on experimental chert tools. A multi-scalar approach combining digital 3D, optical, and scanning electron microscopy," *J. Archaeol. Sci. Rep.*, vol. 30, p. 102236, Apr. 2020, doi: 10.1016/j.jasrep.2020.102236.

[105] M. Abd Mutalib, M. A. Rahman, M. H. D. Othman, A. F. Ismail, and J. Jaafar, "Chapter 9 - Scanning Electron Microscopy (SEM) and Energy-Dispersive X-Ray (EDX) Spectroscopy," in *Membrane Characterization*, N. Hilal, A. F. Ismail, T. Matsuura, and D. Oatley-Radcliffe, Eds. Elsevier, 2017, pp. 161–179.

[106] S.-Y. Lien, C.-H. Yang, K.-C. Wu, and C.-Y. Kung, "Investigation on the passivated Si/Al2O3 interface fabricated by non-vacuum spatial atomic layer deposition system," *Nanoscale Res. Lett.*, vol. 10, Feb. 2015, doi: 10.1186/s11671-015-0803-9.

[107] "Klebosol®." https://www.merckgroup.com/en/brands/pm/klebosol.html (accessed Dec. 22, 2019).

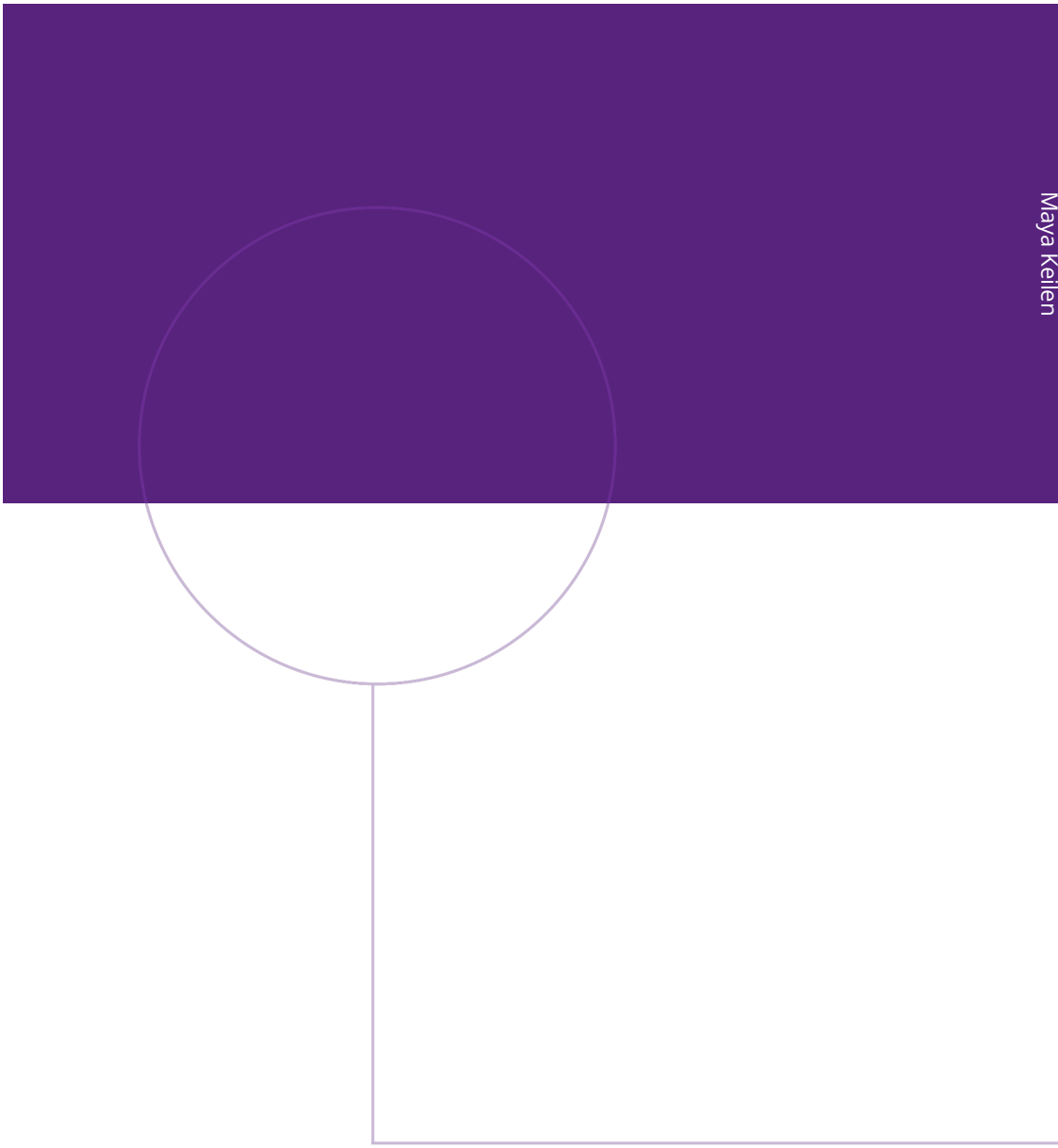

Maya Kellen

NTNU
Norwegian University of
Science and Technology